UCLA
UCLA Electronic Theses and Dissertations

Title
Characterization of particulate matter from non-exhaust traffic emissions

Permalink
https://escholarship.org/uc/item/42n4957j

Author
Oroumiyeh, Farzan

Publication Date
2021

Peer reviewed|Thesis/dissertation

eScholarship.org Powered by the California Digital Library
University of California

UNIVERSITY OF CALIFORNIA

Los Angeles

Characterization of particulate matter from non-exhaust traffic emissions

A dissertation submitted in partial satisfaction of the

requirements for the degree

Doctor of Philosophy in Environmental Health Sciences

by

Farzan Oroumiyeh

2021

© Copyright by

Farzan Oroumiyeh

2021

ABSTRACT OF THE DISSERTATION

Characterization of particulate matter from non-exhaust traffic emissions

by

Farzan Oroumiyeh

Doctor of Philosophy in Environmental Health Sciences

University of California, Los Angeles, 2021

Professor Yifang Zhu, Chair

Ambient air pollution has been one of the leading risk factors in the global burden of disease, whose contribution to mortality as well as various adverse health outcomes has been well-documented. Among the various sources of air pollution, urban traffic emissions have been reported to be among the largest contributors to various criteria pollutants, including particulate matter (PM). A large body of research has linked traffic-related PM with various health outcomes in metropolitan areas. Therefore, the governments have used their legislative power to reduce vehicle exhaust emissions for the benefit of public health. On the other hand, vehicular non-exhaust emissions from abrasion of auto parts (e.g., brake and tire) have been less investigated, and their impact on public health has not been clearly identified. The current dissertation aimed to provide insight on vehicular non-exhaust emissions, including factors affecting them, their spatial variation, health effects, and contributing sources. The dissertation is divided into the following

chapters: Chapter 1 discusses the background and significance of vehicular non-exhaust emissions, chapter 2 presents the literature review, chapters 3 and 4 summarize the original research, and chapter 5 presents the conclusions and future directions.

Chapter 2 summarizes the conducted literature review on vehicular non-exhaust emissions. The majority of the literature review was focused on the brake and tire wear particles, which are the most significant vehicular non-exhaust emission sources. Based on the literature review, brake and tire wear particles were both found to have a unimodal mass-based particle size distribution, while their reported particle number distributions were reported to be more variable with mode diameters in different size ranges. The reported brake and tire wear $PM_{2.5}$ (particulate matter with aerodynamic diameter $\leq$2.5 μm) and PM_{10} (particulate matter with aerodynamic diameter $\leq$ 10 μm) emission factors were found to be largely variable, indicating the need for updating the non-exhaust emission inventories in future. The inorganic elements associated with brake (Ba, Cr, Cu, Fe, Mn, Sb, Sn, Zr) and tire (Zn), as well as their organic content (e.g., Polycyclic aromatic hydrocarbons (PAHs) and phenolic compounds) have been reported to be associated with oxidative stress and various health effects. Further, the effects of transportation electrification on non-exhaust emissions and the potential contribution of electric vehicle (EV) Li-ion batteries to non-exhaust emissions were investigated.

In Chapter 3, we evaluated the impact of braking deceleration rate and vehicle's mass on the generated brake and tire wear particles during real-world driving cycles for three test vehicles with different masses (2800 – 5800 lbs.). Regardless of the braking intensity, the brake and tire wear $PM_{2.5}$ and PM_{10} concentrations of the heaviest vehicle were significantly higher than the lightest vehicle. Moreover, a positive association was observed between the braking deceleration rate and the peak values in brake and tire wear $PM_{2.5}$ and PM_{10} concentrations of all test vehicles,

underscoring the important role of driving style and braking intensity on the generated brake and tire wear particles.

In Chapter 4, we analyzed the spatial variation of ambient $PM_{2.5}$ and $PM_{2.5-10}$ (particulate matter with 2.5 < aerodynamic diameter $\leq$ 10 μm) elemental composition across the greater Los Angeles area. Traffic-related elements associated with brake wear (e.g., Ba, Cu, Mo, Sb, Zr), tire wear (Zn), and exhaust (Pd) particles were shown to be 3-5 times higher at the locations with high traffic intensity than the background sites. With respect to the previous findings in Los Angeles area, the $PM_{2.5}$ elemental concentrations have generally increased, despite the reduction in $PM_{2.5}$ concentration. The significant increase in Li concentration in this region could be linked to the EV Li-ion battery degradation, while the reduction in Ni and V concentrations was potentially due to the regulations on marine fuel composition. Using principal component analysis, four and three source factors were extracted for $PM_{2.5}$ and $PM_{2.5-10}$, respectively, whose relative contributions were further quantified based on multiple linear regression analysis. For $PM_{2.5}$, traffic was the dominant source with 27% contribution, while mineral dust had the largest contribution (45%) to $PM_{2.5-10}$.

The dissertation of Farzan Oroumiyeh is approved.

Michael Leo B. Jerrett

Suzanne E. Paulson

Beate R. Ritz

Yifang Zhu, Committee Chair

University of California, Los Angeles

2021

Table of contents

List of figures

List of tables

Acknowledgement

My PhD research has been a long journey, during which I was faced with different challenges. I was incredibly fortunate to be surrounded by kind and devoted instructors, colleagues, friends, and family members who made this journey smoother and more enjoyable for me.

First, I would like to express my deepest gratitude to my advisor Dr. Yifang Zhu for her unwavering support and priceless guidance throughout the course of my PhD. You have been instrumental to my academic growth, and the successful completion of my research at UCLA would not have been possible without your encouragement, advice, and nurturing.

I would like to extend my sincere thanks to my committee members, Dr. Michael Jerrett, Dr. Suzanne Paulson, and Dr. Beate Ritz, whose help for providing insightful suggestions and invaluable contributions to my research cannot be overestimated. I also wish to thank my mentors and collaborators, Dr. James Schauer, Dr. Martin Shafer, Dr. Scott Weichenthal, Mr. Paul Jacobs, and Mr. Mehran Avini for their gracious feedback.

I would like to express my sincere appreciation to my family and loved ones for their unconditional love and support in every step of my journey. You were my constant source of energy and inspiration, and I am eternally indebted to you. Words cannot express how grateful I am for having you in my life. I would also like to thank my amazing friends, Amir, Babak, Behnam, Chloe, and Julien for having my back through the past few years. I would also like to thank Behnaz and Nader for being my family away from home.

The research presented in this dissertation is supported by the generous funding from the California Air Resources Board (contract # 18MLD028 and 17RD012) and UCLA Center for Occupational and Environmental Health.

Vita

Education

2017 – present	Ph.D. candidate in Environmental Health Sciences, UCLA
2015 – 2017	M.S. in Environmental Engineering, University of Cincinnati
2009 – 2014	B.S. in Chemical Engineering, University of Tehran

Selected Publications

Oroumiyeh F, Jerrett M, Del Rosario I, Lipsitt J, Liu J, Paulson SE, Ritz B, Schauer JJ, Shafer MM, Shen J, Weichenthal S, Banerjee S, Zhu Y. Elemental composition of fine and coarse particles across the Greater Los Angeles area: spatial variation and contributing sources. *Environmental Pollution 2022.*

Oroumiyeh F, Zhu Y. Brake and tire particles measured from on-road vehicles: Effects of vehicle mass and braking intensity. *Atmospheric Environment: X 2021*.

Sadeghpour A, **Oroumiyeh F**, Zhu Y, Ko DD, Ji H, Bertozzi AL, Ju YS. Experimental study of a string-based counterflow wet electrostatic precipitator for collection of fine and ultrafine particles. *Journal of the Air & Waste Management Association 2021*.

Selected Presentations

Shen J, **Oroumiyeh F**, Taghvaee S, La C, Jerrett M, Weichenthal S, Liu J, Del Rosario I, Schauer JJ, Shafer MM, Ritz B, Zhu Y, Paulson SE. Associations between aerosol oxidative potential measured with the Dithiothreitol and Hydroxyl radical assays and metals, emission sources, and socioeconomic status in the Greater Los Angeles area. *(American Geophysical Union, AGU 2021*)

Liu J, Del Rosario I, Lipsitt J, **Oroumiyeh F**, Shen J, Paulson SE, Ritz B, Su J, Weichenthal S, Zhu Y, Jerrett M. Cokriging with a low-cost air sensor network to estimate spatial variation of brake and tire-wear related heavy metals and reactive oxygen species in Southern California, United States. (*American Association for Aerosol Research, AAAR 2021*)

Oroumiyeh F, Del Rosario I, Jerrett M, Lipsitt J, Liu J, Paulson S, Ritz B, Shen J, Y. Zhu. Spatial pattern of trace metal concentrations in southern California associated with brake and tire wear emissions. (*American Association for Aerosol Research, AAAR 2020*)

Liu J, I. Del Rosario I, Jerrett M, Lipsitt J, **Oroumiyeh F**, Paulson S, Ritz B, Shen J, Y. Zhu Statistical analysis and geospatial exposure model of air pollution derived from brake and tire wear. (*American Association for Aerosol Research, AAAR 2020*)

Oroumiyeh F, Zhu Y Estimation of brake and tire wear contribution to particulate pollution using on road measurements. (*American Association for Aerosol Research, AAAR 2019*)

Zhu Y, **Oroumiyeh F**, Wang Z. Long-term field evaluation and application of low-cost air monitoring sensors in a California community. (*American Geophysical Union, AGU 2019*)

Balachandran S, Corey J, **Oroumiyeh F**, Tadepally H, Spatiotemporal trends of fine and ultrafine particulate matter in Cincinnati, OH. (*American Association for Aerosol Research, AAAR 2017*)

Balachandran S, Corey J, Dillner A, **Oroumiyeh F**, Ren H, Tadepally H. Real-time measurements of $PM_{2.5}$, black carbon, sound and traffic dynamics near a major highway. (*American Association for Aerosol Research, AAAR 2016)*

Fellowships & Awards

Student Award, UCLA Center for Occupational and Environmental Health (2018)

Graduate Summer Research Mentorship (GSRM) award, UCLA (2018)

Graduate Student Fellowship, UCLA (2017 – 2022)

Graduate Student Scholarship, University of Cincinnati (2015 – 2016)

1. Background and introduction

Particulate matter (PM) exposure has been one of the significant contributors to mortality and disability-adjusted life years (DALYs). The estimation of the global burden of disease (GBD) attributed 4.2 and 4.6 million deaths to PM exposure in 2015 and 2017, respectively (Bu et al., 2021; Forouzanfar et al., 2015). A further analysis based on the global exposure mortality model (GEMM) has linked a higher number of 8.9 million premature deaths to PM exposure (Burnett et al., 2018). Moreover, both $PM_{2.5}$ (fine particles, aerodynamic diameter ≤ 2.5 μm) and PM_{10} (aerodynamic diameter <10 μm) have been associated with various health outcomes, including cardiovascular and respiratory diseases (Shiraiwa et al., 2017; Sicard et al., 2019). Due to the significant contribution of PM exposure to adverse health outcomes and mortality, a large body of research has focused on understanding PM emission sources.

In urban environments, $PM_{2.5}$ and PM_{10} can be generated by various emission sources, including industrial sources, biomass burning, and traffic (Fulvio Amato et al., 2016). Traffic is one of the major sources of PM in urban environments, with an average contribution of 25% to $PM_{2.5}$ and PM_{10} emissions in major cities (Karagulian et al., 2015). Traffic-related PM has been linked to various health outcomes, including cardiovascular diseases and cardiopulmonary health effects (Bai et al., 2018; Fan et al., 2009; X. Yang et al., 2018). Therefore, traffic-related PM can impose substantial costs on the governments due to their contribution to mortality and adverse health effects (Cakmak et al., 2019; Owusu and Sarkodie, 2020).

Due to the negative impact of traffic-related emissions on public health, the governments and environmental organizations have enforced various emission control policies to reduce traffic emissions through different strategies focused on vehicle usage (vehicle operation restriction, low

emission zone, air pollution charging fee), or vehicle and fuel technology (vehicle emission regulation, public transportation regulation, and alternative fuel technology) (Sanchez et al., 2020). In response to these efforts, the contribution of traffic emissions to $PM_{2.5}$ and PM_{10} has been continuously decreasing in the past few decades (Farrow and Oueslati, 2020). For instance, a meta-analysis of PM source apportionment results in 169 cities worldwide has shown that the contribution of traffic emissions to $PM_{2.5}$ has decreased by 28% since 2005 (Heydari et al., 2020). Heydari et al. (2020) reported that the largest reductions in traffic emission contributions were in Europe, North America, and Oceania due to the strict environmental legislation on vehicle exhaust emissions.

Despite the consistent legislative efforts that resulted in successful control of vehicles exhaust emissions on the global and local scale, non-exhaust emissions have not received enough attention in the past. Non-exhaust emissions are a major subcategory of traffic emissions that encompass vehicular abrasion particles (e.g., brake and tire wear particles) as well as resuspended road dust. With the continuous downward trend of exhaust emissions, non-exhaust emissions are expected to become the dominant source of traffic-related PM (Altuwayjiri et al., 2021; Farrow and Oueslati, 2020; Jeong et al., 2020). Non-exhaust emissions are predicted to become even more important with the fast-paced changes in the auto fleet composition worldwide (Rexeis and Hausberger, 2009). Since electric vehicles (EVs) with zero exhaust emissions are expected to form approximately 40% of the global auto fleet composition by 2035 (Rietmann et al., 2020), the relative importance of non-exhaust emissions, which can be generated by both EVs and internal combustion engine vehicles (ICEVs) is expected to increase.

Non-exhaust particles have been reported to have a considerable metallic content (Piscitello et al., 2021). Brake and tire wear particles, as well as resuspended dust are rich in many inorganic

elements, including Ba, Cr, Cu, Fe, Zn, and Zr that have been reported to contribute to adverse health outcomes by inducing oxidative stress (Gao et al., 2020b; Weichenthal et al., 2019). Moreover, the abundance of several toxic organic compounds (i.e., Polycyclic aromatic hydrocarbons (PAHs) and phenolic compounds) in brake and tire wear particles has been documented in more recent studies (Alves et al., 2021, 2020). Therefore, the impact of non-exhaust particles on public health can be serious and should be investigated.

Despite the ongoing research that emphasizes the role of non-exhaust particles in contributing to overall traffic emissions and PM health effects, there is a lack of relevant environmental policies for mitigating non-exhaust emissions. In the United States, while several states have launched a few initiatives for controlling the chemical composition of brake pads, brake and tire emissions have not been systematically regulated on the federal level (Grigoratos, 2018). The limited knowledge on non-exhaust particles and their specific health effects is presumably one of the reasons for this clear policy gap.

The current dissertation aimed to achieve a comprehensive understanding of vehicular non-exhaust emissions. First, we conducted a literature review on the vehicular non-exhaust emissions and summarized the information on the brake and tire wear particle size distribution, chemical composition, and emission factors. We also discussed the effect of auto electrification on non-exhaust emissions in the future and explored the potential health effects of non-exhaust particles based on their inorganic and organic chemical composition. Chapter 3 investigated the effect of driving behavior and vehicle mass on the brake and tire wear particles during braking, based on real-world braking conditions. In chapter 4, we studied the elemental composition of ambient $PM_{2.5}$ and $PM_{2.5-10}$ in the greater Los Angeles area, identified the elements associated with exhaust and non-exhaust emissions, and estimated the contribution of various sources to $PM_{2.5}$ and $PM_{2.5-}$

$_{10}$. We also compared the $PM_{2.5}$ and $PM_{2.5-10}$ elemental concentrations with previous studies in this area and identified the elements that substantially increased.

2. Vehicular non-exhaust emissions: a review

2.1. Introduction

Traffic is one of the most important sources of air pollution in urban environments. Traffic-related air pollution has been associated with a wide range of adverse health effects such as asthma and respiratory symptoms (Jerrett et al., 2008), cardiovascular diseases (Le Tertre et al., 2002), birth defects (Brauer et al., 2008), and increased mortality (Beelen et al., 2008). The large body of literature on health effects linked to traffic-related air pollution exposures has led to the implementation of various regulations and policies to mitigate vehicle exhaust emissions. On the other hand, the significance of non-exhaust emission sources has remained underestimated, and these emission sources have not been directly targeted by the previous emission control policies.

Non-exhaust emissions include both non-vehicular and vehicular sources. The vehicular non-exhaust emissions are generated from the abrasion of auto parts, mainly from brake and tire wear, while non-vehicular emission sources include mineral dust and resuspended road dust (Pant and Harrison, 2013). Non-exhaust particulate matter (PM) emissions are among the major anthropogenic sources of metals and trace elements (Grieshop et al., 2006; Lawrence et al., 2013). PM metals can increase PM toxicological effects by facilitating the generation of free radicals and contributing to oxidative stress (Bates et al., 2019; Gao et al., 2020b; Padoan and Amato, 2018; Rönkkö et al., 2018).

Source apportionment studies have shown that non-exhaust emissions contribute to both $PM_{2.5}$ (aerodynamic diameter < 2.5 μm) (Habre et al., 2020; Mousavi et al., 2018) and PM_{10} (aerodynamic diameter < 10 μm) (Fulvio Amato et al., 2016; Lawrence et al., 2013). Environmental organizations in Europe and the United States have reported a gradual increase in the relative contribution of non-exhaust emission sources to overall PM_{10} traffic emissions in

recent years, reporting a relative contribution in the range 75-95% in 2015 (Farrow and Oueslati, 2020). In addition, it has been shown that the contribution of non-exhaust emission sources to $PM_{2.5}$ in metropolitan areas has increased by 21%-27% per year between 2011 to 2016 (Jeong et al., 2020).

Despite the growing body of research that emphasizes the important role PM-metals in contributing to overall PM health effects, the knowledge on vehicular non-exhaust emission sources as one of the major contributors to PM-metals is limited. Moreover, with the rapid growth in the hybrid and electric vehicles (EVs) market, more emerging sources of non-exhaust emissions such as Li-ion batteries are introduced, whose contributions to non-exhaust PM emissions have not been studied in the past. The knowledge gap in this area prevents an organized effort for regulating vehicular non-exhaust emissions in the future. The goal of this work is to provide insight into the vehicular non-exhaust emission sources and identify the most influential factors affecting them by reviewing the current state of knowledge in this area to facilitate future regulatory efforts for mitigating these emerging traffic sources.

2.2. Research approaches for studying vehicular non-exhaust emissions

Based on the literature review, it has been found that vehicular non-exhaust emissions have been studied through various study designs, including ambient measurements, laboratory simulation, and on-road sampling. Each of these study approaches can investigate different aspects of non-exhaust emissions. In ambient measurement studies, the overall contribution of vehicular non-exhaust emission sources, including brake and tire wear particles, to traffic emissions are quantified by source apportionment techniques, including receptor modeling. However, studies based on ambient measurements and source apportionment cannot address the effects of individual vehicle properties on brake and tire wear particles. Therefore, laboratory studies that can better

control experimental variables are necessary for understanding the role of different variables on brake and tire wear emissions.

Laboratory studies can simulate the behavior of brake and tire wear particles while parts are detached from the vehicle and studied separately. The brake wear particles have been studied using different brake dynamometers (Alemani et al., 2018; Farwick zum Hagen et al., 2019a; Garg et al., 2000; Hagino et al., 2015; Kukutschová et al., 2011; Sanders et al., 2003) and pin-on-disc tribometers (Nosko and Olofsson, 2017; Wahlström, 2015; Wahlström et al., 2010b). In addition, tire wear particles have been studied in laboratory settings using road and tire simulators (Dahl et al., 2006; Gustafsson and Eriksson, 2015; Kim and Lee, 2018).

Laboratory studies on the brake and tire wear particles have also been performed while driving vehicles under different emission test cycles using chassis dynamometers (Kwak et al., 2013; Mathissen et al., 2019). While studies based on sampling on chassis dynamometers are limited, these studies can provide valuable information about the effect of driving conditions on brake and tire wear particles and their chemical composition. On-road sampling studies are required for understanding the behavior of brake and tire wear particles under more realistic driving conditions, which cannot be simulated in the laboratory studies (Beji et al., 2020; Farwick zum Hagen et al., 2019b; Kwak et al., 2013; Mathissen et al., 2019, 2018, 2012; Oroumiyeh and Zhu, 2021). The on-road studies have investigated the effects of various factors, including brake temperature (Farwick zum Hagen et al., 2019b; Mathissen et al., 2018), vehicle velocity (Beji et al., 2020; Mathissen et al., 2012), road condition (Mathissen et al., 2012), driving condition, and lateral acceleration (Kwak et al., 2013), as well as vehicle mass and braking intensity (Oroumiyeh and Zhu, 2021) on the generated brake and tire wear particles. In the following sections, vehicular non-exhaust emission sources and their physical and chemical characteristics are discussed in detail.

2.3. Characterization of vehicular non-exhaust emission sources

2.3.1. Brake wear emissions

Light-duty vehicle (LDV) brake systems are categorized into two general groups of drum and disc brakes. The disc brake technology has been introduced more recently compared to drum brake system that has been used in the auto industry for a longer period. While some of the LDVs are still equipped with rear-wheel drum brakes, front-wheel brakes, responsible for more than 70% of total vehicle braking force, are increasingly equipped with disc brakes due to their superior performance (Grigoratos and Martini, 2015).

Disc brakes generally consist of a rotor, a brake caliper assembly, and brake pads. During a braking event, the applied hydraulic force generated by brake pedals moves the piston inside the caliper assembly and presses the brake pads to the rotor, which is connected to the wheel hub. As a result of this procedure, the required friction force for stopping the vehicle is supplied. The mechanical interaction between the brake pad and brake rotor can produce brake wear particles in different sizes (Wahlström et al., 2009).

While cast iron has been reported as the most common brake rotor material, steel, ceramic, carbon-carbon, and Al, Si, and Ti have also been used as the base material for brake rotors (Kukutschová and Filip, 2018; Qu et al., 2009; Sadagopan et al., 2018). Other elements, including Mn, P, and minor amounts of other alloying elements, including Cr, have been used to improve the wear properties of brake rotors (Filip, 2013). In contrast, the chemical composition of brake pads is largely variable, and it has improved over time. The brake lining friction components, their function, and their material are summarized in Table 2.1 (Eriksson et al., 2002; Grigoratos and Martini, 2015; Thorpe and Harrison, 2008):

Table 2.1: Brake lining components and materials

Brake lining component	Function	Material
Binders	Adhering the brake lining material together	Mostly phenolic resins (high resistance against temperature and strong wear properties)
Structural fibers and particulates	mechanical strength	Metallic, mineral, carbon, and ceramic material
Fillers	Minimizing production costs; improving thermal properties	Inert or active materials, including minerals (i.e., stone powders, mica, silicates, glass, and vermiculite) and antimony sulfate, chromium oxides, and barium sulfate
Frictional additives	Improving frictional properties while reducing the wearability	Include lubricant (Graphite, organic materials such as nut powders, as well as metal sulfides and rubber) and abrasives (metal oxides and minerals such as silica and zircon)

While the brake lining materials have been generally classified into four classes of non-asbestos organic (NAO), low-metallic (10-30% metals), semi-metallic (metals <65%) brakes in older brake lining material classifications (Thorpe and Harrison, 2008), newer brake lining materials including ceramic brake pads were developed more recently, which should also be considered as a major type of brake lining materials (Kumar and Kumaran, 2019).

Ceramic brake pads have been developed more recently compared to other brake lining materials. Despite their substantial price, ceramic brakes have been increasingly used in passenger cars with the expansion of ceramic technology in the auto industry over the past few years (Li et al., 2020). The high frictional properties and reliable thermal resistance at a wide range of operating temperatures up to 1000 ºC are the advantages of ceramic brake pads (Kumar and Kumaran, 2019; Li et al., 2021).

2.3.1.1. Chemical composition

The chemical compositions of brake components, including brake pads, discs, and rotors, have been changing by brake manufacturers in the past few decades to improve braking capacity while providing optimized frictional, mechanical, and wear properties. The elemental compositions of brake components have been analyzed through multiple laboratory measurement studies (Chandra Verma et al., 2015; Hagino et al., 2016; Hulskotte et al., 2014; Iijima et al., 2007; Kukutschová et al., 2011; Liati et al., 2019; Schauer et al., 2006; Verma et al., 2016; Von Uexküll et al., 2005; Wahlström et al., 2010a). For instance, the elemental compositions of conventional low-metallic and semi-metallic European brake pads and brake rotors have been investigated by X-ray fluorescence (XRF) spectroscopy, and it has been found that Cu and Fe, as the primary brake elements, as well as a few other elements, including Sb, Sn, and Zn contribute to up to 90% of the weight of the brake elements (Hulskotte et al., 2014). Elemental speciation of Low-metallic and NAO brakes has been reported to be dominated by oxygen and metals such as Ba, Cu, Fe, Mn, Ti, and Zn (Wahlström et al., 2010a), while other elements, including Al, Ca, Cd, Cr, K, Mo, Ni, Pb, Si, and Zr have also been observed in different brake pads (Figi et al., 2010; Hjortenkrans et al., 2008; Kukutschová et al., 2011; Sethupathi et al., 2021; Vontorová et al., 2017). While previously rare-earth elements (REEs) were reported to be predominantly associated with mineral dust (Fulvio Amato et al., 2016; Pakbin et al., 2011), a group of RREs, including Gd, Ho, Lu, Pr, and Tb has been recently reported in brake pads (Mleczek et al., 2021). On the other hand, Fe has been reported to be the most dominant element in the brake discs, while a few other elements, including Al, Cd, Cu, Mn, Mo, Ni, P, Sb, Sn, Ti, and Zn had lower mass concentrations in brake discs (Hulskotte et al., 2014).

While the majority of the previous studies have focused on the elemental composition of brake components, fewer studies have investigated the organic constituents of brake pads (Gadd and Kennedy, 2000; Hagino et al., 2016; Plachá et al., 2015; Rogge et al., 1993; Zhao et al., 2015). The total carbonaceous fraction of brake wear PM_{10} has been reported to be largely variable (5%-76%) depending on the brake pad material, braking velocity, and brake temperature (Alves et al., 2021; Hussain et al., 2014; Malachova et al., 2016). More recently, approximately 150 organic compounds have been identified in brake wear PM_{10}, including n-alkanes, n-alkenes, n-alkanols, glycerol compounds, phenolic compounds, and polycyclic aromatic hydrocarbons (PAHs) (Alves et al., 2021). The concentrations of organic compounds were shown to be higher during light braking than heavy braking events, indicating the potential degradation of organic compounds during heavy braking conditions (e.g., high temperature and pressure), which shows the effect of driving style on the chemical composition of the generated brake wear particles (Alves et al., 2021; Menapace et al., 2019).

Various elements have been used as brake wear tracers for source apportionment of fine and coarse particles. Ba, Cu, Sb, and Sn have been most frequently used as brake wear tracers (Almeida et al., 2020; Gietl et al., 2010; Hagino et al., 2016; Iijima et al., 2008; Jeong et al., 2020; Lawrence et al., 2013; Oroumiyeh et al., 2022; Schauer et al., 2006; Sternbeck et al., 2002). In addition, a few other elements, including As, Cr, Fe, Mn, Mo, Sr, Ti, Zn, and Zr have been recommended as brake wear tracers in some of the previous studies (Bukowiecki et al., 2009; Duong and Lee, 2011; Jeong et al., 2019; Wang et al., 2021). However, many of the elements from the second group have been associated with other emission sources. For instance, Zn has been associated with tire wear emissions and industrial emissions (Jeong et al., 2019), and Fe, Ti, Mn, and Sr have been associated with various sources, including road dust and industrial emissions (Cesari et al., 2016; Pakbin et

al., 2011; Querol et al., 2007). Since Ba, Cu, Sb, and Sn are more specific to brake wear emissions, they are expected to be the most suitable brake wear tracers.

Due to the potential contribution of brake wear emissions to adverse health effects, brake wear materials have been subject to various environmental regulations in different parts of the world, which have been previously discussed in detail (Grigoratos, 2018). In Europe, Pb, Cd, Cr, and Hg have been eliminated from brakes since 2003 under the End of Life Vehicle Directive. In the United States, brake wear emissions have not been directly regulated through federal legislation to this date. However, some of the states, including California, New York, Rhode Island, and Washington have enforced various legislations to gradually reduce toxic species, including Cu from auto brakes by 2025, while monitoring Ni, Sb, and Zn for the potential further regulations (Grigoratos, 2018). These states have also specified maximum concentration limits of 0.1% weight for Cr, Pb, Hg, and 0.01% weight for Cd in the manufactured brake pads. With the continuous changes in brake wear chemical composition by the brake manufacturers, as well as the enforcement of new regulations on brake materials, the chemical composition of brake wear particles is expected to alter in the next decade. Therefore, continuous analysis of the chemical speciation of the brake components is crucial for understanding the physiochemical characteristics of brake wear particles and their associated health effects.

2.3.1.2. Size distributions

The brake wear particle size distribution has been investigated using various sampling approaches, as discussed in section 2.2. As shown in Figure 2.1, while a mass-based particle size distribution with mode diameter in fine and ultrafine size range has been reported in a previous brake dynamometer study (Alemani et al., 2016), the majority of the previous studies have reported a unimodal brake wear mass-based particle size distribution with mode diameters in the range of 1-

10 μm using various sampling approaches (Hagino et al., 2016; Iijima et al., 2008, 2007; Kukutschová et al., 2011; Oroumiyeh and Zhu, 2021; Sanders et al., 2003; Von Uexküll et al., 2005).

The reported brake wear particle number distributions, however, are more variable than brake wear mass-based particle size distributions (Figure 2.1). As shown in Figure 2.1, the mode diameter of brake wear particle number distributions has been reported from nano-scale to coarse size range. While a few studies observed a unimodal brake wear particle number distribution, the distributions were reported to be bimodal and multimodal in the majority of the previous studies.

The brake wear particle number distribution has been shown to be affected by a few factors, including brake lining material (Park et al., 2021; Sanders et al., 2003) and brake pad maintenance history (Farwick zum Hagen et al., 2019b). As shown in Figure 2.1, the measurement instruments and sampling approaches should also be considered while comparing the reported brake wear particle size distributions. For instance, Iijima et al., (2007) and Iijima et al., (2008) measured brake wear particles using Aerodynamic Particle Sizers (APS 3321, TSI Inc., Shoreview, MN) and reported a unimodal brake wear particle number distribution, without reporting a second mode in the ultrafine size range (diameter <0.1 μm), due to the limited detection size range of APS (0.5-20 μm). On the other hand, many studies reported multimodal brake wear particle size distributions with mode diameters in the fine and ultrafine size ranges (Alemani et al., 2016; Farwick zum Hagen et al., 2019b, 2019a; Nosko and Olofsson, 2017; Park et al., 2021).

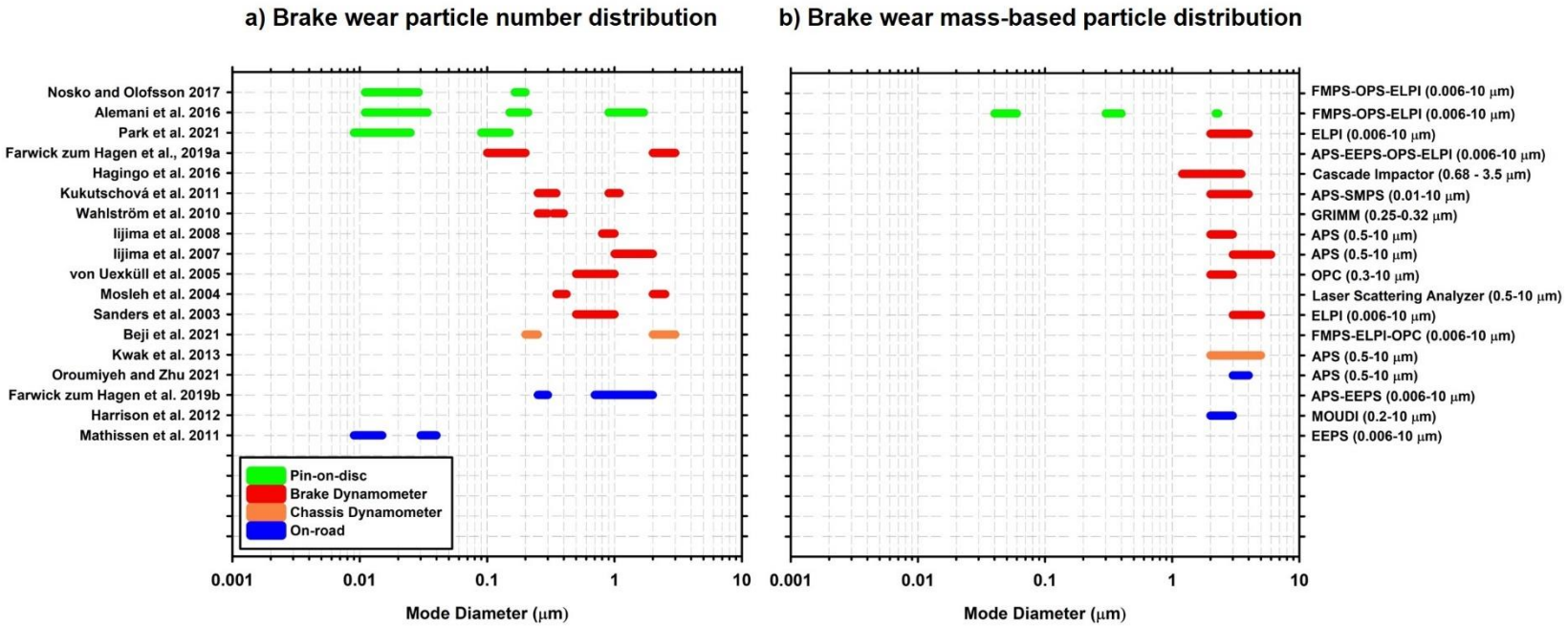

Figure 2.1: Overview of the reported mode diameters of size distributions in the previous studies based on different measurement methods for (a) brake wear particle number distribution and (b) brake wear mass-based particle size distribution. The reported numbers in the parentheses show the detection size range of the measurement instruments: Engine Exhaust Particle Sizer (EEPS), Aerodynamic Particle Sizer (APS), Electrical Low Pressure Impactor (ELPI), Fast Mobility Particle Sizer (FMPS), Optical Particle Counter (OPC), Laser Scattering Analyzer, Optical Particle Sizer (OPS), Scanning Mobility Particle Sizer (SMPS)

Previous on-road and laboratory studies have shown that beyond a specific brake temperature (140 °C <T_{crit} < 240 °C), ultrafine brake wear particles were generated, while at lower temperatures, ultrafine particles were not observed (Alemani et al., 2018, 2016; Farwick zum Hagen et al., 2019b, 2019a; Garg et al., 2000; Niemann et al., 2020; Nosko and Olofsson, 2017). T_{crit} has been shown to increase during multiple runs of laboratory analysis of brake wear particles, presumably due to the differences in the volatilization onset temperatures of the brake wear organic material (Farwick zum Hagen et al., 2019a). For instance, T_{crit} for brake pads with organic binder content (i.e., phenolic resin) has been shown to be 180 °C, while higher T_{crit} of 240 °C has been reported for brake pads with inorganic binder content, underscoring the effect of organic content of brakes on reducing T_{crit} (Alemani et al., 2018; Niemann et al., 2020).

2.3.1.3.Emission factors

Brake wear PM emission factors (EFs) have been estimated based on different sampling approaches introduced in section 2.2. The brake wear $PM_{2.5}$ EFs have been reported to be in the range of 0.5 - 5.5 mg km^{-1} Veh^{-1} in previous dynamometer studies (Garg et al., 2000; Hagino et al., 2016; Iijima et al., 2008), while PM_{10} EFs have been estimated to be 2.9 – 8.1 mg km^{-1} Veh^{-1} (Farwick zum Hagen et al., 2019a; Garg et al., 2000; Hagino et al., 2016; Iijima et al., 2008; Sanders et al., 2003). While previous source apportionment studies reported PM_{10} EFs of 8.0 – 80.0 mg km^{-1} Veh^{-1} (Abu-Allaban et al., 2003; Bukowiecki et al., 2010, 2009; Luhana et al., 2004), a lower PM_{10} EFs of 1.4 – 2.1 mg km^{-1} Veh^{-1} have been reported in an on-road study based on Los Angeles City Traffic cycle (Farwick zum Hagen et al., 2019b). The reported brake wear PM EFs are largely variable and comparing them is challenging due to the differences in sampling approaches and experimental variables. Therefore, the updated emission inventories, which take

into account multiple factors, including braking activity and vehicle miles traveled, are required for providing a more holistic insight into the emission factors of brake wear particles.

The environmental organizations and governmental agencies have provided various methods for estimating the brake wear $PM_{2.5}$ and PM_{10} EFs. United Kingdom National Atmospheric Emissions Inventory (NAEI) reported the average brake wear $PM_{2.5}$ and PM_{10} EFs to be 3 and 7 mg km^{-1} Veh^{-1}, respectively (NAEI, 2018). Moreover, the United States Environmental Protection Agency (USEPA), under Motor Vehicle Emission Simulator (MOVES) program, provided the brake wear emission factors for different vehicle classes (Figure 2.2) (USEPA, 2020). Various factors, including vehicle braking activity, average deceleration rate, and vehicle weight have been included for estimating the brake wear emission factors. According to MOVES emission inventory, brake wear $PM_{2.5}$ EFs are in the range of 1.0 - 9.6 mg km^{-1} Veh^{-1}, while brake wear PM_{10} EFs are 7.8 – 77.0 mg km^{-1} Veh^{-1}. As shown in Figure 2.2, intercity bus and refuse trucks have the highest brake wear $PM_{2.5}$ and PM_{10} emission factors, despite their lower weights compared to vehicles in higher weight classes (e.g., combination trucks). This clearly shows the effect of vehicle braking activity as both refuse trucks and intercity buses have more frequent braking events compared to the vehicles in other weight classes.

European Environment Agency (EEA) has provided a more detailed method for calculating brake wear $PM_{2.5}$ and PM_{10} EFs at different vehicle speeds as previously detailed (European Environment Agency, 2019). In summary, brake wear PM EFs can be estimated based on EF values of brake wear total suspended particles (TSP) using Eqs (2.1) and (2.2) (European Environment Agency, 2019):

$$EF_{PM_{2.5}} = 0.39 * EF_{TSP,B} * S_B(V) \quad (2.1)$$

$$EF_{PM_{10}} = 0.98 * EF_{TSP,B} * S_B(V) \quad (2.2)$$

Where $EF_{TSP,B}$ is the EF of brake wear TSP, and $S_B\ (V)$ is the correction factor for average vehicle velocity and is calculated from Eq (2.3). $S_B\ (V)$ is equal to 1.67 and 0.185 for vehicle speeds below 40 km/h and above 95 km/h, respectively. For vehicle speeds in the range of 40-95 km/h, SB (V) is calculated using a linear equation:

$$S_B(V) = -0.027 * V + 2.75 \quad (2.3)$$

Table 2.2 presents $EF_{TSP,B}$ for LDVs for use in Eqs (2.1) and (2.2):

Table 2.2. Brake wear TSP emission factors for different vehicle classes (European Environment Agency, 2019)

Vehicle category	Brake wear TSP emission factor (µg/km)	Range
Two-wheel vehicles	3.7	2.2 - 5.0
Passenger cars	7.5	4.4 - 10.0
Light-duty trucks	11.7	8.8 - 14.5

$EF_{TSP,B}$ for heavy-duty vehicles (HDVs) can be calculated using adjusted values from Eq (2.4):

$$EF_{TSP,B,HDV} = 3.13 * LCF_B * EF_{TSP,B,PC} \quad (2.4)$$

Where $EF_{TSP,B,HDV}$ and $EF_{TSP,B,PC}$ are TSP EFs for HDV and passenger car, respectively, and LCF_B is the load correction factor for brake wear particles, and it is calculated using Eq (2.5):

$$LCF_B = 1 + 0.79 * LF \quad (1.5)$$

Where LF is the loading factor between zero (empty truck) to one (fully loaded truck).

As shown in Figure 2.2, for a similar vehicle category, higher brake wear $PM_{2.5}$ EFs have been reported by EEA than USEPA, while EEA PM_{10} EFs were generally lower. For instance, the reported brake wear $PM_{2.5}$ EFs of passenger vehicles by EEA are 1.9 times higher than USEPA brake wear EFs for passenger cars. On the other hand, USEPA brake wear PM_{10} EFs are 1.6 times higher than EEA for passenger cars. Similar differences are observed between the reported brake wear EFs for light-duty trucks (light commercial trucks in EEA), and different classes of heavy-duty trucks by the two models. This is likely due to the fact that the reported brake wear EFs in the MOVES model are estimated based on a limited number of older studies of brake wear emissions, assuming brake wear PM_{10} EFs to be approximately 8.0 times higher than $PM_{2.5}$ (Sanders et al., 2003; USEPA, 2020). Since more recent studies have shown that a larger fraction of brake wear particles is confined in fine PM, an updated MOVES model based on more recent findings in the literature is crucial for improving the accuracy of vehicle brake wear PM emission inventory in the US.

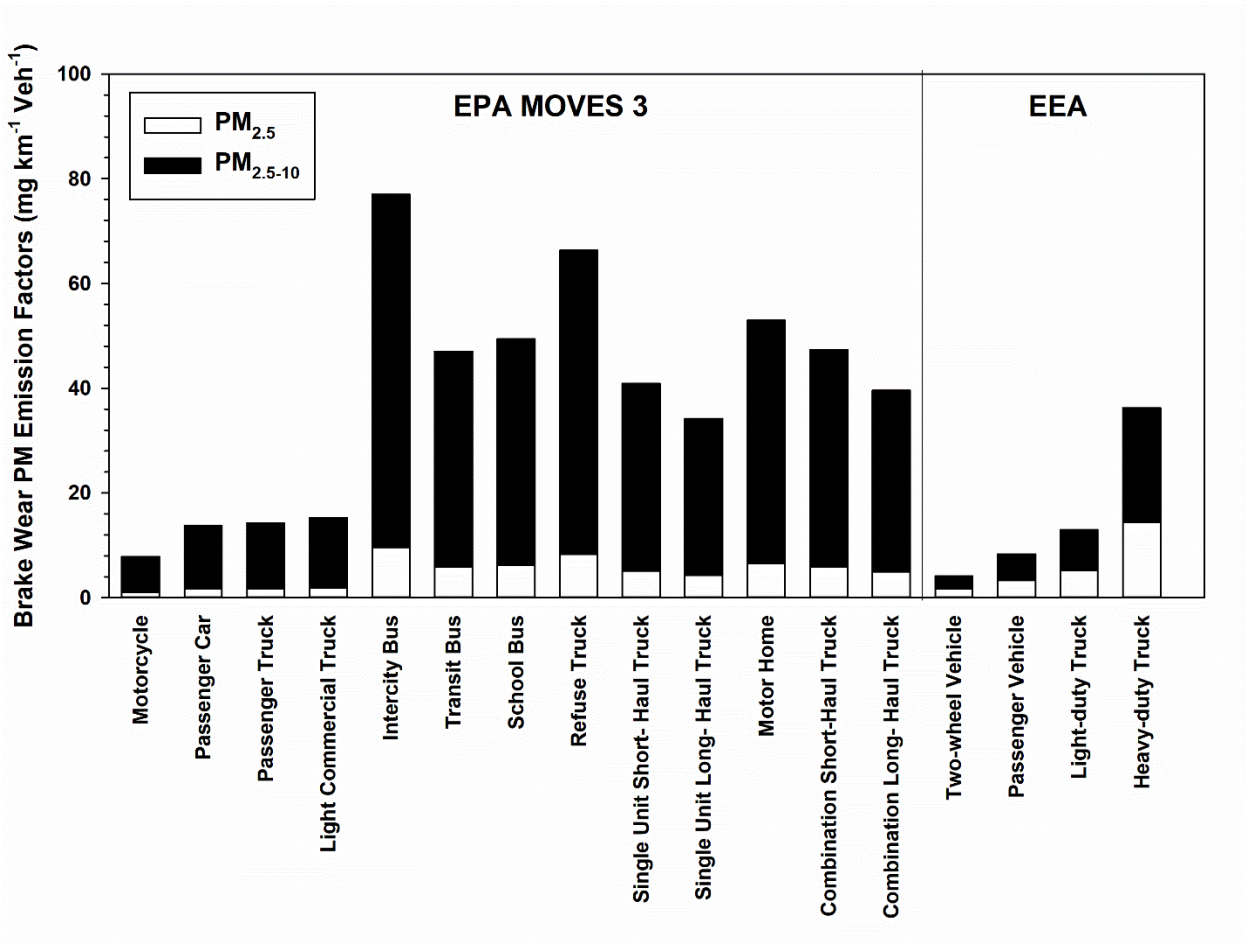

Figure 2.2. Average brake wear PM emission factors based on the estimated values by United States Environmental Protection Agency (USEPA) (vehicles sorted by weight for calendar year 2017) and European Environment Agency (EEA). EEA brake wear PM EFs are estimated for vehicle speed of 60 km/h. EEA heavy-duty truck brake wear PM EFs were estimated for a half full truck with 4 axles.

2.3.2. Tire wear emissions

In real-life driving conditions, tire wear particles are generated through the contact and friction between the tire and pavement material during different modes of driving as a result of mechanical and thermomechanical processes. Tire treads are generally made of a mixture of rubbers, fillers, vulcanizing agents, anti-degradants, and plasticizers (Grigoratos and Martini, 2014). The global annual emissions of tire treads have been estimated to be approximately 5.9 million tons year^{-1},

with population-normalized values in the range of 0.2 to 5.5 kg year^{-1} capita^{-1} (Baensch-Baltruschat et al., 2020). Since the physical and chemical characteristics of generated tire wear particles are different from the original polymeric tread particles due to heat, pressure, and mixing with road dust, tire and road wear particles (TRWP) is a more representative term for referring to the wear products of tire and road interaction (Baensch-Baltruschat et al., 2020; Beji et al., 2020).

TRWPs can become airborne or deposit on the road and further be transported to aquatic environments, based on their physical and chemical properties and local geographical features (Gill et al., 2017; Jan Kole et al., 2017; Panko et al., 2018; Wagner et al., 2018). A recent study in Germany has estimated that 66-76% of total tire wear emissions deposit on near-roadway soils, while 12-20% of the emissions are directed to surface waters and aquatic environments (Baensch-Baltruschat et al., 2021). On the other hand, a smaller fraction of tire wear emissions has been previously reported to be airborne. While the average airborne fraction of TRWPs has been reported to be less than 2% (Panko et al., 2013; I. Park et al., 2018), some studies have documented a higher fraction of airborne TRWPs in the range of 5-7% (Gualtieri et al., 2008; Wik and Dave, 2009).

2.3.2.1. Chemical composition

A limited number of studies have investigated the chemical composition of tire tread particles. The distinction between TRWPs and tread particles should be considered when comparing the results of the previous studies. For instance, it has been shown that tread particles have a higher polymer content than TRWPs, while the concentrations of minerals have been shown to be higher in TRWPs, indicating the effect of road dust on TRWPs (Kreider et al., 2010; Piscitello et al., 2021). Road simulator results from testing various studded and non-studded tires on different road materials associated S and Zn to tread particles, while the presence of Al and Si was linked to

pavement wear despite showing a high contribution to TRWPs (Alves et al., 2020; Beji et al., 2020; Gustafsson et al., 2008). Alves et al. (2020) reported the abundance of other elements, including Ca, Fe, K, Mg, Na, Ti in TRWPs and tire treads to be in the range of 1400 – 37700 and 48 – 4300 μg g^{-1}, respectively. On the other hand, a few other elements, including rare-earth elements As, Se, Sn, Cd, and Sb were only observed in TRWPs, indicating their association with the road dust rather than tire tread (Alves et al., 2020).

Kreider et al. (2010) also showed that while TRWPs have higher Si and Al content due to the mixing with road dust compared to tread particles, the concentration of Zn is higher in tread particles, presumably due to the wide usage in tire production in the form of ZnO (Milani et al., 2004). The association of Zn with tread particles was confirmed during sampling on a chassis dynamometer (Kwak et al., 2013). Zn has been frequently used as a tracer for TRWPs for source apportionment in many of the previous studies of ambient PM measurement (Harrison et al., 2012; Lawrence et al., 2013; Lin et al., 2015; Querol et al., 2008; Srimuruganandam and Shiva Nagendra, 2012; Thorpe and Harrison, 2008; Yu and Park, 2021). However, since Zn has been linked to sources, including brake wear emissions (Bukowiecki et al., 2009; Schauer et al., 2006), lubrication oil (Sternbeck et al., 2002; Wang et al., 2021), and industrial emissions (Jeong et al., 2019), it cannot be used an exclusive tracer for tire wear emissions.

Tires are manufactured from various organic materials. It has been reported that carbonaceous species constitute 65-72% of total tire tread material (Aatmeeyata and Sharma, 2010a; Park et al., 2017). EC and OC have been shown to account for 18-40% and 54% of tire material weight, respectively (Jan Kole et al., 2017; Park et al., 2017). A recent study has found approximately 300 organic species in conventional tire treads and TRWPs, including phthalates, PAHs, n-alkanols, phenolic compounds, levoglucosan, steranes, and various aliphatic species (Alves et al., 2020).

Alves et al. (2020) reported n-undecane as the dominant aliphatic compound, while naphthalene was shown to have the highest concentration among the 22 extracted PAH compounds. On the other hand, Pyrene and fluoranthene have been shown to be the dominant PAHs in TRWPs in other studies (Boonyatumanond et al., 2007; Depaolini et al., 2017; Kreider et al., 2010; Llompart et al., 2013; Markiewicz et al., 2017; Sadiktsis et al., 2012). While the abundance of PAHs in tire tread has been documented, the concentrations of PAHs have been found to be substantially higher in road wear particles than tread particles (Alves et al., 2020; Kreider et al., 2010). Therefore, the concentration of PAHs is expected to be higher in TRWPs than tire tread particles.

Due to the documented toxicity of PAHs (Bortey-Sam et al., 2017; Marris et al., 2020; Ren et al., 2011; Vardoulakis et al., 2020), European Union banned the usage of highly aromatic (HA) oils in tire manufacturing for tires produced after 2010 under the REACH legislation, which has led to a gradual decrease in PAH content of tires (Diekmann et al., 2019). In fact, a statistically significant reduction in the PAH content of European-made tires has been observed between the tires produced before and after 2010 (Depaolini et al., 2017). On the other hand, the PAH content of tires manufactured outside Europe did not show a significant reduction during the same period (Depaolini et al., 2017). An analysis of PAH emission factors from traffic sources has demonstrated that tires are still one of the leading non-exhaust emission source of PAHs in Europe (Markiewicz et al., 2017). Markiewicz et al. (2017) estimated the range of emission factors for 16 USEPA priority PAHs from traffic sources to be 900-3900 $\mu g\ km^{-1}\ Veh^{-1}$ in Sweden. While vehicle exhaust (24-2300 $\mu g\ km^{-1}\ Veh^{-1}$) has been reported to be the dominant traffic-related PAH source, tire wear (1.5-630 $\mu g\ km^{-1}\ Veh^{-1}$) was the most significant non-exhaust emission source of PAHs (Markiewicz et al., 2017). The abundance of PAHs in tire particles have been reported to be largely variable since tire particles can be impacted by various factors. For instance, the collected tire wear

samples during studded tire season showed a higher correlation (r=0.96) with PAH than the samples collected during non-studded tire season (r=0.88), due to the differences in tire material and temperature (Järlskog et al., 2021).

2.3.2.2. Size distributions

The reported tire wear particle sizes in the previous studies show a considerable variation from 1 nm to 1000 μm (Klöckner et al., 2021; Park et al., 2017). While less than 10% of tire wear particles have been reported to be airborne, many studies have focused on the airborne fraction of tire wear particles due to its potential contribution to adverse health effects. Figure 2.3 shows the previously reported mode diameters of tire particle size distributions in the airborne size range (Aatmeeyata et al., 2009; Alves et al., 2020; Beji et al., 2020; Dahl et al., 2006; Dall'Osto et al., 2014; Foitzik et al., 2018; Grigoratos et al., 2018; Gustafsson et al., 2008; Hussein et al., 2008; Kim and Lee, 2018; Mathissen et al., 2011; Olofsson et al., 2018; Oroumiyeh and Zhu, 2021; Panko et al., 2009; Sjödin et al., 2010). The majority of these studies have reported unimodal mass-based particle size distributions with mode diameters in the range of 1-10 μm for tread wear particles and TRWPs (Alves et al., 2020; Grigoratos et al., 2018; Hussein et al., 2008; Kim and Lee, 2018; Kupiainen et al., 2005; Kwak et al., 2013; I. Park et al., 2018; Sjödin et al., 2010), while bimodal mass-based particle size distributions have also been reported with a second mode in the fine and ultrafine size ranges (Figure 2.3) (Beji et al., 2020; Olofsson et al., 2018).

As shown in Figure 2.3, the reported tire wear particle number distributions are largely variable. The reported tire wear particle size distributions have been unimodal, bimodal, and multimodal, with mode diameters in the range of 0.01 to 5 μm. The majority of the studies have observed at least one peak in the ultrafine size range. It has been reported that the generation of ultrafine tire wear particles is enhanced at higher driving velocities and larger slip angles, as well as longitudinal

acceleration and deceleration (Foitzik et al., 2018). Other studies have reported the impact of tire condition, including tire type, tire studding, tire tread rating, tire travel distance, and tire temperature, as well as the vehicle mass and deceleration rate on the generated tire particles (Alves et al., 2020; Grigoratos et al., 2018; Oroumiyeh and Zhu, 2021; Park et al., 2017). For instance, Park et al. (2017) reported that at tire surface temperatures of 160 ºC and above, the generation of nanoparticles is initiated, and it is gradually enhanced at higher temperatures up to 400 ºC.

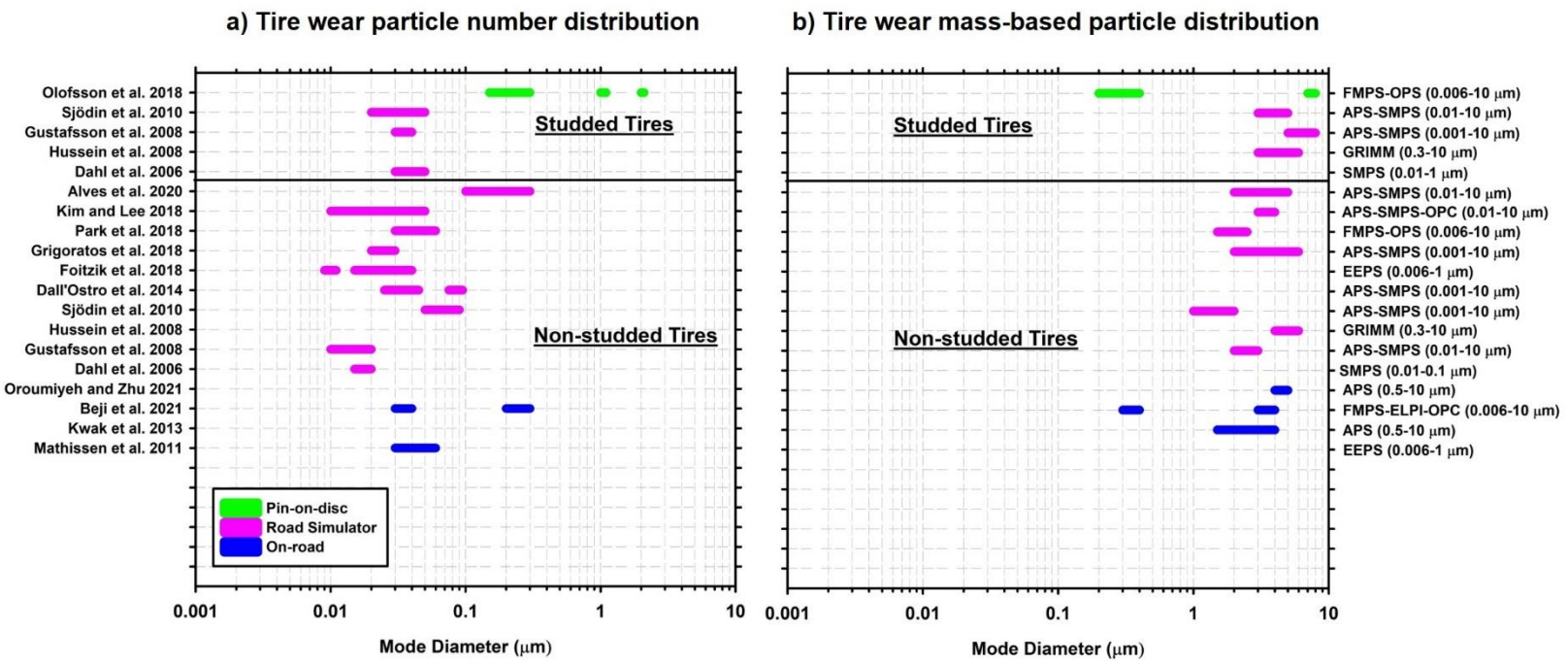

Figure 2.3. Overview of the reported mode diameters of size distributions in the previous studies based on different measurement methods for (a) tire wear particle number distribution and (b) tire wear mass-based particle size distribution. The reported numbers in the parentheses show the detection size range of the measurement instruments: Engine Exhaust Particle Sizer (EEPS), Aerodynamic Particle Sizer (APS), Electrical Low Pressure Impactor (ELPI), Fast Mobility Particle Sizer (FMPS), Optical Particle Counter (OPC), Laser Scattering Analyzer, Optical Particle Sizer (OPS), Scanning Mobility Particle Sizer (SMPS)

As mentioned in section 2.3.2, only a limited fraction of tread particles has been reported to be airborne. Moreover, tire wear particles are one of the major sources of microplastics in the environment with a wide range of particle diameters (1-1000 μm) (Hartmann et al., 2019; Sommer et al., 2018). A significant correlation ($P < 0.05$) has been observed between the microplastic concentration in urban areas and traffic density (Kitahara and Nakata, 2020). In fact, tire wear particles have been reported to be the dominant source of microplastics in the environment contributing to 50-60% of annual microplastics emissions (Boucher and Friot, 2017; Hüffer et al., 2019; Lassen et al., 2015). Therefore, many studies have investigated the tire particle size distribution in the super-coarse (aerodynamic diameter ≥ 10 μm) size range to investigate the fate and transport of tire wear particles in the soil, vegetation, and aquatic environments.

Both tread wear particles and TRWPs have been reported in a wide size range up to 1000 μm (Klöckner et al., 2021). For instance, the size distribution of TRWPs has been reported to be unimodal with a mode diameter of 25 μm (Klöckner et al., 2021; Kovochich et al., 2021). On the other hand, Kreider et al. (2010) reported a bimodal TRWP size distribution with mode diameter of 5 and 25 μm while observing a unimodal distribution for tread wear particles with mode diameter of 25 μm. A few factors, including vehicle load, payment roughness, and temperature been reported to affect the tire wear particle size distribution in the super-coarse size range (Grigoratos et al., 2018; Gustafsson et al., 2008; Järlskog et al., 2021; Sjödin et al., 2010). For instance, the wear mechanism during driving on a surface with higher roughness is dominated by mechanical abrasion, which leads to the generation of larger particles, while lower particles are generated due to fatigue wear at lower roughness conditions (Chang et al., 2020).

2.3.2.3. Emission factors

Previous studies have estimated tire wear $PM_{2.5}$ and PM_{10} EFs using various sampling approaches discussed in section 2.2. Tire wear $PM_{2.5}$ EFs have been reported to be in the range 0.3 – 11 mg km^{-1} Veh^{-1} (Aatmeeyata et al., 2009; Kupiainen et al., 2005; Luhana et al., 2004; Panko et al., 2013). While road simulator studies have observed a relatively wide range of 1.9-11 mg km^{-1} Veh^{-1} for tire wear PM_{10} EFs (Aatmeeyata et al., 2009; Alves et al., 2020; Dahl et al., 2006; Kupiainen et al., 2005; Sjödin et al., 2010), studies based on ambient measurements have reported tire wear PM_{10} EFs to be in the range of 7-7.4 mg km^{-1} Veh^{-1} (Luhana et al., 2004; Panko et al., 2013). It is important to note that tire wear concentrations and EFs are a function of road conditions, including surface wetness and temperature (Gustafsson et al., 2008; Mathissen et al., 2011), as well as the vehicle type and size (Beddows and Harrison, 2021; Kim and Lee, 2018; Oroumiyeh and Zhu, 2021; Salminen, 2014). Therefore, the reported EFs in the previous studies are not always comparable. Instead, emission inventories can be used for a more comprehensive understanding of the tire wear EFs.

UK NAEI has estimated tire wear $PM_{2.5}$ and PM_{10} EFs to be 5 and 7 mg km^{-1} Veh^{-1}, respectively (NAEI, 2018). MOVES model by USEPA included a few factors, including vehicle speed and number of axles to estimate the tire wear $PM_{2.5}$ and PM_{10} EFs (Figure 2.4). However, vehicle weight which is an important variable in determining tire wear emissions has not been considered in the MOVES model. As shown in Figure 2.4, tire wear $PM_{2.5}$ EFs are in the range of 0.4 – 2.6 mg km^{-1} Veh^{-1}, while tire wear PM_{10} EFs are estimated to be 2.7-17.1 mg km^{-1} Veh^{-1}. The combination long-haul and short-haul trucks, as well as intercity bus and refuse truck were shown to have the highest tire wear $PM_{2.5}$ and PM_{10} EFs.

The most comprehensive method for estimating tire wear $PM_{2.5}$ and PM_{10} EFs has been proposed by EEA (European Environment Agency, 2019). Tire wear PM EFs are estimated based on the concentration of tire wear total suspended particles (TSPs) (European Environment Agency, 2019). In summary, tire wear PM EFs can be calculated using Eqs (2.6) and (2.7):

$$EF_{PM_{2.5}} = 0.42 * EF_{TSP,T} * S_T(V) \quad (2.6)$$

$$EF_{PM_{10}} = 0.60 * EF_{TSP,T} * S_T(V) \quad (2.7)$$

Where $EF_{TSP,T}$ and $S_T\,(V)$ are the tire wear TSP EF and average vehicle velocity correction factor. $S_T\,(V)$ is equal to 1.39 and 0.90 for vehicle speeds below 40 km/h and above 90 km/h, respectively, while it is calculated from Eq (2.8) for velocities in the range of 40-90 km/h:

$$S_T(V) = -0.00974 * V + 1.78 \quad (2.8)$$

Table 2.3 presents $EF_{TSP,T}$ for LDVs for use in Eqs (2.6) and (2.7):

Table 2.3. Tire wear TSP emission factors for different vehicle classes (European Environment Agency, 2019)

Vehicle category	Tire wear TSP emission factor (µg/km)	Range
Two-wheel vehicles	4.6	4.2 – 5.3
Passenger cars	10.7	6.6 – 16.2
Light-duty trucks	16.9	9.0 – 21.7

For HDVs, $EF_{TSP,T}$ is calculated by Eq (2.9):

$$EF_{TSP,T,HDV} = {}^{N_{axle}}/_{2} * LCF_T * EF_{TSP,B,PC} \quad (2.9)$$

Where $EF_{TSP,T,HDV}$ and $EF_{TSP,T,PC}$ represent EFs for HDV and passenger car, respectively, and LCF_{B} is the load correction factor for tire wear particles from Eq (2.10):

$$LCF_T = 1.41 + (1.38 * LF) \quad (2.10)$$

Where LF is the loading factor is in the range of zero to one for empty to fully loaded HDVs.

The EEA tire wear PM_{10} EFs for passenger vehicle and light-duty truck are 1.5 and 2.3 times higher than MOVES tire wear EFs, respectively. In addition, tire wear $PM_{2.5}$ EFs of passenger vehicles and light-duty trucks are 6.0 and 10.6 times higher in EEA emission inventory than MOVES, respectively. Similar to MOVES brake wear EFs, since the model has not been updated in the past decade, a large discrepancy between the EEA and MOVES tire wear EFs is observed. While the MOVES model has used a tire wear $PM_{10}/PM_{2.5}$ ratio of 6.7, the MOVES report discusses that more recent studies have shown a smaller tire wear $PM_{10}/PM_{2.5}$ ratio in the range of 2.0-2.5, which is expected to be applied in the next versions of the model (Grigoratos, 2018; USEPA, 2020).

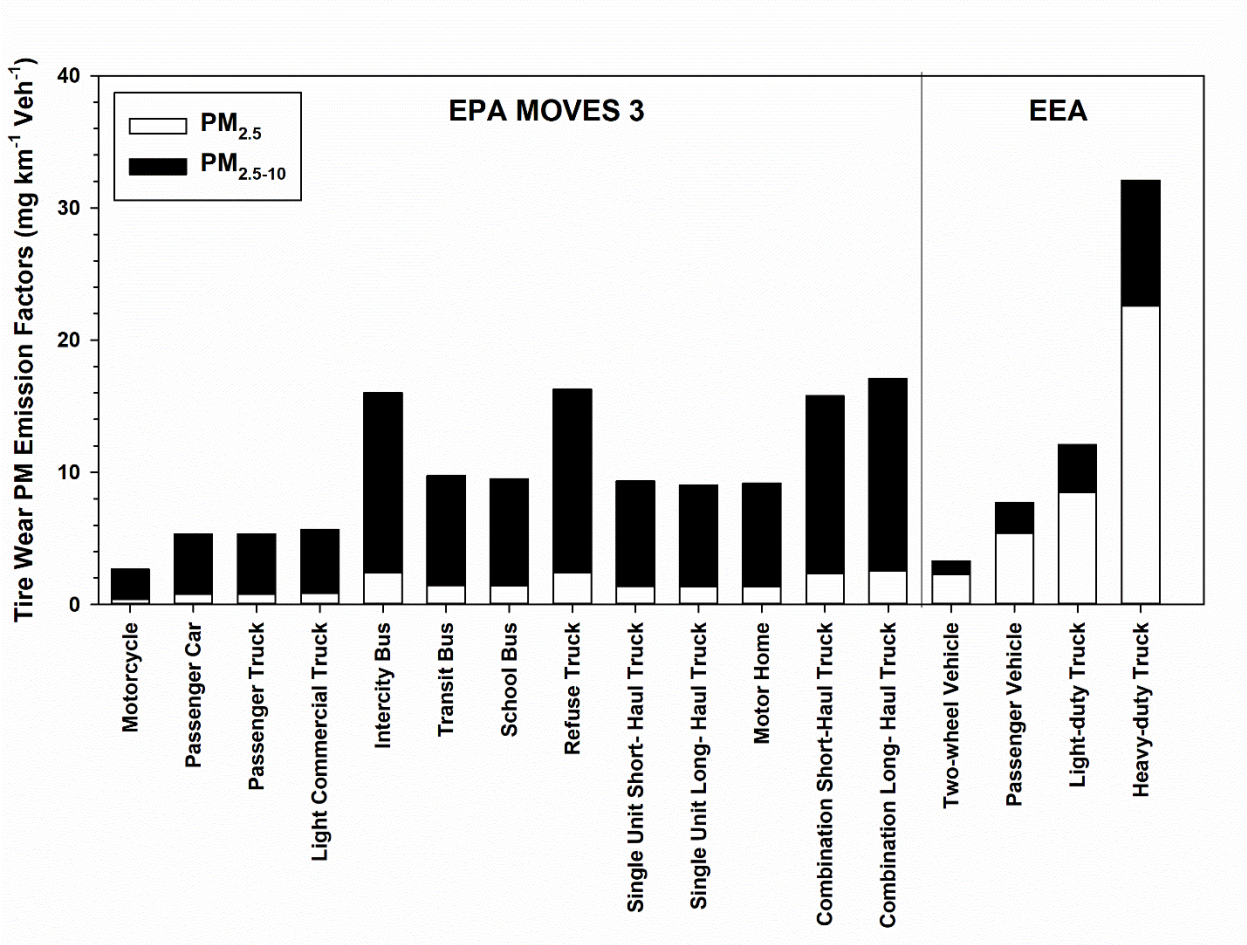

Figure 2.4. Average tire wear PM emission factors based on MOVES 3 (vehicles sorted by weight for calendar year 2017) and EEA. EEA tire wear PM EFs are estimated for vehicle speed of 60 km/h. EEA heavy-duty truck tire wear PM EFs were estimated for a half full truck with 4 axles.

2.4. Effect of auto electrification on the vehicular non-exhaust emissions

The global vehicle fleet has been changing in the past few years with the advancements in electric vehicles (EV) technology. EVs are becoming more affordable, and the EV market has been expanding at a higher rate. While the total share of EVs from the global vehicle market was only 2.5% in 2019 (Barkenbus, 2020), the global EV market is expected to reach 30% by 2030 and 42.5% by 2035 (Rietmann et al., 2020; Rietmann and Lieven, 2019). The expansion in the EV market is occurring at a faster rate in some of the countries due to governmental policies and

significant national and local incentives to encourage auto shoppers (Zhou et al., 2015). For instance, the EV market in Sweden is predicted to exceed 50% prior to 2035 (Rietmann et al., 2020), while the EV sales in Norway exceeded 50% in 2021, according to the International Energy Agency (IEA) (IEA, 2021).

EVs have an intrinsic environmental advantage over internal combustion engine vehicles (ICEVs) due to their zero exhaust emissions. While the impact of auto electrification on reducing exhaust emissions has been shown to be dependent on various factors such as electricity source (L. Wang et al., 2020), EVs have the potential to mitigate traffic-related pollutants, including NO_x, SO_2, and CO_2, in the countries with more sustainable energy sources (Buekers et al., 2014; Burchart-Korol et al., 2018; de Souza et al., 2018).

Despite the advantage of EVs over ICEVs in reducing exhaust emissions, EVs can still contribute to non-exhaust emissions. EVs have been reported to be 24-56% heavier than ICEVs in an equal class, due to the application of heavy EV batteries for achieving a longer range per charge (Moawad et al., 2011; Timmers and Achten, 2018, 2016). Therefore, EVs have been reported to have higher brake and tire wear EFs than ICEVs in an equal output power level due to the extra weight of the batteries (Beddows and Harrison, 2021). However, it is important to note that brake wear EFs of EVs could decrease with the application of regenerative braking system, which minimizes the vehicle's frictional braking force and converts the wheels' kinetic energy into electricity to power the vehicle (Beddows and Harrison, 2021; Hall, 2017). Moreover, advancements in battery technology to produce high-capacity EV batteries as well as other lightweight design strategies, including the application of lightweight composite material, carbon fiber, and aluminum alloys in vehicle manufacturing, can reduce EV non-exhaust emissions in the future (Delogu et al., 2017; Xu et al., 2020).

The battery is one of the most important components of an EV because of its crucial role in generating power for the vehicle. With the substantial rate of auto electrification, emerging battery emissions are expected to be introduced to the environment, which have been rarely investigated, and their contribution to airborne traffic emissions has never been estimated. In this section, the potential contribution of EV batteries to non-exhaust emissions is briefly discussed.

Lithium-ion batteries (LIBs) are currently the most common energy source of EVs. They are categorized into various types based on their positive and negative electrode components (i.e., Lithium Nickel Manganese Cobalt Oxide (NMC), Lithium Manganese Oxide (LMO), and Lithium Nickel Cobalt Aluminum Oxide (NCA)) (Miao et al., 2019). The most common LIB electrolytes include Lithium salts such as $LiPF_6$, organic carbonates such as dimethyl carbonate (DEC), as well as polymer and ceramic electrolytes (Essl et al., 2020; Miao et al., 2019; Que et al., 2016). In addition, a porous membrane is integrated inside the battery to prevent a short circuit between the electrodes while allowing for the permeation of Li ions (Hannan et al., 2018).

Upon the first usage of the battery, a layer (solid-electrolyte interface (SEI)) formed by the dissociation of battery electrolytes covers the separating membrane, which can affect the battery performance and battery aging over time (Wang et al., 2018; F. Yang et al., 2018). At elevated temperatures, SEI undergoes a series of chain reactions, which can eventually lead to the emission of flammable gasses and toxic materials from LIBs and thermal runaway (Essl et al., 2020; Golubkov et al., 2018; Huang et al., 2015).

The majority of the previous studies on hazard analysis of LIBs are based on extreme or abnormal conditions associated with the battery failure, including overheating and thermal runaway conditions. Particle measurements during extreme conditions such as thermal runaway are logistically challenging due to the high battery temperature of up to 1000 ºC (Golubkov et al.,

2015). The limited number of studies on the battery emissions were not focused on airborne fraction of PM due to the extreme battery temperature and safety concerns for aerosol sampling. Instead, deposited PM samples were collected upon returning the battery to normal temperature and further analyzed for size distribution and chemical speciation. Therefore, the collected PM has been reported to be in the size range of 0.1-8.0 mm, without accounting for airborne battery particles (Zhang et al., 2019b). Approximately 44% and 36% of the collected battery PM has been reported in the size range of 0.1-0.8 mm and 0.8-1.7 mm, respectively (Zhang et al., 2019b). Moreover, it has been reported that 11-29% of the cell mass can be lost in the form of particles and gas, depending on the battery charging level and battery material (Lai et al., 2021; Zhang et al., 2019a, 2019b).

The chemical composition of the generated PM depends on different factors, including the battery type, electrolyte material, and state-of-charge (SOC) (Essl et al., 2020). It has been reported that the major elemental components of the emitted particles from an NMC/LMO battery are C, Li, Co, Ni, Mn, and Al (Lai et al., 2021). Other elements including Cu, Fe, K, S, as well as trace amounts of Ba, Ca, Cr, Mg, Mo, Na, Sb, Sn, Sr, Si, Ti, V, Zn, and Zr, have also been reported in chemical speciation of the emitted particles during the thermal runaway of NMC batteries (Zhang et al., 2019b). Metallic elements have been reported to constitute 43% of the total emitted PM mass, indicating that EV LIBs could be among the important contributors of traffic-related PM metals (Zhang et al., 2019b).

At the lower temperatures, as a result of SEI decomposition, the reaction between electrolyte and lithium generates heat and produces gaseous compounds, which are continuously produced through the thermal runaway conditions (Essl et al., 2020). The primary gaseous compounds produced during this process are CH_4, C_2H_4, CO, CO_2, H_2, and HF, depending on the LIB material

(Fernandes et al., 2018; Larsson et al., 2016; Sturk et al., 2019). During this stage of LIB degradation, solid materials including LiF, Li_2CO_3, and $LiPF_6$ can also be generated, which can contribute to particle generation upon venting from the battery (Fernandes et al., 2018; Wang et al., 2006; Wilken et al., 2013).

The results of the previous studies clearly show that EV batteries could generate large particles with high metallic content during battery failure conditions. However, none of the previous studies have investigated the contribution of battery emissions to airborne PM. Moreover, there is a significant lack of knowledge about the potential battery emissions during normal operating conditions of the batteries. Therefore, future research is necessary to (i) investigate and quantify airborne EV battery PM emissions in temperatures below the thermal runaway, and (ii) investigate the potential contribution of evaporation/condensation processes in generating particles from the emitted gaseous compounds from the batteries.

2.5. Health effects associated with vehicular non-exhaust emissions

The chemical composition of fine and coarse particles has been shown to affect PM toxicity (Rönkkö et al., 2018; Weichenthal et al., 2019). Non-exhaust PM metals have been associated with various health outcomes, including cancer (Chen et al., 2021; Raaschou-Nielsen et al., 2016), reduced lung function (Huang et al., 2018), cardiovascular and cardiopulmonary diseases (Magari et al., 2002; Samoli et al., 2016; Ye et al., 2018), birth defects (Basu et al., 2014; Pedersen et al., 2013), and increased mortality (Basagaña et al., 2015; Ostro et al., 2015, 2010, 2007; Valdés et al., 2012; Wang et al., 2017). These metals can trigger oxidative stress by inducing the disproportionate generation and consumption of reactive oxygen species (ROS), including hydroxyl radicals, oxygen radicals, peroxides, and oxygen superoxide (André Nel, 2005; Bates et al., 2019; Hadei and Naddafi, 2020; J. Park et al., 2018; Wei et al., 2009). The oxidative potential

is defined as PM capacity for producing ROS, which is substantially dependent on PM chemical composition, and has been used for determining PM toxicity (Fang et al., 2019; Weichenthal et al., 2019; Yadav and Phuleria, 2020).

Oxidative potential can be measured by various cellular and acellular assays and has been associated with different health outcomes, including asthma (Yang et al., 2016), diabetes (Strak et al., 2017), and hospital admissions for cardiovascular and respiratory causes (Abrams et al., 2017; Bates et al., 2015; Gao et al., 2020b). Among the transition metals, Cu and Fe, which are both associated with brake wear emissions, have been frequently reported to be correlated with oxidative potential in different studies based on various acellular assays (Gao et al., 2020a, 2020b; Hakimzadeh et al., 2020; Mousavi et al., 2019; Perrone et al., 2019; Rao et al., 2020; Shirmohammadi et al., 2017; Weichenthal et al., 2019; Yang et al., 2015). Other metals associated with brake and tire wear emissions, including Ba (Mousavi et al., 2019; Perrone et al., 2019; Shirmohammadi et al., 2017; Weichenthal et al., 2019; Yang et al., 2015), Cr (Crobeddu et al., 2017; Liu et al., 2018), Mn (Gao et al., 2020a; Perrone et al., 2019), Mo (Calas et al., 2018), Sb (Crobeddu et al., 2017; Shirmohammadi et al., 2017), Sn (Calas et al., 2018), Zn (Liu et al., 2018; Shirmohammadi et al., 2017), and Zr (Calas et al., 2018) have also been reported to be associated with oxidative potential. While some studies reported the association of total metals with oxidative potential, other studies documented the association of water-soluble (WS) fraction of metals with oxidative potential as it has been reported that solubility of metals can enhance their bioavailability (Mukhtar and Limbeck, 2013). The association of the WS fraction of some of the brake and tire wear metals, including WS-Ba, WS-Cr, WS-Cu, WS-Fe, WS-Mo, and WS-Zn has been documented in a number of studies (Cheung et al., 2012; Hu et al., 2008; Pietrogrande et al., 2018; Shirmohammadi et al., 2015; Strak et al., 2012).

The impact of organic content of vehicular non-exhaust emissions on PM health effects should also be considered. In general, exhaust and non-exhaust traffic emissions both contribute to organic carbon (OC) in urban areas (F. Amato et al., 2016; Gianini et al., 2013; Hasheminassab et al., 2014; Taghvaee et al., 2019; Veld et al., 2021; von Schneidemesser et al., 2010). In Los Angeles, the relative contribution of non-exhaust emissions to OC has been reported to increase from 14% in 2005 to 28% in 2015, while the contribution of exhaust emissions to OC has decreased (Altuwayjiri et al., 2021). A considerable fraction of OC has been attributed to road dust, which can also be linked to non-exhaust emissions (Mousavi et al., 2018). As mentioned in previous sections, organic materials have been shown to constitute both brake and tire wear particles (Aatmeeyata and Sharma, 2010b; Alves et al., 2021, 2020; Dall'Osto et al., 2014; Gadd and Kennedy, 2000; Jan Kole et al., 2017; Park et al., 2017; Plachá et al., 2015). OC, water-soluble OC (WSOC), and volatile organic compounds, including PAHs have been reported to be associated with oxidative potential (Calas et al., 2018; Hakimzadeh et al., 2020; Janssen et al., 2015; Kramer et al., 2021; Liu et al., 2020; Lovett et al., 2018; Mousavi et al., 2019; Perrone et al., 2019; Pietrogrande et al., 2018; Strak et al., 2012, 2017; Taghvaee et al., 2019; Zhang et al., 2016). Some of the organic constituents of brake and tire wear particles, including PAHs, glycerol compounds, heavy alkanes, and phenolic compounds are toxic and contribute to overall PM health effects (Alves et al., 2021, 2020; Markiewicz et al., 2017). For instance, PAHs have been associated with various health outcomes, including birth defects (Ren et al., 2011), cancer (Armstrong et al., 2004; Vardoulakis et al., 2020), and cardiovascular diseases (Marris et al., 2020; Xu et al., 2010) and respiratory diseases (Bortey-Sam et al., 2017). Moreover, it has been shown that the presence of organic material can increase the toxicity of transition metals by increasing the solubility of metals (Gao et al., 2020b; Tapparo et al., 2020).

The majority of previous studies have not apportioned the contribution of exhaust and non-exhaust emissions to oxidative potential, and they have estimated the overall contribution of vehicular emissions, including gasoline and diesel vehicles (Bates et al., 2015; Hakimzadeh et al., 2020; Liu et al., 2018; Mousavi et al., 2019; Taghvaee et al., 2019). Only a few studies have distinguished the contribution of exhaust and non-exhaust emission sources through source apportionment techniques (Jeong et al., 2020; Shirmohammadi et al., 2016, 2015). Jeong et al. (2020) reported a higher correlation between the $PM_{2.5}$ oxidative potential and non-exhaust emissions than exhaust emissions in Toronto, highlighting the role of non-exhaust emissions in contributing to $PM_{2.5}$ oxidative potential. Shirmohammadi et al. (2016) estimated the contribution of various sources to $PM_{2.5}$ and $PM_{0.18}$ oxidative potential in southern California and reported that while exhaust emissions were a significant source of $PM_{0.18}$ oxidative potential, vehicular abrasion source, including brake and tire wear particles was a significant source of $PM_{2.5}$ oxidative potential. Shirmohammadi et al. (2015) studied the contribution of water-soluble and water-insoluble metals to $PM_{2.5-10}$ oxidative potential and reported vehicular abrasion and resuspended dust as the primary contributors to $PM_{2.5-10}$ oxidative potential in southern California. Future ambient measurement studies can better understand the relative contribution of exhaust and non-exhaust emissions to $PM_{2.5}$ and $PM_{2.5-10}$ and their oxidative potential.

2.6. Conclusions

Exhaust emissions have significantly decreased in different parts of the world, due to the prohibitive environmental policies, as well as scientific improvements in the auto industry that have led to the manufacturing of fuel-efficient vehicles with low exhaust emissions. On the other hand, the role of non-exhaust emissions has been underestimated in the emission inventories, while their relative contribution to traffic-related emissions is on the rise.

Brake components have been reported to have a high metallic content. While Fe has been shown to be the dominant element in brake rotors and brake pads, many other elements, including Al, Ca, Cd, Cr, K, Mn, Mo, Ni, Pb, Si, Ti, Zn, and Zr have also been observed in brake wear particles in fine and coarse PM. Overall, Ba, Cu, Sb, and Sn were found to be the most appropriate brake wear tracers. Moreover, carbonaceous species have been reported to have a considerable contribution to the total weight of brake wear particles. Approximately 150 organic compounds, including n-alkanes, n-alkenes, n-alkanols, glycerol compounds, phenolic compounds, and polycyclic aromatic hydrocarbons (PAHs) have been observed in brake wear particles.

The mass-based particle size distribution of brake wear particles has been reported to be unimodal with mode diameter in the range of 1-10 μm. The reported brake wear particle size distributions have been reported to be variable, depending on the sampling approach and instrumentation. A unimodal, bimodal, and multimodal brake wear particle size distribution with mode diameters in the ultrafine and fine size ranges has been reported in the previous studies. Brake temperature, brake lining material, and brake maintenance history have been shown to have a significant impact on the brake wear particle size distribution.

It has been shown that approximately 2-7% of the tire tread particles are airborne, while the remainder transport to the aquatic environment or deposit on the roads. Many elements, including Al, Si, Zn, Ca, Fe, K, Mg, Na, K, S, and Ti have been reported to be abundant in tire-road wear particles (TRWPs). Zn and S have been shown to be highly associated with tire treads, while some of the reported elements in TRWPs, including Al, Si, and Ti have been associated with other emission sources, including road dust. Despite the association of Zn with tire tread particles, selecting Zn as a tire wear tracer should be taken with caution due to the association of Zn with other emission sources. Carbonaceous species constitute up to 72% of tire tread weight, and

various organic species, including PAHs, n-alkanols, phenolic compounds, levoglucosan, steranes, and aliphatic species have been reported in TRWPs. Overall, TRWPs were shown to be the leading non-exhaust emission source of PAHs. Among the reported PAHs, pyrene, fluoranthene, and naphthalene have been reported to have the highest concentrations.

The airborne tire wear particle size distributions have been reported to be unimodal, bimodal, and multimodal, with mode diameters in the range of 0.01 to 5 μm. Moreover, the majority of the studies reported a minimum of one peak in the ultrafine size range. Tire wear particles can contribute to up to 60% of the microplastics with diameters in the range of 1-1000 μm. The mass-based particle size distribution of larger tire tread particles has been reported to be unimodal with mode diameters of 25 μm, while a bimodal TRWP size distribution has been documented.

Various studies have reported the brake wear $PM_{2.5}$ and PM_{10} emission factors (EFs) to be in the range of 0.5-5.5 and 1.4-80.0 mg km^{-1} Veh^{-1} , respectively. In addition, tire wear $PM_{2.5}$ EFs have been shown to be 0.3-11.0 mg km^{-1} Veh^{-1}, while tire wear PM_{10} EFs were 1.9 – 11.0. Due to the large variation in $PM_{2.5}$ and PM_{10} EFs, emission inventories can be used for comparing the brake and tire wear PM EFs of vehicles. USEPA estimated lower brake wear $PM_{2.5}$ EFs and tire wear $PM_{2.5}$ and PM_{10} EFs than European Environment Agency (EEA), while reporting a higher brake wear PM_{10} EFs for the vehicles in different size classes. Moreover, a lower $PM_{2.5}/PM_{10}$ EF ratio is reported by USEPA than EEA, which can have significant policy implications since most of the PM health effects have been documented in the fine size.

Non-exhaust emissions are an important source of PM metals with various health effects. Metals associated with the brake and tire wear emissions could induce various health outcomes, including cancer, reduced lung function, cardiovascular and cardiopulmonary diseases, birth defects, increased mortality, and oxidative potential. Moreover, the brake and tire wear organic content

includes toxic organic compounds such PAHs, phenolic compounds, and glycerol compounds that can contribute to overall PM health effects.

The current work aimed to provide a comprehensive understanding of the vehicular non-exhaust emissions, their physical and chemical characteristics, and their associated health effects. This literature review study also provided insight into the future trend of non-exhaust emissions with the growth of auto electrification.

3. Brake and tire particles measured from on-road vehicles: effects of vehicle mass and braking intensity

Published in Atmospheric Environment: X (2021, Volume 12)

DOI: 10.1016/j.aeaoa.2021.100121

3.1. Abstract

Vehicle exhaust emissions have been decreasing due to stricter regulations and advancements in control strategies. However, non-exhaust emissions from brake and tire wear have not been extensively regulated in the past, and their relative contribution to particulate matter (PM) in urban areas is increasing. We examined the effect of a vehicle's mass and braking intensity on brake and tire particles based on on-road data collected from three different types of vehicles under real-world driving conditions. $PM_{2.5}$ and PM_{10} concentrations and particle size distributions were measured near the center and rear of the right front wheel, respectively. During the braking, the highest peaks in brake $PM_{2.5}$ (520-4280 μg/m^3) and PM_{10} (950-8420 μg/m^3) concentrations were observed from the heaviest vehicle, while the lowest peaks in brake $PM_{2.5}$ (250-2440 μg/m^3) and PM_{10} (430-3890 μg/m^3) concentrations were observed from the lightest vehicle. Similarly, the observed peaks in tire $PM_{2.5}$ (340-4750 μg/m^3) and PM_{10} (810-8290 μg/m^3) concentrations of the heaviest vehicle were shown to be the highest among the test vehicles, while the peaks in tire $PM_{2.5}$ (220-2150 μg/m^3) and PM_{10} (370-3840 μg/m^3) concentrations of the lightest vehicle were lower than other vehicles. A statistically significant difference in the peak values of $PM_{2.5}$ and PM_{10} concentrations was observed between the heaviest and lightest vehicles for both brake and tire particles. The braking deceleration rate was found to be an important factor in predicting the peaks in $PM_{2.5}$ and PM_{10} concentrations during major braking events for all three test vehicles. Brake particles showed a unimodal mass size distribution with a mode diameter of 3-4 μm, while tire

particles showed a slightly larger mode diameter of 4-5 μm. The finding of this study provides insight into the effects of driving conditions and vehicle mass on brake and tire emissions.

3.2. Introduction

During the past decades, remarkable efforts have been made to reduce vehicle exhaust emissions, which are one of the major sources of particulate matter (PM) in urban environments. These efforts were based on a large body of research that has been focused on exhaust emissions such as particle size distribution, spatiotemporal distribution, and associated health effects (Beelen et al., 2008; Wang et al., 2016; Zhu et al., 2006). As a result, governments have gradually increased regulations to reduce exhaust emissions. In contrast, non-exhaust emission sources, including brake and tire wear, have not been investigated comprehensively, and therefore, have not been extensively regulated.

It has been shown that the contribution of the non-exhaust emission sources to PM_{10} (PM with aerodynamic diameters less than or equal to 10 μm) is at a comparable level to the exhaust emissions (Bukowiecki et al., 2010). Moreover, the contribution of non-exhaust emission sources to $PM_{2.5}$ (PM with aerodynamic diameters less than or equal to 2.5 μm) has increased in recent years, while exhaust emissions have been continuously decreasing (Jeong et al., 2020). Given a predicted increase in the sales of electric and hybrid vehicles with low or zero exhaust emissions in the future (Axsen and Wolinetz, 2018), non-exhaust sources are likely to become more important worldwide (Rexeis and Hausberger, 2009).

The key contributors to non-exhaust PM are road dust and brake and tire wear, with minor contributions from the clutch and engine dust (Pant and Harrison, 2013). The contribution of brake wear particles to non-exhaust PM_{10} varies depending on the sampling location and measurement method. Previous studies have shown that brake wear particles could contribute to 55% of non-

exhaust PM_{10} in areas with high braking frequency (Harrison et al., 2012). It has been shown that the contribution of brake wear particles to $PM_{2.5}$ at highways is approximately three times higher than the downtown sampling location (Jeong et al., 2019). In addition, the contribution of brake wear particles to $PM_{2.5}$ has been reported to increase during morning rush hours as a result of congested traffic condition. Brake wear particles have been found in ultrafine, fine, and coarse size ranges (Garg et al., 2000; Kwak et al., 2013; Sanders et al., 2003). More recently, brake wear particles have been reported in the nanometer size range (Farwick zum Hagen et al., 2019b; Liati et al., 2019; Puisney et al., 2018). A few factors, such as the driving style and braking intensity (Kwak et al., 2013), brake temperature (Gramstat et al., 2020; Kukutschová et al., 2011), and maintenance condition of the brakes (Grigoratos and Martini, 2015), have been reported to affect brake wear emissions.

On the other hand, fewer studies have focused on investigating tire wear emissions. Previous studies have shown that tire wear particles could contribute to 11% of total PM_{10} (Baensch-Baltruschat et al., 2020). While tire wear particles were mostly reported in the coarse size range (Gustafsson et al., 2008; Mathissen et al., 2011; Sommer et al., 2018)), ultrafine particles have been observed in a few studies (Kim and Lee, 2018; Kumar et al., 2013), which are presumably generated during the evaporation and condensation processes of volatile tire compounds (Baensch-Baltruschat et al., 2020). The physical and chemical characteristics of the tire wear particles were shown to be a function of road features (Gustafsson et al., 2008), tire characteristics (Gustafsson and Eriksson, 2015), driving conditions and inertia load (Kim and Lee, 2018) based on different experimental setups.

A number of methods have been used for the measurement of brake and tire wear particles. Aside from the studies based on source apportionment, a large number of the previous studies on brake

and tire wear emissions were performed in laboratory settings. Brake dynamometers were used for measuring brake wear particles where the brake pads were tested under different conditions inside a chamber without being attached to any vehicle (Garg et al., 2000; Iijima et al., 2008; Kukutschová et al., 2011). Moreover, road simulator systems have been used for modeling the interaction between the road surface and tire, and studying tire wear particles under different road conditions (Gustafsson et al., 2008; Gustafsson and Eriksson, 2015). While laboratory measurements provide consistency across different tests, they cannot adequately represent real-world driving conditions. A few studies have been carried out on brake and tire wear emissions using on-road sampling (Farwick zum Hagen et al., 2019b; Kwak et al., 2013; Mathissen et al., 2011; Pirjola et al., 2010; Sanders et al., 2003). While these previous studies have discovered valuable information on the brake and tire wear particles, each study only focused on one vehicle, thus could not address the differences of brake and tire wear emissions across different vehicles.

In this study, we measured the brake and tire mass concentrations and size distributions from three test vehicles under real-world driving and braking conditions and investigated the effects of the vehicle mass and braking intensity on the brake and tire particles. To the best of our knowledge, this is the first study to investigate the effect of these factors on brake and tire particles using on-road measurements.

3.3. Methods

3.3.1. Experimental design

A schematic of the sampling system is provided in Figure 3.1. The brake and tire particles were sampled from the right front wheel of the test vehicles. This is because during the braking event, the weight of the vehicle shifts forward; therefore, the front wheels experience more friction (Grigoratos and Martini, 2015). Three sampling inlets were installed near the brake and tire of the

right front wheel as well as on the roof of the test vehicle for ambient PM measurements. A custom-made apparatus was used, which provided sufficient space between the sampling probe and the wheel under both straight and cornering driving conditions. The brake sampling probe was located 5 cm from the center of the wheel, while the tire sampling inlet was installed 2.5 cm from the top of the wheel. The brake and tire inlets were installed 30 cm apart from each other. Isokinetic sampling probes (8 mm ID) were used. Particle losses due to settling and curvature as well as aspiration efficiency were calculated based on classic aerosol theories (Hinds, 1999). The details of the isokinetic sampling design are discussed in Section S1 of the Supplemental Information.

In this study, "brake particles" and "tire particles" refer to the particles collected from the brake and tire sampling inlets, respectively. While these particles were collected near the brake and tire, they could be mixed with other emission sources, whose relative contribution cannot be estimated without chemical speciation analysis and source apportionment. The mixing between the brake and tire particles at both inlets is also plausible. Therefore, the collected data should not be interpreted as solely constitute the brake and tire wear particles. Nevertheless, we do expect brake and tire wear emissions to have a great impact on the particles collected from their respective sampling inlets.

Since adding substantial and balanced loading to a vehicle without changing its center of gravity was not feasible, the on-road sampling was performed on three vehicles with different masses. A full-sized SUV (2016 Chevrolet Suburban), a mid-sized sedan (2016 Honda Accord), and a compact sedan (2017 Nissan Sentra) were tested on a predetermined route. The details of the test vehicles are presented in Table 3.1. All of the test vehicles were equipped with all-season non-studded tires as well as ceramic disc brakes. Ceramic brakes can provide a stable thermal performance (Kumar and Kumaran, 2019; Sundarkrishnaa, 2015) and generate less PM compared

to other types (Seo et al., 2021). While ceramic brake pads have been mostly popular in high-end vehicles due to their high cost (Li et al., 2020), they have become more widespread in recent years due to their durability and superior performance (Li et al., 2021).

The sampling route was a 5.5 km path in the Westwood neighborhood in Los Angeles. The sampling route included a mildly downhill terrain, with fairly straight residential streets, multiple stop signs, and low traffic. The instantaneous driving speed during the measurement did not exceed 75 km/h. On-road sampling took place between March and June 2019. Measurements generally took place between 7 PM to 11 PM when traffic was minimal. For each vehicle, brake temperature was measured before and after each round of sampling using a digital infrared thermometer (1052D, Etekcity Corp., Anaheim, CA). There was a minimum of 30 minutes resting period between two consecutive sampling sessions to ensure the brake temperature was less than 80 °C before each experiment. Section S2 in the supplementary information summarizes the average brake temperatures before and after sampling sessions for each vehicle. The average ambient temperature and relative humidity during the sampling sessions were 21.2 °C and 73.7%, respectively.

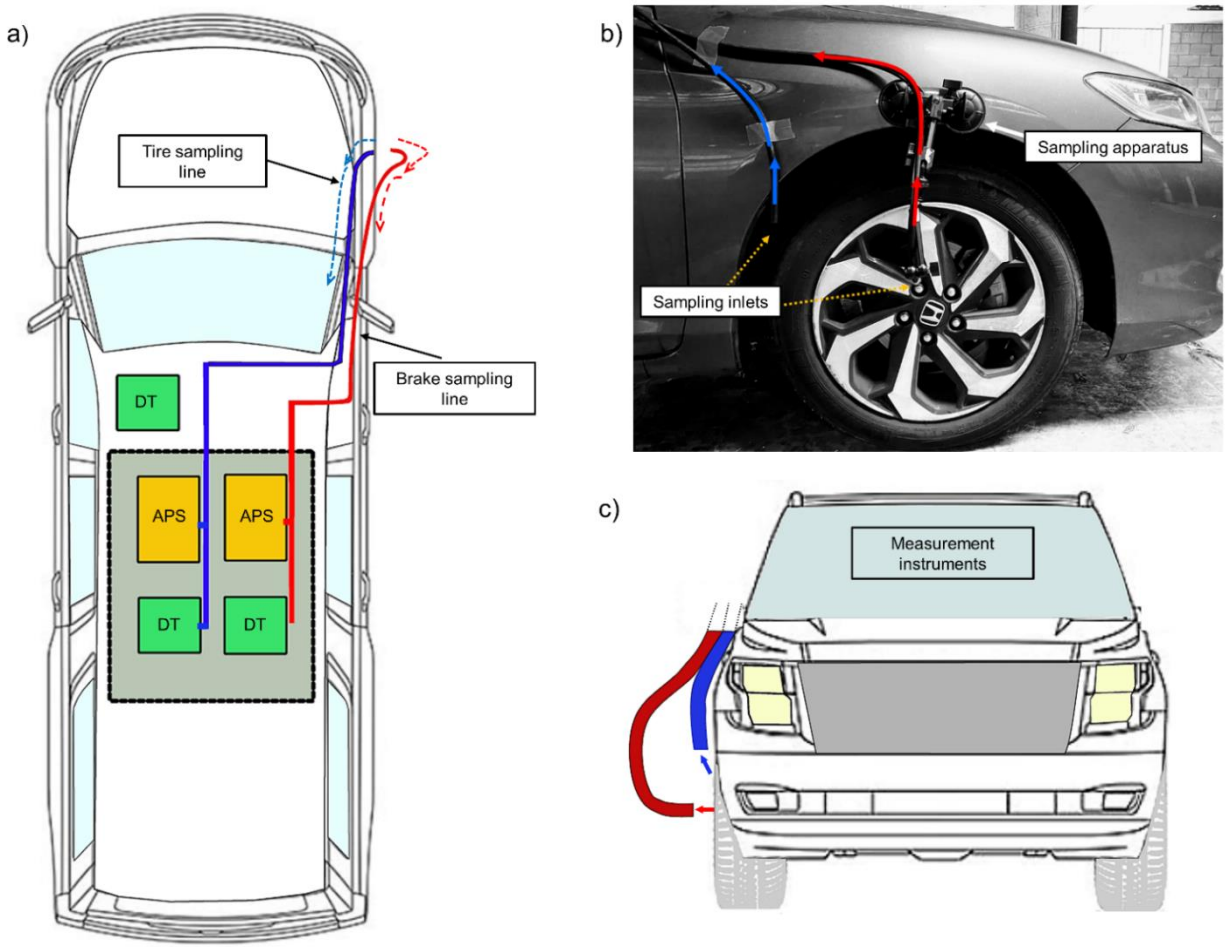

Figure 3.1. Schematic diagrams for the test vehicle with the sampling configuration. (a) Top view. Illustration of the sampling instruments installed inside the vehicle, including APS (TSI APS 3321) and DT (TSI DustTrak 8532). (b) The test vehicle and sampling apparatus. Arrows show the direction of the sampling flow from the brake and tire. (c) Front view. The tire particles are measured from the rear side of the right front wheel. The brake particles are measured at the center of the right front wheel.

Table 3.1: Specifications of the test vehicles

Make/Model	Year/Trim	Vehicle type	Mass (lbs)	Brake pad thickness (mm)	Tire make/model
Nissan Sentra	2017/S	Compact sedan	2857	6.2	Michelin Primacy MXV4
Honda Accord	2016/LX	Midsize sedan	3543	8.8	Michelin Primacy MXV4
Chevrolet Suburban	2016/LS	Full size SUV	5808	7.5	Michelin Defender LTX

3.3.2. Instrument

Three DustTraks (8532, TSI Inc., Shoreview, MN) were used to concurrently measure $PM_{2.5}$ and PM_{10} concentrations from the brake and tire as well as in the ambient air. The brake and tire particle size distributions in the size range of 0.5–20 μm were determined by two Aerodynamic Particle Sizers (APS 3321, TSI Inc., Shoreview, MN) with a log interval of 1 s, respectively. Velocity and GPS coordinates were logged using the GlobalSat data logger (DG-500, New Taipei City, Taiwan). The total sampling flow rate was 8 liter per minute (LPM), which was provided by APS (5 LPM) and DustTrak (3 LPM). The electric power for running APS inside the vehicle was provided by a marine dual-purpose AGM Battery (AGM 105, West Marine, Watsonville, CA) and a power inverter (TruePower 2000PS, Promariner, Menomonee Falls, WI).

3.3.3. Quality assurance and quality control

Before the sampling began, the DustTrak monitors were zero-calibrated in the laboratory, and the GlobalSat data logger was synced to the global time. The DustTrak monitors were also collocated for 10-minute before and after sampling on each vehicle. The resulting linear relationships were applied to adjust DustTrak data. Section S3 of the supplemental information presents the collocation test results.

Previous studies have calibrated DustTrak data against gravimetric measurements for brake wear particles and reported an underestimation. A calibration factor of 5.7±2.1 was reported during the measurement of $PM_{2.5}$ from brake wear particles (Hagino et al., 2015). While a calibration factor for PM_{10} was found to be 2.3±0.2 during on-road brake wear sampling (Farwick zum Hagen et al., 2019b), laboratory measurements reported a calibration factor of 6.4±0.7 for brake wear PM_{10} (Farwick zum Hagen et al., 2019a). Based on these reported calibration factors in the literature, the average calibration factors of 5.7 and 4.4 were used for correcting brake and tire $PM_{2.5}$ and PM_{10} data from DustTrak in this study. $PM_{2.5}$ and PM_{10} DustTrak data collected at the roof of the vehicles were corrected with previously reported ambient calibration factors of 0.52 and 0.33, respectively (Chung et al., 2001; Rivas et al., 2017).

3.3.4. Data analysis

The correlation between the brake and tire PM concentrations and the average deceleration rates for all three vehicles was determined by linear regression analysis. Shapiro-Wilk and Kolmogorov-Smirnov tests were used to examine if the maximum brake and tire $PM_{2.5}$ and PM_{10} datasets at different braking intensity levels are normally distributed. Kruskal-Wallis ANOVA on ranks with a Bonferroni-Dunn post hoc was used to determine the significant differences in the brake and tire PM concentrations among different vehicles since some of the datasets did not pass the normality tests. R 3.4.0 and Microsoft Excel 2016 (Microsoft, Seattle, WA, USA) were used to summarize data and perform statistical analysis. All figures were generated with Sigmaplot 14.0 (Systat Software Inc., San Jose, CA).

3.4. Results and discussion

3.4.1. Determining major braking events

A decrease in the vehicle's velocity can occur with or without braking. Previous studies reported various ranges for the longitudinal deceleration rates during the braking events (Maurya and Bokare, 2012; Smith et al., 2003). It has been shown that only 5% of braking events occur under the deceleration rate of 0.5 m/s^2 and lower (Lee et al., 2007). In this study, deceleration events with (**a)** continuous deceleration for more than 3 s and (**b)** instantaneous deceleration rates of 0.5 m/s^2 or greater in magnitude were selected as major braking events. For each braking event, the arithmetic mean of the instantaneous deceleration rates was calculated to represent the braking intensity.

Figure 3.2 shows a representative time series of the $PM_{2.5}$ concentration measured at the brake inlet of the Chevrolet Suburban and its instantaneous velocity. As shown in Figure 3.2, braking leads to substantial increases in brake and tire PM concentrations and generates a peak in the PM concentration profile. Peak values in brake and tire $PM_{2.5}$ and PM_{10} concentrations during each braking event were identified and further used for analysis on the effect of braking intensity and mass. Figure 3.2 also shows that there could be a delay between the onset of the braking and the observation of a peak in PM concentrations. This lag effect was taken into consideration when identifying major braking events and their associated PM concentrations. A similar effect was reported in a recent study, presumably due to the particle residence time in the sampling line (Farwick zum Hagen et al., 2019b).

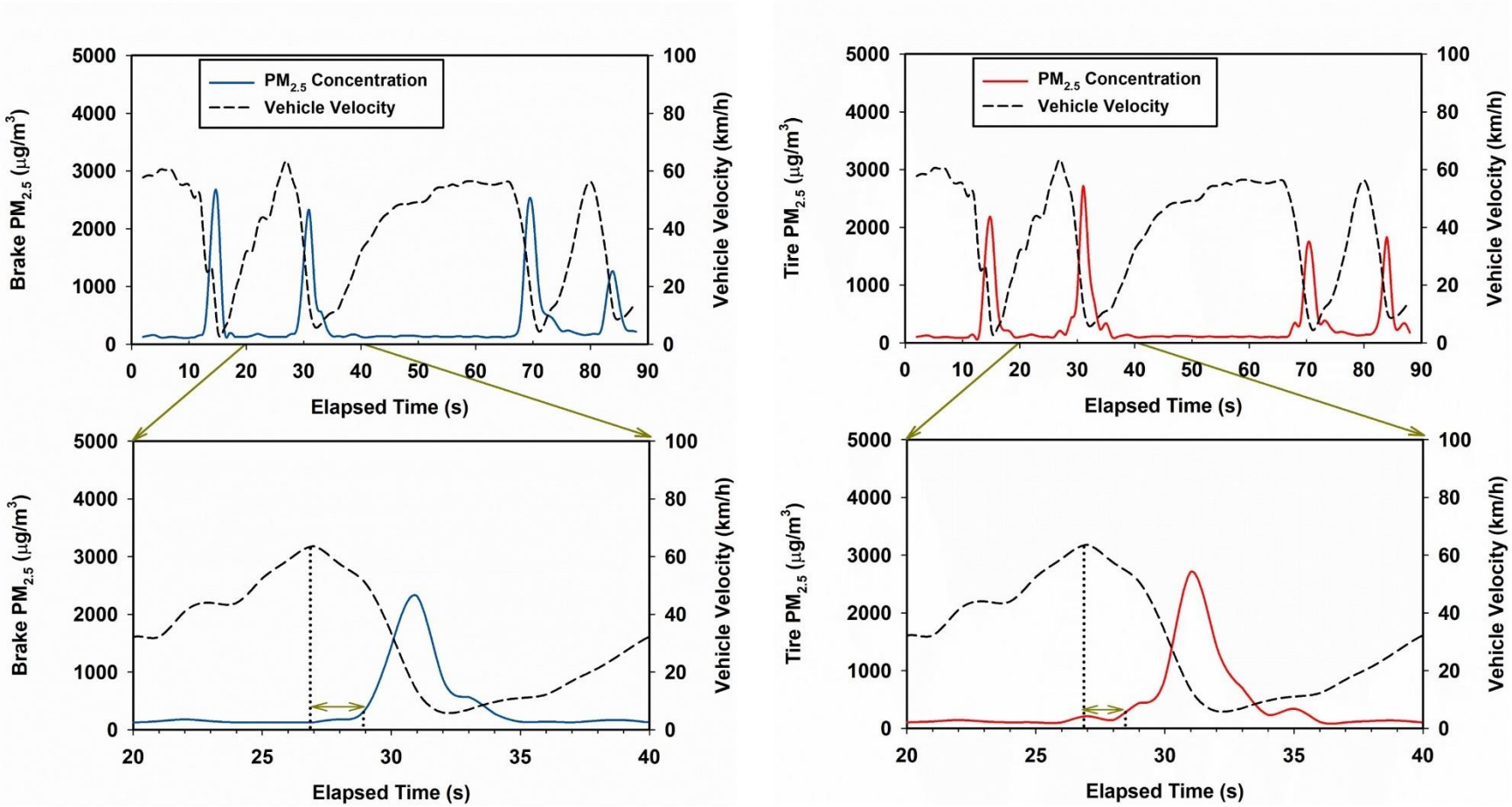

Figure 3.2. A typical temporal profile of $PM_{2.5}$ concentration and driving velocity of the Chevrolet Suburban (a) brake $PM_{2.5}$, (b) tire $PM_{2.5}$

3.4.2. Effect of the braking intensity and vehicle mass on PM mass concentration

Figure 3.3 shows that the deceleration rate was a statistically significant predictor of the brake and tire $PM_{2.5}$ and PM_{10} concentrations during major braking events. The strength of the linear regression (R^2) varies across the vehicles. In general, the correlation improves as the vehicle's mass increases, except for the Accord's brake $PM_{2.5}$, which shows a slightly stronger correlation compared to Chevrolet Suburban. For brake particles, PM_{10} shows a stronger positive correlation with the deceleration rate (p<0.001, R^2 = 0.47-0.53) than $PM_{2.5}$ (p<0.001, R^2 = 0.35-0.47). A similar trend was observed for tire particles, where a stronger linear relationship existed between the deceleration rate and PM_{10} (p<0.001, R^2 = 0.26-0.50) than $PM_{2.5}$ (p<0.001, R^2 = 0.22-0.33). In comparison, the deceleration rate was a stronger predictor for brake $PM_{2.5}$ (p<0.001, R^2 = 0.35-0.47) than tire $PM_{2.5}$ (p<0.001, R^2 = 0.22-0.33). For both $PM_{2.5}$ and PM_{10} concentrations, the slope of the regression for the brake PM concentrations was consistently greater than that for the tire. Section S2 in the supplementary information summarizes the average ambient $PM_{2.5}$ and PM_{10} concentrations during the on-road sampling for each test vehicle.

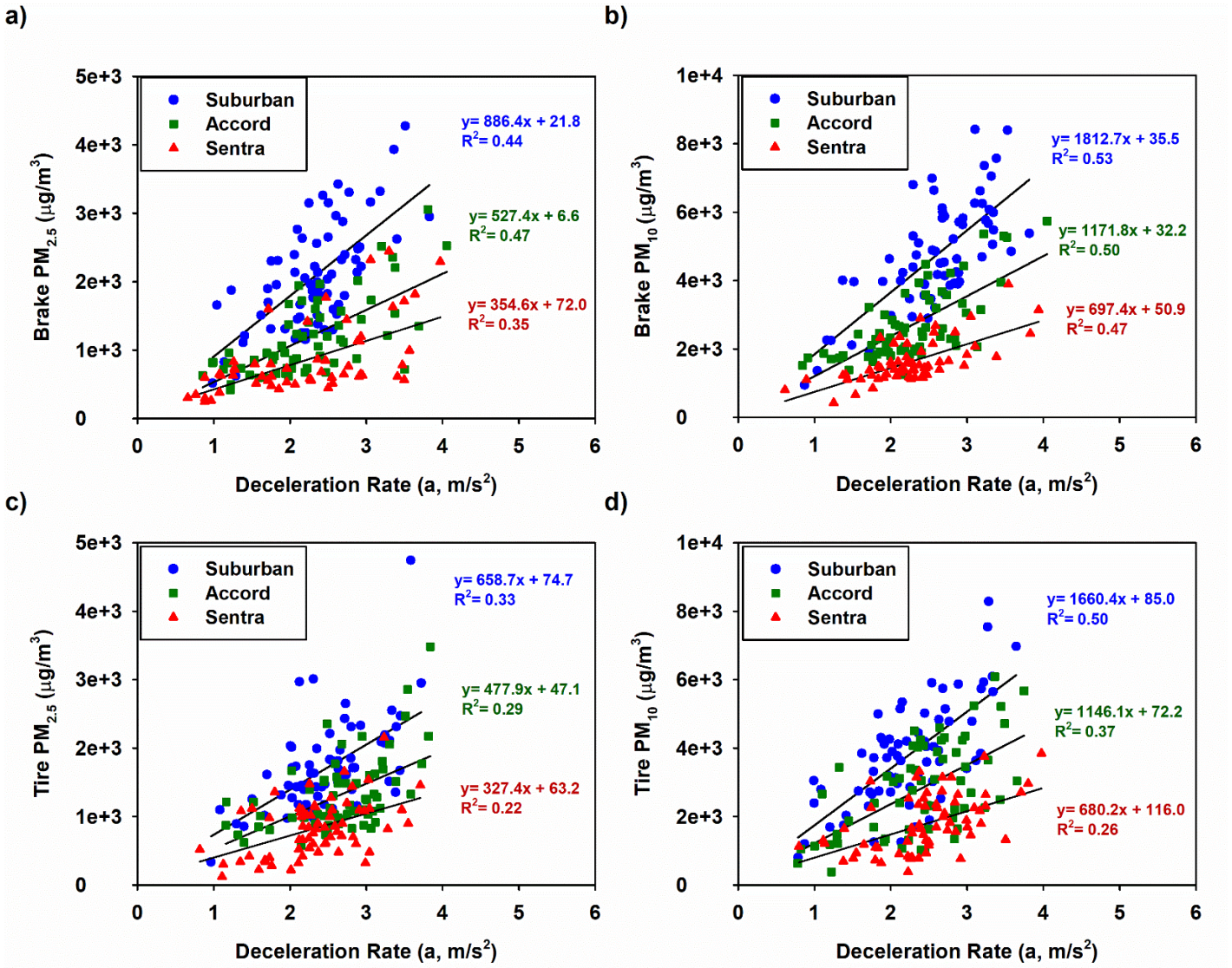

Figure 3.3. Relationships between the peak values in PM concentrations and the average deceleration rate (p-value< 0.001) (a) brake $PM_{2.5}$, (b) brake PM_{10}, (c) tire $PM_{2.5}$, (d) tire PM_{10}

The braking intensity was defined based on the arithmetic mean of the vehicle's instantaneous deceleration rate during each braking event. A braking deceleration of 0.2 g (g=9.81 m/s^2) has been used as the comfortable braking index level (Wu et al., 2009). Moreover, while 50% of the braking longitudinal declaration rates were reported to be under 0.2 g, only 15% of the braking events were shown to have deceleration rates higher than 0.3 g (Lee et al., 2007). Therefore, braking events with an average deceleration rate of 0.3 g and higher were marked as heavy brakes ($a>3.0$ m/s^2); braking events with an average deceleration rate of 0.2 g and lower were marked as light brakes ($0.5<a<2.0$ m/s^2); and those in between were categorized as moderate brakes.

As the braking becomes more intense, a more rapid decrease in the velocity of the vehicle and an elevated deceleration rate occurs. During heavy braking, as the vehicle's velocity decreases quickly, the kinetic energy of the vehicle is absorbed and further transformed into heat through abrasion processes. The required friction force is mainly generated by the abrasion between the brake pad and the disc as well as the friction between the tire and the road pavement. The generated thermal energy affects the friction surfaces and eventually produces wear particles in various sizes. Since a stronger friction force is required for stopping heavier vehicles, a higher concentration of brake and tire particles would be expected. To verify this, the distribution of the brake and tire wear $PM_{2.5}$ and PM_{10} concentrations for three vehicles during the major braking events with respect to the braking intensity were compared.

Figure 3.4 demonstrates the distribution of the brake and tire $PM_{2.5}$ and PM_{10} concentrations for three test vehicles with respect to the braking intensity. For both brake and tire particles, the differences in the median values of $PM_{2.5}$ and PM_{10} concentrations are statistically significant among the three vehicles regardless of the braking intensity level (Kruskal-Wallis P <0.05), suggesting that there is a statistical difference between at least one pair of vehicles. A multiple

comparison procedure (Dunn's Method) was then used to determine if the PM concentration distribution of a vehicle or vehicles was statistically different from the others. The $PM_{2.5}$ concentrations were significantly different between the Chevrolet Suburban and Nissan Sentra, regardless of the braking intensity level for both brake and tire particles (Dunn's Method, $p<0.05$). Likewise, a significant difference was observed in the PM_{10} concentration between the Chevrolet Suburban and Nissan Sentra for both brake and tire particles regardless of the braking intensity level (Dunn's Method, $p<0.05$). The differences in the $PM_{2.5}$ and PM_{10} concentrations between the Chevrolet Suburban and Honda Accord were always significant during heavy and moderate brakes for both brake and tire particles. However, for the light braking intensity, the difference between the Chevrolet Suburban and Honda Accord was not significant. A statistically significant difference was not observed between the Honda Accord and Nissan Sentra, presumably due to a smaller difference in the mases of the two vehicles.

There are few studies that have discussed the effect of vehicle mass on non-exhaust PM emissions. Computer modeling of tire wear properties has previously suggested that vehicle inertia load can affect tire wear particle generation (Salminen, 2014). Moreover, studies on brake wear particles have discussed that inertia load is likely to affect brake wear particles (Garg et al., 2000). In addition, life cycle data have been used for estimating non-exhaust emissions based on the mass of the vehicles, expressing the significance of inertia load on non-exhaust PM generation (Simons, 2016). Overall, the results of this study confirm the findings in the previous works and indicate that vehicle mass can play a major role in predicting brake and tire PM concentrations during the braking.

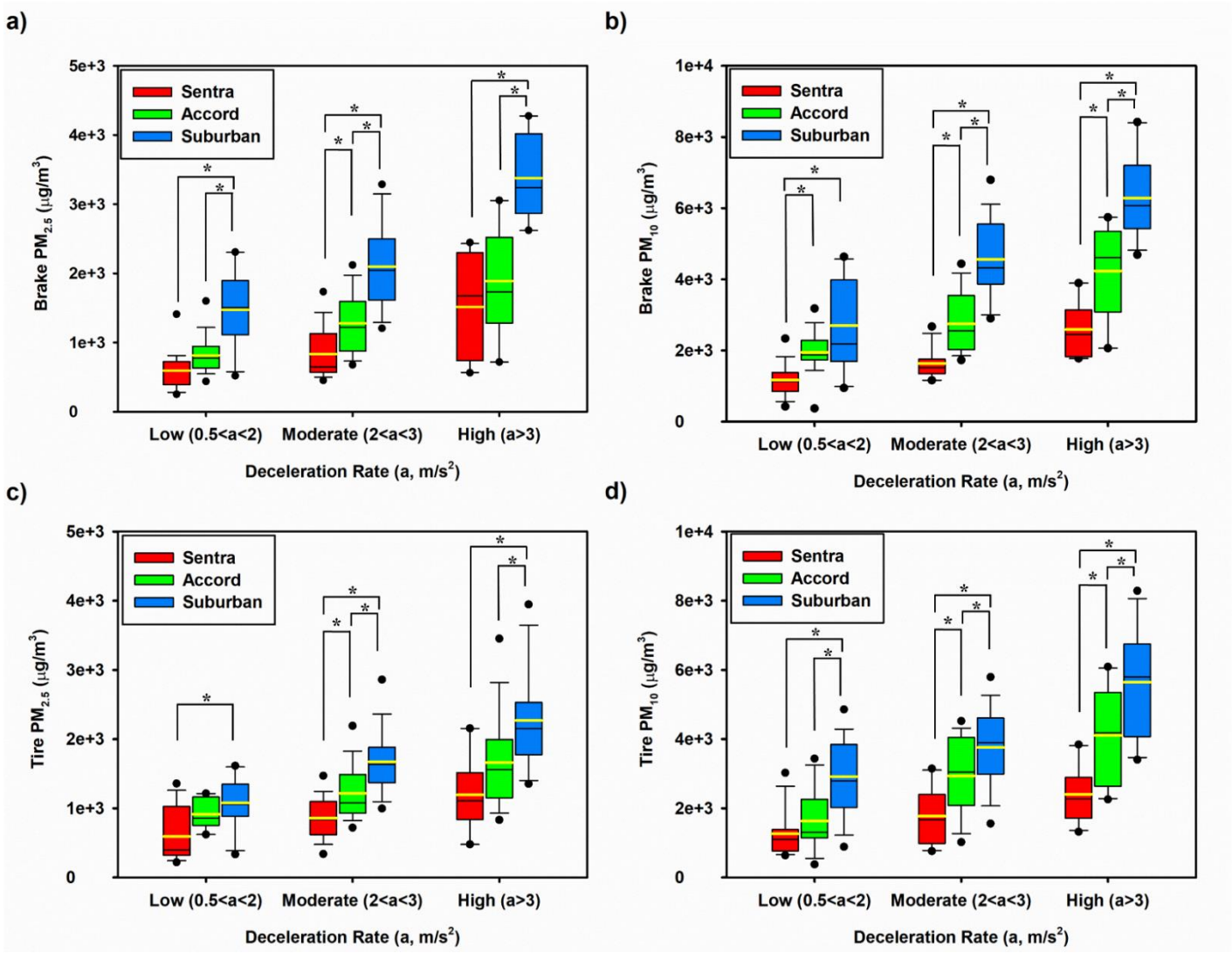

Figure 3.4. Peak values in PM concentrations for the test vehicles at three deceleration rate (i.e., braking intensity) levels (a) brake $PM_{2.5}$, (b) brake PM_{10}, (c) tire $PM_{2.5}$, (d) tire PM_{10}

3.4.3. Particle size distribution

Mass-based particle size distributions of the brake and tire particles are shown as contour plots in Figure 3.5. To obtain mass-based size distributions, we assume particles are perfect spheres with a uniform density of 2.6 and 2.8 g/cm^3 for brake and tire wear particles, respectively (Alemani et al., 2016; Hussein et al., 2008; Kwak et al., 2013). In Figure 3.5, the x and left y coordinates present the sampling elapsed time in seconds and the aerodynamic particle diameter in the logarithmic scale, respectively. The normalized mass concentration ($dM/dlogd_p$) for the particle diameters in the range of 0.5–20 μm at a given time is shown in different contour colors. The right y-axis shows the average deceleration rate during the braking events. As shown in Figure 3.5, while not all braking events increase PM mass concentration, high PM concentrations were observed for most of them. Similar to Figure 3.4, for both the brake and tire particles, higher PM concentrations are generated from the heavier vehicles during braking. This is more noticeable for the Chevrolet Suburban, presumably because its mass is approximately twice as heavy as that of the Nissan Sentra and approximately 60% heavier than that of the Honda Accord. A substantial difference between the mass-based size distribution of the brake and tire particles was not observed.

Figure 3.6 plots the average mass-based particle size distributions for the three test vehicles. Both brake and tire particles showed a unimodal mass size distribution with a mode diameter of 3-4 μm and 4-5 μm, respectively. The reported brake particle size distributions in the previous studies vary depending on the sampling setup and instrumentation. The brake particles have been reported in various size ranges, including ultrafine, fine, and coarse sizes (Farwick zum Hagen et al., 2019a; Kwak et al., 2013; Nosko and Olofsson, 2017). The results of this study are in agreement with the findings of the previous study that reported a mass-based particle size distribution in the 1-10 μm size range (Kwak et al., 2013). Moreover, unimodal tire mass-based particle size distributions with

mode diameters of 2−3 μm, 3−5 μm, and 3−4 μm have been reported (Hussein et al., 2008; Kim and Lee, 2018; Kwak et al., 2013). In general, our results on tire particle size distributions agree with the findings of these studies.

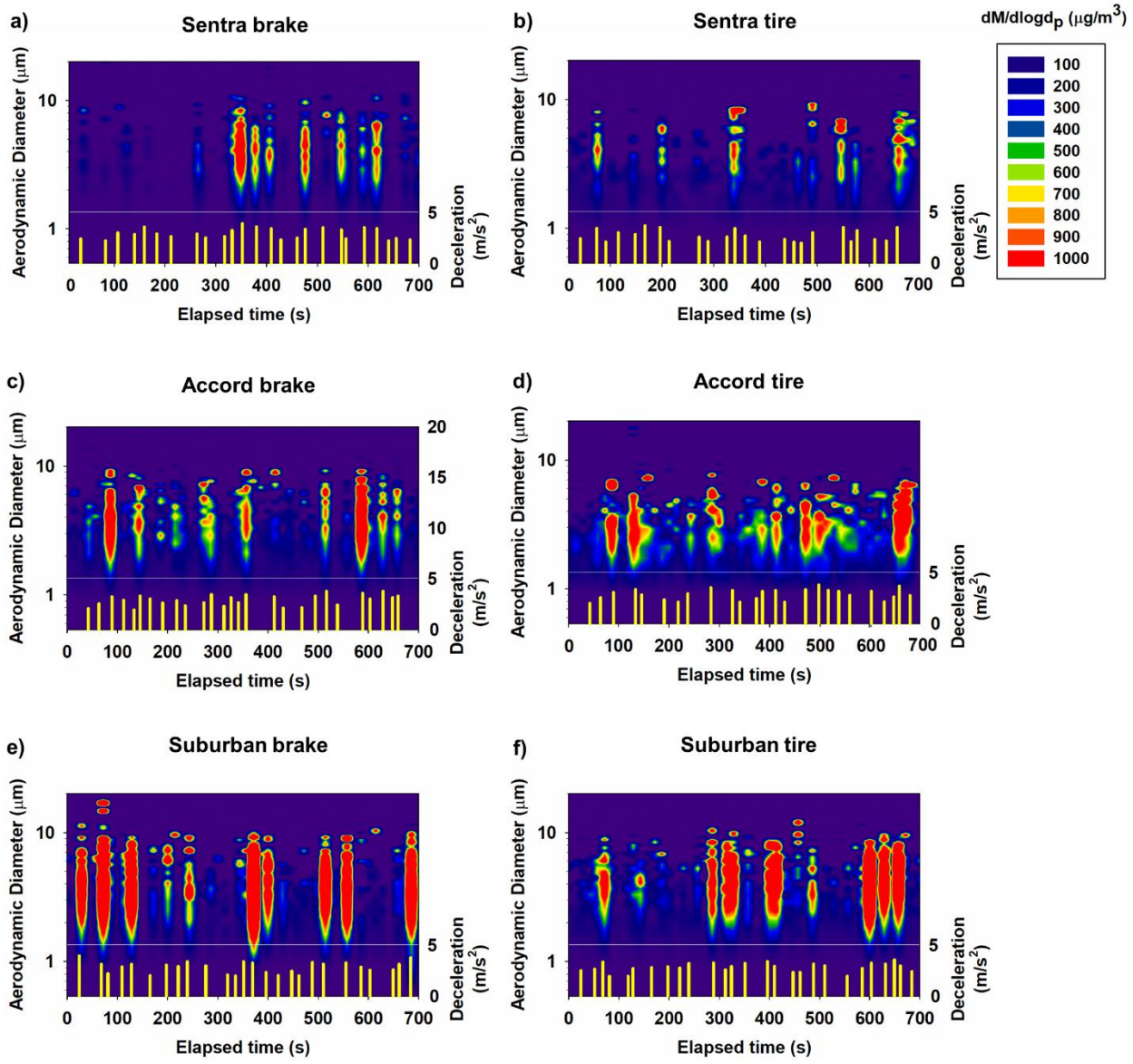

Figure 3.5. Mass-based particle size distributions for brake and tire particles with regard to the braking deceleration rate during moderate and heavy braking events (a) Sentra brake, (b) Sentra tire, (c) Accord brake, (d) Accord tire, (e) Suburban brake, (f) Suburban tire

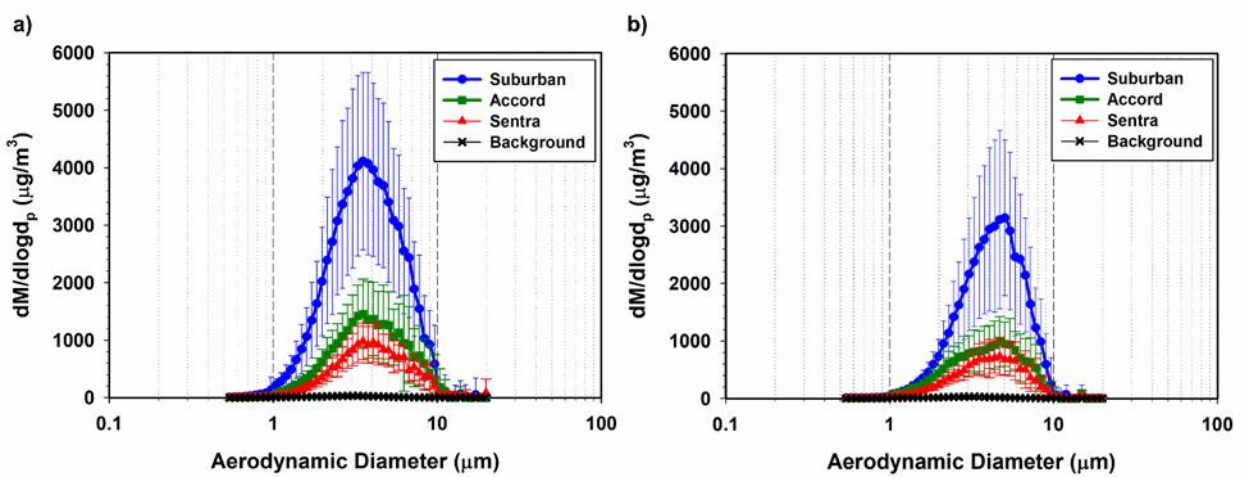

Figure 3.6. Average mass-based particle size distribution during braking events for (a) brake particles and (b) tire particles (error bars: standard deviation)

3.5. Discussion

One of the goals of this work was to study the effect of braking intensity on brake and tire particles. As shown in section 3.2, for each vehicle, higher brake and tire $PM_{2.5}$ and PM_{10} concentrations are observed during more intense braking events. However, it is important to note that at any given initial and final speed, the braking events with higher deceleration rates take less time, and therefore the particles are produced for a shorter period of time. Overall, the average durations of light ($0.5<a<2$ m/s^2) vs. heavy ($a>3$ m/s^2) braking events for all test vehicles were 7.3±0.5 s and 5.2± 0.4 s, respectively, showing an approximately 40% difference. This shorter braking time offsets the total amount of generated brake and tire particles during heavy breaking events.

There are a few other factors that can affect the brake and tire particles. For instance, the aerodynamic drag may affect the vehicle braking intensity and concentrations of brake and tire particles. The aerodynamic drag has been reported to increase during windy conditions (Selvaraju and Parammasivam, 2019; Windsor, 2014) and affect the stopping distance and stopping time at higher driving speeds (V > 100 km/h) (Haggag and Mansouri, 2016). However, in this study, the

effect of aerodynamic drag on braking intensity was expected to be negligible due to low to medium driving speeds and low wind.

The brake temperature can also affect the brake wear particle size distribution. At a certain critical brake temperature (T_{crit}), particle number concentration has been shown to rapidly increase due to the generation of ultrafine particles (Alemani et al., 2018; Farwick zum Hagen et al., 2019b). While T_{crit} has been shown to be a function of brake lining material, most studies reported T_{crit} to be in the range of 140-190 °C (Alemani et al., 2018; Farwick zum Hagen et al., 2019b, 2019a; Nosko and Olofsson, 2017). A previous study using the Los Angeles City Traffic (LACT) cycle has shown that temperature transition occurs gradually (Farwick zum Hagen et al., 2019b). In fact, the brake temperature was reported to reach T_{crit} after 1 hour of continuous driving (Farwick zum Hagen et al., 2019b). In this study, the brake temperature was below 80 °C at the beginning of each sampling session and reached up to 120 °C at the end of each 12-min session (Table S2). Therefore, the range of brake temperature in this study was expected to be well below the T_{crit} (140-190 °C) which is required for excessive ultrafine particle generation.

The goal of this work was to study the effect of vehicle mass on non-exhaust PM during different braking intensity levels. The effects of vehicle mass on non-exhaust PM emissions have received more attention in recent years with the global efforts for transportation electrification. Battery electric vehicles have shown to be heavier than vehicles with internal combustion engines due to the excessive battery weight (Timmers and Achten, 2018). While recent studies have shown the frequency of braking in the battery electric vehicles can be eight times lower due to the application of the regenerative braking system (Hall, 2017), more recent studies based on updated emission inventories have discussed that excessive weight of battery electric vehicles can minimize the positive effect of regenerative braking in reducing non-exhaust PM emissions (Beddows and

Harrison, 2021). Therefore, future research is needed to better understand the overall impact of vehicle electrification on brake and tire wear emissions. The findings from the current study can provide insight into the effect of vehicle mass on brake and tire particles during various braking intensity levels and alleviate the gap of knowledge in this area.

3.6. Study limitations and future work

Chemical speciation has been shown to be useful in the identification of brake and tire wear particles (Lough et al., 2005). For instance, specific chemical elements have been used for tracing brake and tire wear particles (Wang et al., 2021). However, chemical speciation analysis would require collecting a large amount of PM samples during lengthy on-road sampling sessions, which was logistically prohibitive in the current study.

Accurate calibration factors for correcting PM concentrations measured by DustTrak is important. To the best of our knowledge, the DustTrak calibration factor for tire wear particles is not available in the literature. While DustTrak calibration factors for brake wear particles have been reported, they vary widely across different brake lining materials and sampling methods. Therefore, future studies are needed to provide more details about the DustTrak calibration factors of brake and tire wear particles.

Finally, the results of the current study showed that there could be a lag between the onset of the braking and observation of an increase in the concentration of the brake and tire particles. A similar observation has been reported previously during the on-road sampling of the brake wear particles (Farwick zum Hagen et al., 2019b). Since the instrument response time can vary, future research is needed to investigate the instrument response time during the real-time measurement of brake and tire wear particles.

3.7. Conclusion

In this study, three vehicles with different masses were tested to investigate their effects on brake and tire particles under real-world driving conditions. On-road measurements were performed on three test vehicles with masses ranging from 2800-5800 lbs. A significant difference was observed in the brake and tire $PM_{2.5}$ and PM_{10} concentrations between the heaviest and lightest vehicles, indicating that there is a positive association between the vehicles' mass and the PM concentration at the brake and tire inlets. This study also demonstrated that the braking intensity is a strong predictor of the brake and tire $PM_{2.5}$ and PM_{10} concentrations. The brake and tire particles were measured in size range of 0.5-20 μm. Brake particles showed a unimodal mass size distribution with a mode diameter of 3-4 μm, while tire particles showed a slightly larger mode diameter of 4-5 μm. The findings of the current work provide novel information on the effect of vehicle and driving conditions on brake and tire particles.

4. Elemental composition of fine and coarse particles across the Greater Los Angeles area: spatial variation and contributing sources

Published in Environmental Pollution (2022, Volume 292 Part A)

(DOI: 10.1016/j.envpol.2021.118356)

4.1. Abstract

The inorganic components of particulate matter (PM), especially transition metals, have been shown to contribute to PM toxicity. In this study, the spatial distribution of PM elements and their potential sources in the Greater Los Angeles area were studied. The mass concentration and detailed elemental composition of fine ($PM_{2.5}$) and coarse ($PM_{2.5-10}$) particles were assessed at 46 locations, including urban traffic, urban community, urban background, and desert locations. Crustal enrichment factors (EFs), roadside enrichments (REs), and bivariate correlation analysis revealed that Ba, Cr, Cu, Mo, Pd, Sb, Zn, and Zr were associated with traffic emissions in both $PM_{2.5}$ and $PM_{2.5-10}$, while Fe, Li, Mn, and Ti were affected by traffic emissions mostly in $PM_{2.5}$. The concentrations of Ba, Cu, Mo, Sb, Zr (brake wear tracers), Pd (tailpipe tracer), and Zn (associated with tire wear) were higher at urban traffic sites than urban background locations by factors of 2.6 to 4.6. Both $PM_{2.5}$ and $PM_{2.5-10}$ elements showed large spatial variations, indicating the presence of diverse emission sources across sampling locations. Principal component analysis extracted four source factors that explained 88% of the variance in the $PM_{2.5}$ elemental concentrations, and three sources that explained 86% of the variance in the $PM_{2.5-10}$ elemental concentrations. Based on multiple linear regression analysis, the contribution of traffic emissions (27%) to $PM_{2.5}$ was found to be higher than mineral dust (23%), marine aerosol (18%), and industrial emissions (8%). On the other hand, mineral dust was the dominant source of $PM_{2.5-10}$ with 45% contribution, followed by marine aerosol (22%), and traffic emissions (19%). This study

provides novel insight into the spatial variation of traffic-related elements in a large metropolitan area.

4.2. Introduction

Exposures to particulate matter (PM) have been linked to a wide range of chronic and acute health conditions, including cardiovascular diseases, lung cancer, and adverse birth outcomes (Burnett et al., 2018; Gharibvand et al., 2017; Orach et al., 2021; Sapkota et al., 2012). Both fine particles ($PM_{2.5}$, aerodynamic diameter less than or equal to 2.5 μm) and coarse particles ($PM_{2.5\text{-}10}$, aerodynamic diameter ranging from 2.5 to 10 μm) have been associated with increased mortality (B. Wang et al., 2020; Zhang et al., 2017). While most studies addressing the health effects of PM have focused on undifferentiated PM mass, there are a growing number of studies examining PM chemical components, including metals (Franklin et al., 2008; Rönkkö et al., 2018). It has been reported that the metal components are among the major contributors to the overall health effects of PM (Badaloni et al., 2017; Wallenborn et al., 2009). Metals are known to induce oxidative stress (Araujo and Nel, 2009; Gao et al., 2020b), which is one of the most significant physiological mechanisms of PM toxicity (Bates et al., 2019; Miller, 2020). A better understanding of the major sources of PM elements in the environment is required for mitigating their associated health effects.

In Southern California, traffic emissions have been estimated to contribute to 32% and 18% of ambient $PM_{2.5}$ and $PM_{2.5\text{-}10}$, respectively (Habre et al., 2020), and they are one of the dominant sources of PM elements (Mousavi et al., 2018). Significant steps have been taken to control traffic emissions through technological advancements and restrictive policies, which have led to remarkable reductions in exhaust emissions in the past few decades (Pitiranggon et al., 2021; Thorpe and Harrison, 2008). With the continuous reductions in exhaust emissions in light of the

previous emission control strategies, the relative importance of non-exhaust emission sources is increasing in the metropolitan areas (Jeong et al., 2020; Oroumiyeh and Zhu, 2021).

Brake and tire wear particles and resuspended dust are among the primary contributors to non-exhaust PM (Piscitello et al., 2021). Specific elements have been used as tracers for identifying non-exhaust emission sources (Grigoratos and Martini, 2015; Pant and Harrison, 2013). For brake wear particles, Ba, Cu, and Sb are the most common tracers (Gietl et al., 2010; Schauer et al., 2006; Sternbeck et al., 2002), while Cr, Fe, Mo, Sn, Ti, and Zr have also been reported as brake wear tracer (Amato et al., 2011a; Apeagyei et al., 2011). For tire wear particles, Zn has been widely used as a tracer since zinc oxide can contribute up to 1% of tire mass (Farahani et al., 2021; Harrison et al., 2012; Milani et al., 2004; Morillas et al., 2020a). However, Zn is not specific to tire wear because high Zn concentrations have also been reported for other emission sources, including brake wear particles (Lough et al., 2005) and industrial emissions (Jeong et al., 2019; Morillas et al., 2019). In addition, platinum-group elements (PGEs), including Rh, Pd, and Pt, are primarily generated by catalytic converters in light-duty vehicles (LDVs) and can be used as tailpipe tracers (Bozlaker et al., 2014; Das and Chellam, 2020). Moreover, other elements, including Bi, Ce, Ni, and V have been linked to marine fuel emissions (Auffan et al., 2017; Crosignani et al., 2021; Morillas et al., 2019; Spada et al., 2018). On the other hand, using elemental tracers for identifying resuspended road dust should be taken with caution since both crustal and vehicle abrasion sources contribute to resuspended road dust (Denby et al., 2018).

Los Angeles is a megacity and one of the largest metropolitan regions in the United States. Due to its sprawling landscape, Los Angeles is heavily impacted by traffic emissions (Jerrett et al., 2005; Su et al., 2016). Chemical speciation in the Los Angeles area was first studied a few decades ago (Chow et al., 1994). With advancements in analytical measurement technologies, more recent

studies have investigated the spatial variation of a larger spectrum of PM elements in the Los Angeles area (Arhami et al., 2009; Cheung et al., 2011; Habre et al., 2020; Hasheminassab et al., 2020). While these studies provided valuable insights into the chemical speciation and spatial variation of PM elements, they did not cover a large area with a spatial resolution high enough to facilitate research on the association between PM elements and adverse health outcomes. The current study aims to develop a spatially-resolved chemical speciation dataset for $PM_{2.5}$ and $PM_{2.5-10}$ to investigate spatial variations of traffic-related elements in the Greater Los Angeles area to enable future health effect studies.

4.3. Material and methods

4.3.1. Site selection

This study is part of a larger effort to evaluate the association between brake and tire wear emissions and adverse birth outcomes in Los Angeles. The sampling sites were selected with the goal of maximizing the variability in PM mass concentration and chemical speciation to facilitate exposure modeling across the Los Angeles basin. While the effect of traffic intensity on the $PM_{2.5}$ and $PM_{2.5-10}$ elemental concentrations was the main focus of the current study, other factors such as road slope and intersection density which likely affect brake and tire wear particles were also considered for sampling site selection (Abu-Allaban et al., 2003; Harrison et al., 2012). Overall, PM samples were collected at 46 locations in the Greater Los Angeles region (Figure S1) during two periods, in September 2019 and February 2020. In each field campaign, samples were collected concurrently over a two-week integrated period with four replicate sampling locations between the two periods. While most of the sampling sites were within Los Angeles County, the study also covered the adjacent parts of Riverside, San Bernardino, and Ventura counties.

The sampling sites can be categorized into four groups: **(a)** urban traffic, **(b)** urban community, **(c)** urban background, and **(d)** desert (see Table S5 in the supplementary information (SI) for more details). The annual average daily traffic (AADT) data from 2018 were collected from the Federal Highway Administration to compare the traffic volume at different urban sampling sites (Table S5). The mean AADT values for each sampling location were calculated based on the AADT values of the major surrounding roads and highways following the buffering method proposed in the previous studies (Henderson et al., 2007).

4.3.2. Sample collection and analytical methods

Ambient $PM_{2.5}$ and $PM_{2.5\text{-}10}$ samples were collected using Harvard cascade impactors (Lee et al., 2006). The cascade impactors were configured for 3-stage collections and were contained inside custom-made pump boxes that operated at 5 LPM. The first stage of the impactor collected super-coarse particles (aerodynamic diameter larger than 10 µm) using pre-cleaned 3/4" diameter Polyurethane foam (PUF) substrates, the second stage collected coarse particles using 3/8" diameter pre-cleaned PUF, and the final stage was configured with pre-cleaned Teflon membrane filters (Teflo, 2 µm, Pall Life Sciences, 37 mm) to collect $PM_{2.5}$. The filters, PUF substrates, and the components of the impactors were rigorously pre-cleaned in the trace element laboratory at the University of Wisconsin-Madison State Laboratory of Hygiene (WSLH) prior to use, following protocols established in previous studies (Dillner et al., 2007; Lough et al., 2005). The impactors were pre-loaded in the laboratory to minimize potential field-handling contamination.

The PM mass loading on all three substrates was determined by micro-gravimetry (weighting precision = 0.001 µg) at the WSLH. The substrates were equilibrated in the dedicated temperature (21±1.5 °C) and humidity-controlled (40±3%) weighing room for 30 hours before taring and post-weighing. Active ionization sources, including Po strips were installed on the microbalances to

remove static charges during weighing. The concentrations of 55 chemical elements in $PM_{2.5}$ and $PM_{2.5-10}$ were determined by Sector Field Inductively Coupled Plasma Mass Spectrometry (SF-ICP-MS) (Thermo-Finnigan Element 2XR) as previously detailed (Dillner et al., 2007; Herner et al., 2006; Lough et al., 2005; Pakbin et al., 2011) (For more information about the quality assurance/quality control procedure and the effect of relative humidity on $PM_{2.5}$ and $PM_{2.5-10}$ concentrations, please refer to section S4 in the SI). The signal-to-noise (S/N) ratios were calculated based on the previously suggested method (Norris et al., 2014). In this study, elements with concentrations exceeding the method detection limit (MDL) in at least 80% of the samples and S/N ratios greater than two were included in subsequent data analysis. Overall, 43 elements were included for data analysis (see Table S6 in SI).

4.3.3. Statistical analysis

Bivariate Spearman correlation analysis was performed to determine the associations between measured elements. The elements with large anthropogenic and crustal contributions were identified by the crustal enrichment factors (EFs) (Harrison et al., 2003; Salomons and Förstner, 1984), calculated using Eq (4.1):

$$EF_x = \frac{\left(\frac{C_x}{C_{ref}}\right)_{Sample}}{\left(\frac{C_x}{C_{ref}}\right)_{Crust}} \quad (4.1)$$

Where C_x is the concentration of the x element in the field sample, and C_{ref} represents the concentration of the reference element. The elemental concentrations of the upper continental crust (UCC) were used as the crustal concentrations in Eq (4.1) for estimating EFs (Taylor and McLennan, 1985), and Al was used as the reference element (Birmili et al., 2006; Gao et al., 2002).

In order to assess the impact of traffic emissions on $PM_{2.5}$ and $PM_{2.5\text{-}10}$ elements, roadside enrichments (REs) were calculated based on Eq (4.2):

$$RE_i = \frac{C_i^H - C_i^L}{C_i^H} \quad (4.2)$$

Where C_i^H and C_i^L, represent the concentration of the i^{th} element at high and low traffic sites, respectively (Amato et al., 2011b; Oliveira et al., 2010). The calculated REs were based on concentrations at three pairs of sampling locations: **(a)** urban community vs. urban background sites, **(b)** urban traffic vs. urban background sites, and **(c)** urban traffic vs. urban community sites. A similar approach was used in a previous study for identifying metals associated with traffic emissions (Amato et al., 2011b). All elements were categorized into three different groups representing strong, weak, and inconsistent roadside enrichment levels (i.e., Types I, II, and III) (see Table S7 for details).

Principal component analysis (PCA) was separately applied to the $PM_{2.5}$ and $PM_{2.5\text{-}10}$ elemental concentration datasets, each with 50 samples to identify the major sources of PM elements. Overall, the standardized format of 43 elements was included in PCA. Varimax orthogonal rotation was used to optimize the variance between the components, and an eigenvalue of unity or larger was used as a threshold for the inclusion of the extracted source factors in PCA. Based on the resulting principal component loadings, the $PM_{2.5}$ and $PM_{2.5\text{-}10}$ sources were identified using the bivariate correlation analysis results, EFs, and REs.

Two separate linear regression models were further developed to compare the sources contributing to $PM_{2.5}$ and $PM_{2.5\text{-}10}$ based on methods suggested in a previous study (Larsen and Baker, 2003). In each model, ambient $PM_{2.5}$ and $PM_{2.5\text{-}10}$ concentrations were treated as dependent variables, and their corresponding principal component scores were the independent variables. The linear

regression models were developed in a stepwise sequence with the aim of maximizing the coefficient of determination (R^2 values) by including noncolinear and statistically significant source factors (p<0.05).

Descriptive statistical analysis, PCA, multi-variable linear models, and significance tests were performed using SPSS 27.0 (IBM, Armonk, NY). Sigmaplot 12.5 (Systat, San Jose, CA) was used for plotting figures.

4.4. Results and Discussion

4.4.1. Spatial variation of PM mass concentrations

The $PM_{2.5}$ and $PM_{2.5-10}$ mass concentrations at the urban traffic, urban community, urban background, and desert sampling sites are presented in Figure 4.1. The average concentrations of $PM_{2.5}$ at those sites were 10.9 μg/m^3, 8.9 μg/m^3, 6.8 μg/m^3, and 10.5 μg/m^3, respectively, while the average concentrations of $PM_{2.5-10}$ at those sites were 9.6 μg/m^3, 8.3 μg/m^3, 7.4 μg/m^3, and 12.4 μg/m^3, respectively. The $PM_{2.5}/PM_{2.5-10}$ ratios were slightly higher at the urban traffic (0.53) and urban community (0.52) sites than at the urban background (0.48) and desert (0.46) sites. Overall, a statistically significant difference was observed between the $PM_{2.5}/PM_{2.5-10}$ ratios across various sampling locations (Kruskal-Wallis method ($p < 0.05$)). Higher $PM_{2.5}/PM_{2.5-10}$ ratios at the urban traffic and urban community sites were presumably due to fresh emissions from traffic and industrial sources. In Europe, lower $PM_{2.5}/PM_{2.5-10}$ ratios were reported at locations with dry weather conditions or in close proximity to desert dust (Eeftens et al., 2012; Querol et al., 2008), while higher $PM_{2.5}/PM_{2.5-10}$ ratios were reported at urban locations with high traffic volumes (Fulvio Amato et al., 2016). Similar findings were reported in Southern California, showing that desert sampling sites had the lowest $PM_{2.5}/PM_{2.5-10}$ ratios, while urban sampling locations had higher $PM_{2.5}/PM_{2.5-10}$ ratios (Kim et al., 2000; Motallebi et al., 2003).

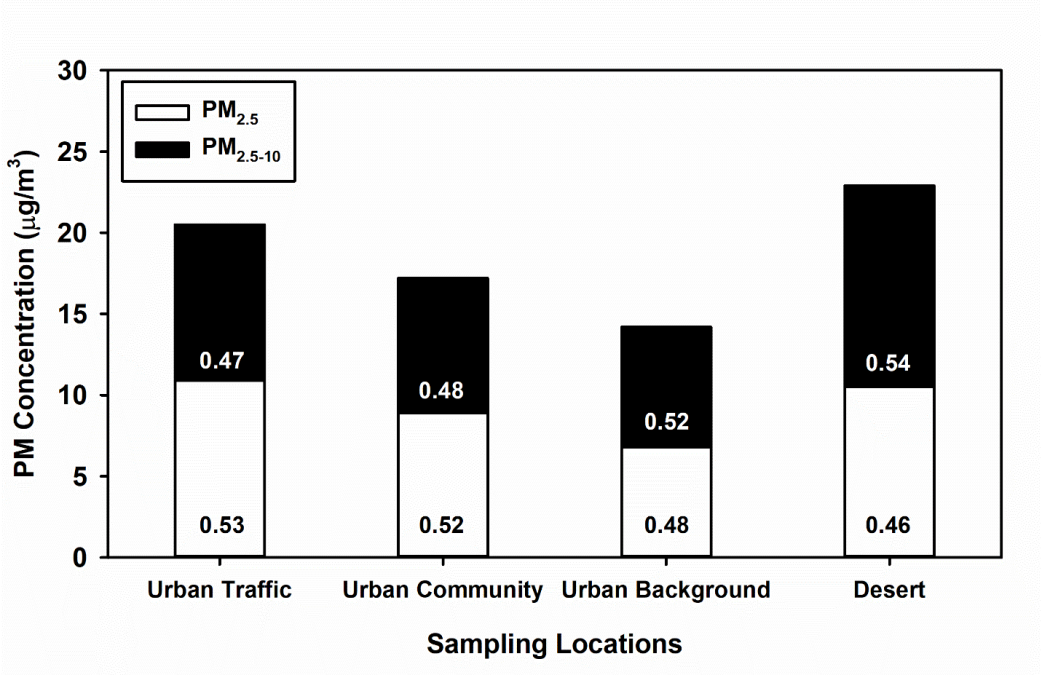

Figure 4.1. $PM_{2.5}$ and $PM_{2.5-10}$ concentrations at different sampling locations. Denoted numbers represent $PM_{2.5}/PM_{10}$ and $PM_{2.5-10}/PM_{10}$ ratios

4.4.2. $PM_{2.5}$ and $PM_{2.5-10}$ elemental concentrations and their spatial variation

Figure 4.2 presents absolute average elemental concentrations in $PM_{2.5}$ and $PM_{2.5-10}$ at different sampling locations. The most abundant elements in both $PM_{2.5}$ and $PM_{2.5-10}$ were Na, S, Fe, Ca, Al, Mg, K, Ba, and Ti. The majority of these elements are naturally abundant in the crust of the earth, while S is also present in the secondary inorganic sulfate. As presented in Figure 4.2, while the concentrations of crustal elements such as Al, Ca, Rb, K, Ti, and Fe were higher in coarse particles, the levels of many of the brake and tire wear tracers (Mo, Cr, Sb, Zn), as well as S, Pb, and Ni were higher in $PM_{2.5}$. The concentrations of Ba, Cu, and Zr in $PM_{2.5}$ and $PM_{2.5-10}$ were comparable. These results are in agreement with findings of previous studies that reported crustal elements such as Al, Ca, Mg, Na, and Si were more abundant in $PM_{2.5-10}$ (Kim et al., 2000; Lough et al., 2005). In addition, other trace elements, including Cd, Pb, and Ni were shown to have higher concentrations in $PM_{2.5}$ than $PM_{2.5-10}$ in previous studies (Poulakis et al., 2015; Querol et al., 2008).

Tables S8 and S9 in SI summarizes the absolute and normalized elemental concentrations in $PM_{2.5}$ and $PM_{2.5-10}$, respectively. Figure S2 presents the relative contributions of $PM_{2.5}$ elements to the elemental concentrations in PM_{10}.

Figure 4.3 represents concentration ratios (panels a and b) and crustal enrichment factor (EF) ratios (panels c and d) of selected traffic (i.e., Ba, Cr, Cu, Mo, Pd, Sb, Zn, and Zr) and crustal (i.e., Ca, Fe, K, Li, Mn, Rb, Ti) elements at the urban traffic, urban community, and desert sites for both fine and coarse particles (Amato et al., 2011a; Apeagyei et al., 2011; Gietl et al., 2010; Pakbin et al., 2011; Schauer et al., 2006; Sternbeck et al., 2002). To calculate the concentration and EF ratios, elemental concentrations and EFs at different sampling sites were normalized by the average concentrations and EFs at the urban background sites, respectively. As shown in Figure 4.3 (panels a and b), urban traffic sites had higher levels of brake and tire wear tracers in comparison to other sampling sites. At the urban traffic sites, the average concentrations of Ba, Cu, Mo, Sb, and Zr in $PM_{2.5}$ and $PM_{2.5-10}$ were 3.3-4.6 and 2.6-4.4 times higher than urban background sites, respectively. In previous studies, the concentrations of traffic tracers such as Ba and Cu in $PM_{2.5}$ were shown to be 3.7 and 4.4 times higher at a freeway site compared to background downtown sites (Jeong et al., 2019). Moreover, the concentrations of the heavy metals in $PM_{2.5-10}$ have been previously reported to be up to 10 times higher at locations with high traffic intensity compared to rural sites (Pakbin et al., 2011). The higher concentrations of Ba, Cu, Sb, and Zn at the urban locations have been attributed to traffic sources, and particularly brake and tire wear emissions (Querol et al., 2007). On the other hand, a large increase in the concentrations of crustal elements was not observed at the urban traffic sites. In fact, average concentrations of crustal elements were only increased by a factor of 1.1-2.1 for $PM_{2.5}$, and 1.1-1.5 for $PM_{2.5-10}$. In contrast, desert sites had the highest concentrations of crustal elements.

The elements with significant anthropogenic sources were identified by EF ratios. As shown in Figure 4.3, in both $PM_{2.5}$ and $PM_{2.5-10}$, the increase in concentrations of traffic tracers at the urban traffic locations led to higher EF ratios, indicating a strong influence of traffic activity on these elements. A similar effect was observed for EF ratios of traffic elements at the urban community locations, while EF ratios of these elements were consistently lower than unity at the desert sites with low traffic activity. On the other hand, while the concentrations of crustal elements at desert sites were up to 3 times higher than those at the background locations, the normalized EFs remained close to unity. Among crustal elements, Fe, Li, Mn, and Ti at the urban traffic sites showed EF ratios greater than unity in $PM_{2.5}$, while their EF ratios were closer to unity in $PM_{2.5-10}$. This indicates that while Fe, Li, Mn, and Ti in $PM_{2.5-10}$ mostly originated from geogenic activities, there were also anthropogenic sources for these elements in $PM_{2.5}$ at the urban traffic locations. Figure S3 in SI presents the calculated EFs for $PM_{2.5}$ and $PM_{2.5-10}$ elements.

Figure S4 presents the Spearman correlation coefficients between AADT values and selected $PM_{2.5}$ and $PM_{2.5-10}$ elemental concentrations. As shown in Figure S4, traffic elements showed a moderate correlation ($\rho > 0.5$) with AADT, except for Zn in $PM_{2.5}$ and Pd in $PM_{2.5-10}$. On the other hand, the crustal elements were poorly correlated ($\rho < 0.4$) with AADT, except for Ti and Fe. It is important to note that while AADT can affect the concentrations of traffic elements, other factors, including wind direction and proximity to areas with high braking activity, including freeways exit ramps, and locations with stop-and-go traffic can also affect the traffic-related elemental concentrations (Abu-Allaban et al., 2003; Harrison et al., 2012). Table S10 in the SI section presents the $PM_{2.5}$ and $PM_{2.5-10}$ elemental concentrations of the selected traffic elements in all of the collected samples.

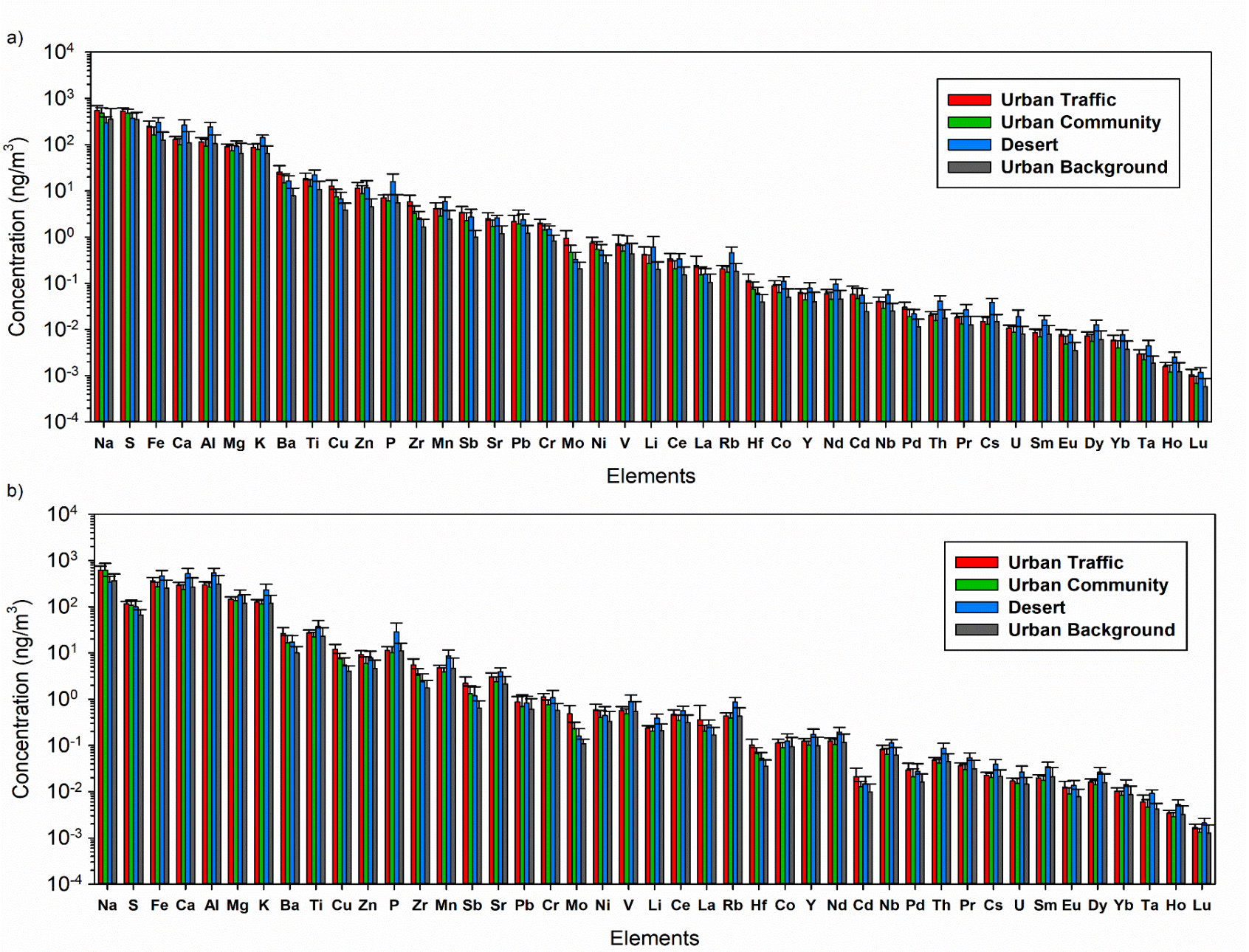

Figure 4.2. Absolute elemental concentrations in (a) $PM_{2.5}$ and (b) $PM_{2.5-10}$ at different sampling locations

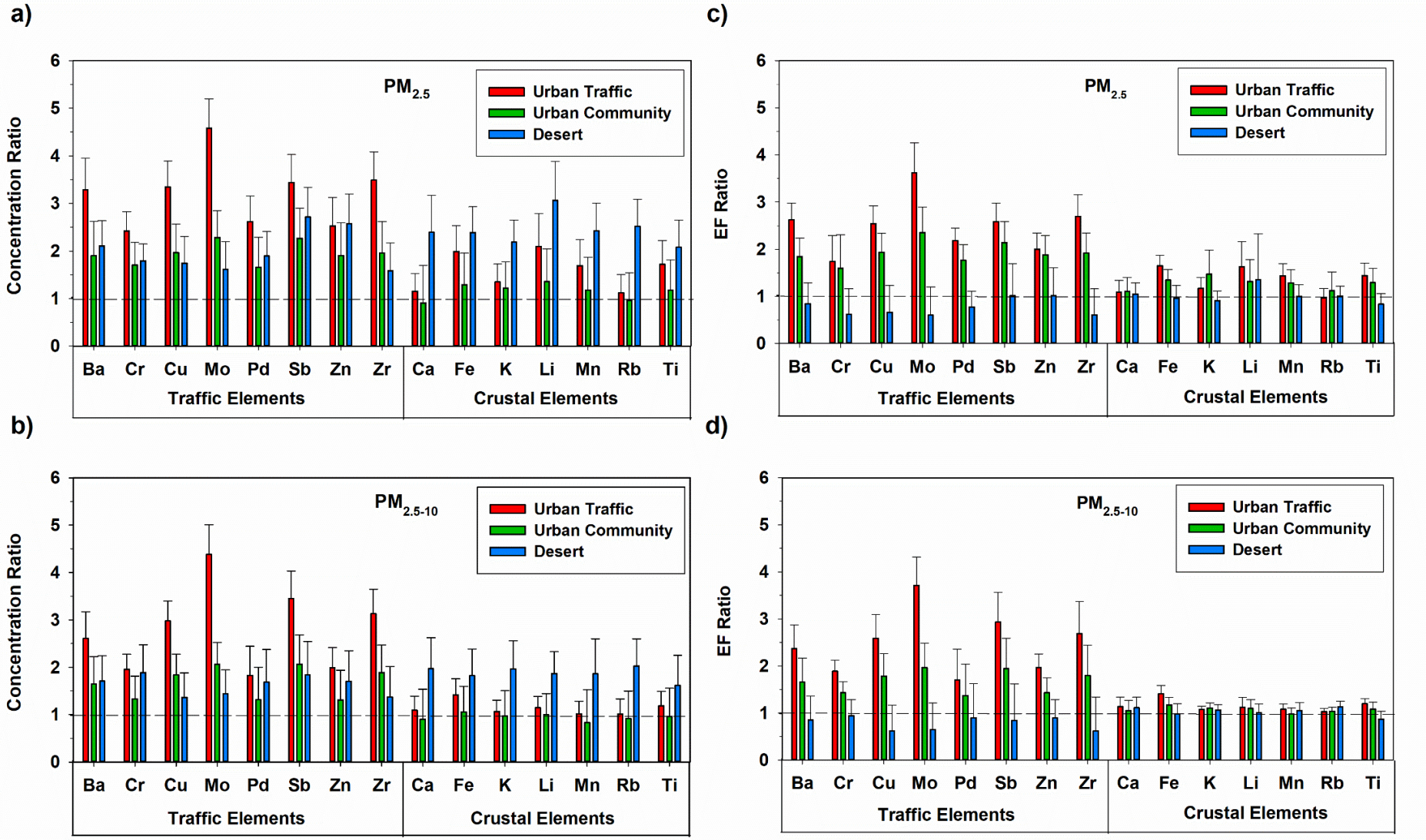

Figure 4.3. Concentration and crustal enrichment factor (EF) ratios at the urban traffic, urban community, and desert sites normalized by the values in urban background sites for the selected crustal and traffic elements (a) $PM_{2.5}$ elemental concentrations, (b) $PM_{2.5-10}$ elemental concentrations, (c) EF values of $PM_{2.5}$ elements, (d) EF values of $PM_{2.5-10}$ elements

4.4.3. Variability in the chemical composition of $PM_{2.5}$ and $PM_{2.5-10}$

Figure 4.4 shows the coefficient of variation (CV = standard deviation/mean) for $PM_{2.5}$ and $PM_{2.5-10}$ elemental concentrations. In the literature, a CV > 20% has been used as a threshold to indicate that an element is heterogeneous within an urban environment (Wilson et al., 2005). As shown in Figure 4.4, the elemental concentrations showed a notably higher variation than $PM_{2.5}$ and $PM_{2.5-10}$ mass concentrations across different sampling sites. Overall, elemental concentrations were more variable in fine particles than in coarse particles, except for a few elements such as Mo, La, P, and Ta.

Figure S5 compares the concentrations of selected $PM_{2.5}$ and $PM_{2.5-10}$ elements in the current study and other cities, including Barcelona, Florence, Lecce, and Taipei City (Fulvio Amato et al., 2016; Hsu et al., 2019; Perrone et al., 2019). As shown in Figure S5, while the $PM_{2.5}$ elemental concentrations of Al, Ba, Cu, and Sb were higher in Los Angeles, the levels of Cr, Mo, V, and Zn were relatively lower. In comparison, the $PM_{2.5-10}$ elemental concentrations in Los Angeles were within the range of the reported concentrations in other cities. It should be noted that the differences across the studies in terms of the type and number of the sampling locations, as well as the sampling seasons, could also contribute to the observed differences.

Figure S6 presents the normalized concentrations of selected elements based on the mean concentrations reported by a previous study of Southern California communities in 2008-2009 (Habre et al., 2020) (see the description of Figure S6 in the SI section for more information about the methodology comparison between the previous and current studies). With respect to the concentrations reported by Habre et al. (2020), the average $PM_{2.5}$ concentration is approximately 35% lower while the majority of $PM_{2.5}$ elemental concentrations present higher values. For instance, at the urban traffic sites, $PM_{2.5}$ elemental concentrations of Ba, Cr, Cu, Mo, Sb, and Pd

were 3.2 to 6.8 times higher than previously reported concentrations. Moreover, concentrations of Al, Ca, Dy, Fe, K, Li, Mn, Rb, and Ti in $PM_{2.5}$ were 3.1 to 5.2 times higher at the desert locations compared to the reported concentrations by Habre et al. (2020). In contrast to $PM_{2.5}$, $PM_{2.5\text{-}10}$ elemental concentrations were not substantially different from the previously reported concentrations.

At the urban traffic sites, the concentration of Li in $PM_{2.5}$ was 3.7 times higher than the previous findings, showing the largest concentration increase among the crustal elements. Moreover, crustal enrichment factors (EFs) of Li were compared to the reported average EFs at industrial and near-roadway sampling locations close to the Port of Los Angeles (Arhami et al., 2009). The EFs of Li in $PM_{2.5}$ and $PM_{2.5\text{-}10}$ have increased by factors of 5.3 and 3.0, respectively, compared to the previously reported EFs (Arhami et al., 2009). In fact, Li had the largest increase in EFs among all of the reported elements by Arhami et al. (2009). This suggests that new anthropogenic sources for Li might be introduced in the Greater Los Angeles area during the past few years. The vehicle fleet composition in Los Angele County shows that the number of electric vehicles has substantially increased from approximately 600 vehicles in 2010 to 369,300 vehicles in 2020 (California Energy Commission, 2021). Therefore, one of the probable sources of Li at the urban traffic locations could be emissions from the venting of Li-ion batteries used in electric vehicles. Li-ion batteries could degrade over time and generate gaseous chemicals (e.g., HF, C_2H_5F) and solid species (LiF) as decomposition byproducts (Sturk et al., 2019; Wilken et al., 2013). The battery degradation can be accelerated at high temperatures or with battery aging (F. Yang et al., 2018). Given the foreseeable surge in electric vehicle adoption, future studies are needed to focus on Li emissions from Li-ion batteries.

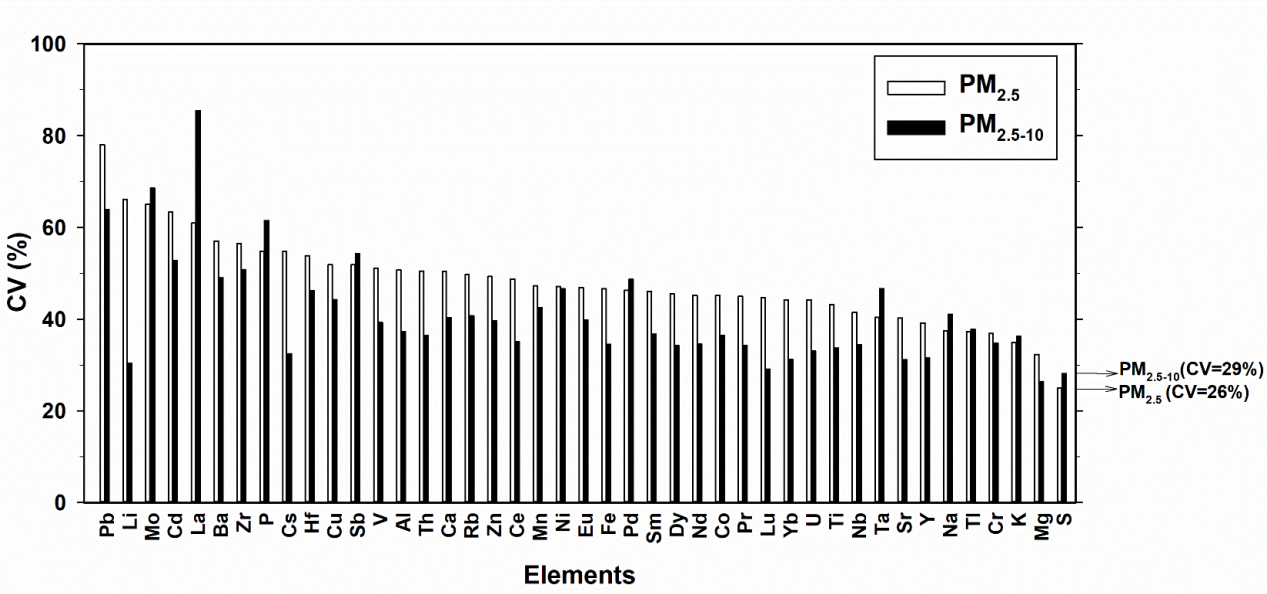

Figure 4.4. Coefficient of variation (CV) of $PM_{2.5}$ and $PM_{22.5-10}$ elements based on absolute elemental concentration

4.4.4. Associations between $PM_{2.5}$ and $PM_{2.5-10}$ chemical elements

Spearman correlation coefficients (ρ) for $PM_{2.5}$ and $PM_{2.5-10}$ elements are shown in Figure S7. The majority of elements associated with exhaust (Pd) and non-exhaust roadway emissions (Ba, Cr, Cu, Sb, Zn, Zr) showed relatively strong inter-element correlations (ρ >0.70) in $PM_{2.5}$ and $PM_{2.5-10}$. In particular, Ba, one of the common brake wear tracers, was strongly correlated (ρ >0.90) with other brake wear tracers, including Cu, Sb, and Zr in $PM_{2.5}$ and $PM_{2.5-10}$. Similarly, Pd, a tailpipe tracer, showed a strong correlation (ρ >0.90) with Ba in both $PM_{2.5}$ and $PM_{2.5-10}$. In addition, Mo showed moderate positive correlations with other traffic-related elements (ρ >0.50), except for Pd in $PM_{2.5-10}$ (ρ <0.50).

In general, crustal elements, including Al, Ca, and K, showed relatively strong inter-element correlations (ρ >0.70) in both $PM_{2.5}$ and $PM_{2.5-10}$. Relatively strong correlations (ρ >0.70) were observed for Fe with most of the traffic-related elements in $PM_{2.5}$ and $PM_{2.5-10}$. A few other elements, including Li, Mn, and Ti showed moderate to strong correlations with traffic-related

elements in $PM_{2.5}$ except for Mo and Cr. However, the correlations of Li, Mn, and Ti with traffic-related elements in $PM_{2.5-10}$ were generally weaker. This agrees with the findings in section 4.2, which discussed the effect of traffic emissions on Li, Mn, and Ti in $PM_{2.5}$.

Correlations among Mg, Na, and V were fairly strong in $PM_{2.5}$. While V has been attributed to marine fuel emissions, especially near the ports, Na and Mg are associated with sea salt aerosol (Fulvio Amato et al., 2016; Pakbin et al., 2011). The high correlation between Na, Mg, and V likely indicates mixed marine aerosols with emissions from the ports of Long Beach and Los Angeles. On the other hand, in $PM_{2.5-10}$, V was not correlated with Na, and both Mg and V showed stronger correlations with crustal elements.

It should be noted that compared with the average concentrations reported by Habre et al. (2020), the concentrations of Ni and V in $PM_{2.5}$ were lower in the current study, except for Ni at the urban traffic locations (Figure S6). During the past decade, a few regulations were implanted to control sulfur in marine fuel, which led to a decrease in Ni and V content of the fuel oils (Spada et al., 2018). These results show that while Ni and V concentrations have decreased during the past decade as a result of the implemented regulations on fuel sulfur content, their concentrations near the ports are still higher than other sampling locations. As shown in Figure S8, the majority of locations with V concentrations of 1.0 ng/m^3 and greater in fine particles were located within 8 miles of the Port of Long Beach. A similar effect was observed for Ni concentrations, which were constantly above 0.6 ng/m^3 at the sampling sites near the ports.

4.4.5. Identification of traffic-related elements using roadside enrichments (REs)

Figure 4.5 and Table S11 present the estimated roadside enrichments (REs) of the $PM_{2.5}$ and $PM_{2.5-10}$ elemental concentrations. The influence of traffic on $PM_{2.5}$ and $PM_{2.5-10}$ elemental concentrations was determined by categorizing the elements into three different classes representing strong, weak, and inconsistent REs (see Table S12). All traffic-related tracers, including Ba, Cr, Cu, Zn, Zr, Mo, Pd, and Sb were categorized as Type I elements with strong RE (RE>20% for all pairs) in both fine and coarse particles. Among traffic tracers in $PM_{2.5}$, the REs of Ba, Cu, Mo, and Zr were higher than 40% for each pair of sampling location types. Type II elements that showed weak RE (positive RE with RE<20% for at least one pair) included elements associated with marine aerosol (Na, Mg), as well as S, Pb, and some of the lanthanoid elements (Lu, Y, Eu) in fine and coarse particles. Crustal elements such as Al, Ca, Rb, as well as some of the rare-earth elements such as Nd, Sm, Dy, Ho were categorized as Type III elements with inconsistent RE (RE<0 for at least one pair).

While for $PM_{2.5}$ most of the elements were categorized as Type I, for $PM_{2.5-10}$ the majority of the elements were classified as Type III. This indicates that while several elements are dominated by traffic emissions in $PM_{2.5}$, they are likely from multiple sources in $PM_{2.5-10}$. For instance, Fe and Li were assigned to Type I in $PM_{2.5}$ due to their roadside enrichments, however in $PM_{2.5-10}$ they met the criteria for Type II and Type III elements, respectively.

Analyses of crustal enrichment factor ratios, bivariate correlation, and roadside enrichments revealed that Ba, Cr, Cu, Mo, Pd, Sb, Zn, and Zr were largely impacted by traffic emissions in both $PM_{2.5}$ and $PM_{2.5-10}$. Previously, Ba, Cr, Cu, Mo, Sb, and Zr have been associated with brake wear particles (Amato et al., 2011a; Apeagyei et al., 2011; Gietl et al., 2010), while Zn has been mostly used as a tracer of tire wear particles (Harrison et al., 2012; Wagner et al., 2018). In

addition, Pd is used in catalytic converters in internal combustion engine vehicles and has been used as a tracer for exhaust emission (Bozlaker et al., 2014; Das and Chellam, 2020). Moreover, based on the findings of the previous sections, it is inferred that Fe, Mn, Li, and Ti show a different behavior in fine and coarse particles. The previous studies have linked Mn to crustal (Cesari et al., 2016), traffic (Lawrence et al., 2013; Schauer et al., 2006; Wang et al., 2021), and industrial sources (Querol et al., 2007). While Fe has been linked to traffic (Amato et al., 2009; Schauer et al., 2006) and road dust (Pakbin et al., 2011), Ti has also been associated with mineral dust (Amato et al., 2011b) and non-exhaust traffic sources (Apeagyei et al., 2011). Therefore, these elements are associated with traffic emissions in $PM_{2.5}$, while they can be generated by other emission sources in $PM_{2.5\text{-}10}$.

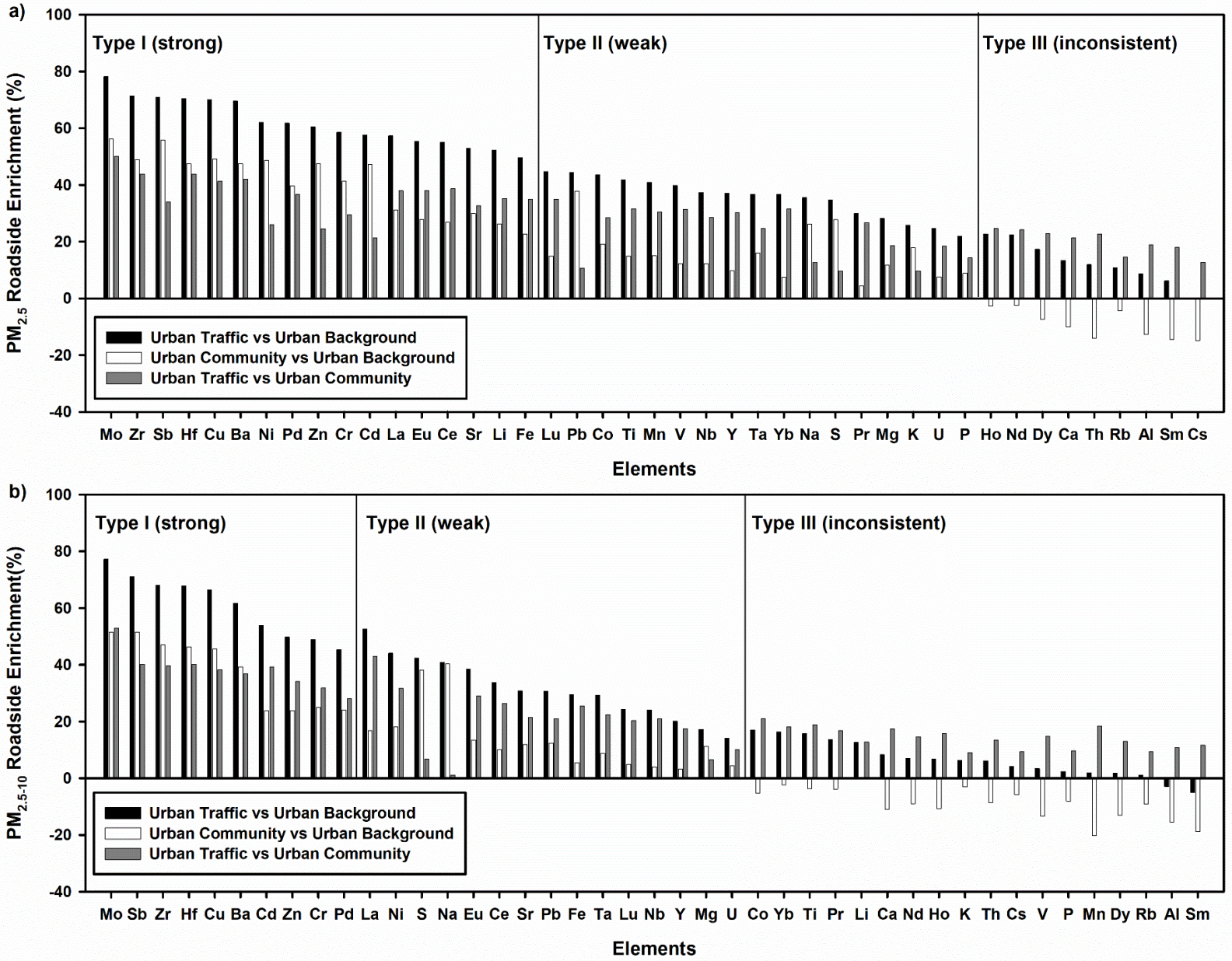

Figure 4.5. Roadside enrichments for different types of elements (a) $PM_{2.5}$, (b) $PM_{2.5-10}$

4.4.6. Source identification using principal component analysis (PCA)

The major sources of PM elements in the region were determined by applying PCA to $PM_{2.5}$ and $PM_{2.5-10}$ elemental concentration datasets. The analyses of Spearman correlation, EFs, and REs were used to help assign sources to PCA factors, and elements with PCA loadings of 0.5 and higher were used for source identification. Table S12a shows PCA results for $PM_{2.5}$ chemical speciation data. For $PM_{2.5}$, four principal components explained 88% of the total variance. The first principal component (PC1), responsible for 42% of the total variance, has substantial contributions from the crustal elements such as Rb, Al, Ca, and K, and it potentially indicates mineral dust. Moreover, this factor has robust loadings from the rare-earth elements such as Dy, Ho, Lu, Nd, Pr, Sm, Y, and Yb that are typically found in mineral dust (Fulvio Amato et al., 2016; Pakbin et al., 2011). The common traffic tracers, including brake wear tracers (Ba, Cu, Mo, Sb, and Zr), tire wear tracer (Zn), and tailpipe tracer (Pd), largely contributed to PC2, which accounts for 31% of the total variance. The elements associated with marine aerosol, including Na and Mg had a substantial contribution to PC3. This factor also explains most of the variability for V and S. While S can have various sources, including marine aerosol, V is indicative of marine fuel emissions (Fulvio Amato et al., 2016; Farahani et al., 2021; Morillas et al., 2020b; Spada et al., 2018), and therefore, PC3 is a mixed source with contributions from marine aerosol and fuel combustion, accounting for 11% of the total variance. The fourth principal component (PC4) accounts for 5% of the total variance, and it has a high contribution from Cd with lower contributions from Pb, Ni, and Zn. The association of Cd with combustion emissions and metal industries has been previously reported (Liang et al., 2017; Pacyna and Pacyna, 2001; Rossini et al., 2005). In addition, Ni and Pb have also been associated with steel production emissions and industrial fuel combustions (Querol et al., 2007), suggesting that PC4 potentially represents industrial emissions.

Table S12b presents the PCA results for $PM_{2.5-10}$ elements. Three components were extracted, which accounted for 86% of the total variance. The majority of crustal elements such as Al, Rb, Ca, as well as rare-earth elements are contained in PC1, presumably indicating mineral dust. The brake, tire, and tailpipe tracers such as Ba, Cu, Mo, Pd, Sb, Zn, and Zr are included in PC2 , which can be attributed to traffic emissions. The contribution of Na, S, and Mg to PC3 likely represents marine aerosol with some contributions from fuel combustion. The mineral dust, traffic, and marine aerosol source factors are responsible for 52%, 26%, and 8% of the total variance, respectively.

While Fe, Li, Mn, and Ti, showed comparable loadings in the mineral dust and traffic source factors in $PM_{2.5}$, they were largely attributed to the mineral dust source factor in $PM_{2.5-10}$. This agrees with the findings in the previous sections, showing that Fe, Li, Mn, and Ti originated from traffic emissions in $PM_{2.5}$, while their concentrations in $PM_{2.5-10}$ are associated with other sources. Similarly, while V was largely attributed to marine aerosol in $PM_{2.5}$, the mineral dust source factor had the highest V loading in $PM_{2.5-10}$.

4.4.7. Comparison of the major sources contributing to $PM_{2.5}$ and $PM_{2.5-10}$

To better understand the major sources of $PM_{2.5}$ and $PM_{2.5-10}$, multiple linear regression analysis was used to investigate the association of the extracted PCA source factors with $PM_{2.5}$ and $PM_{2.5-10}$ mass concentrations. Using the extracted principal component scores as independent variables and the mass concentrations of $PM_{2.5}$ and $PM_{2.5-10}$ as dependent variables, two separate stepwise linear regression models were examined. Eq (4.3) shows the resulting equation for predicting $PM_{2.5}$ concentrations:

$$\hat{Z}_1 = 0.49\,FS_1 + 0.60\,FS_2 + 0.39\,FS_3 + 0.18\,FS_4 \quad (R^2 = 0.76) \qquad (4.3)$$

Where $\hat{Z}_1$ is the standardized format of $PM_{2.5}$ mass concentration, and *FS1 – FS4* represent the factor scores for mineral dust, traffic, marine aerosol, and industrial emissions, respectively (Tables S13a) (Larsen and Baker, 2003). Based on the standardized regression coefficients and coefficients of determination (R^2), the relative contribution of various sources to $PM_{2.5}$ was estimated (Larsen and Baker, 2003; Mousavi et al., 2019; Taghvaee et al., 2019). Traffic emissions had the largest contribution (27%) to $PM_{2.5}$ mass concentrations, followed by mineral dust (23%), marine aerosol (18%), and industrial emissions (8%), while the source of 24% of $PM_{2.5}$ mass was undetermined.

Likewise, Eq (4.4) represents the linear relationship for $PM_{2.5\text{-}10}$

$$\hat{Z}_2 = 0.78\,FS_1 + 0.33\,FS_2 + 0.38\,FS_3 \quad (R^2 = 0.86) \tag{4.4}$$

Where $\hat{Z}_2$ represents the standardized format of $PM_{2.5\text{-}10}$ concentration, and *FS1 – FS3* represent the factor scores for mineral dust, traffic, and marine aerosol, respectively (Tables S13b). Mineral dust was the dominant source of coarse particles with 45% contribution to $PM_{2.5\text{-}10}$, while the contribution of marine aerosol and traffic emissions were 22% and 19%, respectively, and 14% of $PM_{2.5\text{-}10}$ mass had an undetermined source.

It is important to note that the presented source apportionment results are solely based on the $PM_{2.5}$ and $PM_{2.5\text{-}10}$ elemental concentrations, and other important components of fine and coarse particles, including carbonaceous species, have not been included in this model. Therefore, the presented source apportionment results might not provide a comprehensive picture of the factors contributing to $PM_{2.5}$ and $PM_{2.5\text{-}10}$ concentrations in the region. To assess the performance of the model at different sampling locations, an analysis was performed on the model residual values. As shown in Figure S9, the mean absolute percentage error (MAPE) values were lower at the urban

traffic and desert locations, but higher at the urban background and urban community locations (Bai et al., 2019). This finding indicates that the model has a better performance at locations with high elemental concentrations (urban traffic and desert locations), while showing a reduced prediction accuracy at locations with lower elemental concentrations. This could be due to the contribution of other sources, including secondary aerosols, which have not been accounted for in this model.

4.5. Conclusions

$PM_{2.5}$ and $PM_{2.5-10}$ samples were collected at 46 locations in the Greater Los Angeles area representing urban background, urban community, urban traffic, and desert sites. For $PM_{2.5}$, traffic emissions had the largest contribution (27%), followed by mineral dust (23%), marine aerosol (18%), and industrial emissions (8%). For $PM_{2.5-10}$, mineral dust was the dominant source with 45% contribution followed by marine aerosol (22%) and traffic emissions (19%). For elements, Ba, Cr, Cu, Mo, Pd, Sb, Zn, and Zr were affected by traffic emissions in both $PM_{2.5}$ and $PM_{2.5-10}$. However, Fe, Li, Mn, and Ti were associated with traffic emissions mostly in $PM_{2.5}$. Comparison of PM elemental concentrations to previously reported levels in the region showed a decrease in Ni and V in $PM_{2.5}$, presumably due to the regulations on fuel oil sulfur content. In contrast, large increases in crustal enrichment factors of Li in $PM_{2.5}$ and $PM_{2.5-10}$ were observed, which might be associated with Li emissions from the degradation of electric vehicle Li-ion batteries. Overall, these results provide insight into the spatial distribution of PM elements across a large metropolitan area and underscore the role of both exhaust and non-exhaust traffic emissions in generating PM elements.

5. Conclusions and future directions

In the current dissertation, first, we explored the physical and chemical characteristics of vehicular non-exhaust emissions based on the literature review. Both brake and tire wear particles were shown to have a unimodal mass-based particle size distribution with mode diameters in the range of 1-10 μm. On the other hand, brake and tire wear particle number distributions have been reported to be unimodal, bimodal, and multimodal, depending on the sampling approach and the detection limit of the applied sampling instrument. Brake wear particle number distribution was concluded to be substantially affected by brake disc temperature, brake material, and brake maintenance history, while tire wear particle number distribution can be a function of driving condition (velocity, acceleration, and deceleration rate) as well as tire condition (tire type, tread rating, temperature).

The reported brake wear $PM_{2.5}$ (0.5-5.5 mg km^{-1} Veh^{-1}) and PM_{10} (1.4-80.0 mg km^{-1} Veh^{-1}) emission factors (EFs) have been largely variable in previous studies. Similarly, the tire wear $PM_{2.5}$ and PM_{10} EFs were reported to be 0.3-11.0 and 1.9-11.0 mg km^{-1} Veh^{-1} indicating a large variation. The reported brake and tire wear $PM_{2.5}$ and PM_{10} EFs in the European and US emission inventories also showed clear discrepancies. The variability of the reported brake and tire wear PM EFs in the previous studies and emission inventories shows a clear need for a more systematic and universal method for estimating the brake and tire wear PM EFs.

Due to the large variation in the brake and tire wear PM EFs, we hypothesized that other factors, including driving style and vehicle size may also have an impact on the brake and tire wear particles. To test this hypothesis, we measured the brake and tire wear particles from three test vehicles with different masses on a predetermined driving route with multiple braking events. The on-road sampling results showed that more intense braking events lead to substantially higher

brake and tire wear $PM_{2.5}$ and PM_{10} concentrations for all test vehicles, indicating the major role of driving style on the generated brake and tire wear particles. In addition, heavier vehicles generally produced higher concentrations of brake and tire wear particles. In fact, the differences in the brake and tire wear $PM_{2.5}$ and PM_{10} concentrations between the heaviest and lightest vehicle were statistically significant, regardless of the braking intensity. The findings of this study warrant the need for an updated and customized brake and tire wear emission inventory, which takes into account various factors, including driving style, as well as vehicle weight and type.

Vehicular non-exhaust particles have been reported to be rich in metallic species. Non-exhaust PM metals, including Ba, Cr, Cu, Fe, Mn, Mo, Sb, Sn, Zn, and Zr, have been linked with oxidative stress and different adverse health outcomes, including cardiovascular cardiopulmonary diseases, cancer, and birth defects. Investigating the spatial distribution of traffic-related elements is necessary for understanding the health effect of exhaust and non-exhaust particles. For this purpose, we performed ambient measurements and collected 50 $PM_{2.5}$ and $PM_{2.5-10}$ samples at 46 various locations with different traffic volumes and geographic characteristics in the Greater Los Angeles area. Our results confirmed that the concentrations of brake wear tracers (e.g., Ba, Cr, Cu, Mo, Sb, Zr), tire wear tracer (Zn), and exhaust tracer (Pd) in fine and coarse particles were substantially higher at sampling locations with high traffic intensity than background sites. On the other hand, the concentrations of Fe, Mn, and Ti, which have been previously used as brake and tire wear tracers, were shown to be impacted by traffic emissions only in $PM_{2.5}$. In addition, the source apportionment results based on the elemental concentrations showed that while traffic was the dominant source of $PM_{2.5}$ with 27% contribution, mineral dust had the highest contribution (45%) to $PM_{2.5-10}$. Overall, the findings of this study showed that traffic-related elements, which are mostly generated by non-exhaust particles, have a larger effect on $PM_{2.5}$ than $PM_{2.5-10}$.

However, future studies are required for apportioning the contribution of exhaust and non-exhaust particles to $PM_{2.5}$ and $PM_{2.5-10}$ and their oxidative potential.

The vehicle fleet is expected to undergo a dramatic change in the upcoming decade with the fast growth in the electric vehicle (EV) market. The previous studies have shown that under abnormal battery conditions such as thermal runaway, LIBs generate toxic gases and large particles with high metallic content, and therefore, LIBs can contribute to non-exhaust emissions. However, previous studies have been limited to investigating battery emissions under abnormal conditions, and they were only focused on super-coarse particles. Therefore, the potential contribution of LIB PM emissions to $PM_{2.5}$ and PM_{10} under normal operation should be estimated in future studies. Our findings showed that Li concentration in Los Angeles has considerably increased with respect to the elemental concentrations reported in previous studies. Since the temporal analysis of regional vehicle fleet composition also showed a tremendous increase in the number of electric vehicles (EVs) in the area, we concluded that the increase in Li concentration is likely associated with the EV Li-ion battery degradation. Moreover, while the positive effect of auto electrification in reducing exhaust emissions is undeniable, non-exhaust emissions of EVs should be taken into consideration. The current EVs are equipped with relatively heavy lithium-ion batteries (LIBs), which can increase the EV brake and tire wear emissions. While regenerative braking technology can reduce the generation of brake wear particles, the decrease in the EV brake wear emissions due to the regenerative braking should be quantified through laboratory or on-road experiments in the future.

The environmental organizations have estimated the brake and tire wear PM EFs of the heavy-duty vehicles (HDVs) to be considerably higher than light-duty vehicles (LDVs) based on their developed emission inventories. It has been shown that vehicle load, number of axles, and vehicle

speed can affect the brake and tire wear EFs. Moreover, larger HDVs are mostly equipped with air brakes, which use compressed air instead of brake fluid. Air brakes are generally more sophisticated, and their mechanical design is different from hydraulic brakes used in LDVs. Finally, HDVs mostly use larger studded tires that are substantially different from the tires used in LDVs. Therefore, the brake and tire wear particles from HDVs are expected to have different physical and chemical characteristics. Despite the significant brake and tire wear EFs and the potential differences in the characteristics of their tires and brakes, none of the previous studies have directly investigated HDVs brake and tire wear emissions through on-road sampling or laboratory measurements. This clear knowledge gap can prohibit building a more detailed emission inventory for non-exhaust traffic emission sources, and it should be addressed in the forthcoming studies in this area.

Overall, despite the growing body of research that emphasizes the role of non-exhaust emissions in contributing to traffic-related air pollution, non-exhaust emissions have not been directly regulated in different parts of the world. While few attempts have been made in Europe and the US to regulate the chemical composition of brake pads and tire treads, the lack of a comprehensive regulatory strategy has prevented mitigation of these important traffic sources. We predict that the material presented in the current dissertation, combined with previous and future studies in this area, can promote the significance of non-exhaust particles and eventually provide enough evidence for regulating these emerging emission sources.

Appendix

Supplementary information for Chapter 3

S1. Isokinetic sampling

Isokinetic sampling was employed to ensure that samples accurately represent the brake and tire particles. At both brake and tire inlets, the measurement probes were aligned horizontally in line with the ambient air streamlines. The mathematical calculations for isokinetic sampling of brake and tire particles have been previously discussed (Kwak et al., 2013). In summary, it has been shown that air flow velocity behind the tire is not equal to the traveling speed of the vehicle. the air flow velocity behind the vehicle's wheel was estimated using the developed linear model (Kwak et al., 2013). Particles aspiration efficiency (η) was calculated based on the incoming flow velocity (U) and free stream flow velocity (U_0). Sampling loss due to settling, deposition loss due to curvature in sampling line, and sampling penetration efficiencies (P_t) were calculated based on the classical aerosol theories (Hinds, 1999). The sampling penetration and aspiration efficiencies at the brake and tire inlets for particles in the coarse size range are summarized in Table S1.

Table S1 Aspiration and penetration efficiencies for particles in the coarse size range based on driving speed

d_p (μm)	Driving Speed (km/h)	U (m/s)	U_0 (m/s)	η	P_t (Brake)	P_t (Tire)
2.5	50	2.7	2.7	1.00	0.97	0.98
2.5	60	2.7	3.2	1.00	0.98	0.98
2.5	70	2.7	3.7	1.01	0.98	0.98
5	50	2.7	2.7	1.00	0.89	0.92
5	60	2.7	3.2	1.02	0.90	0.92
5	70	2.7	3.7	1.04	0.90	0.93
10	50	2.7	2.7	1.01	0.58	0.67
10	60	2.7	3.2	1.06	0.57	0.64
10	70	2.7	3.7	1.12	0.55	0.61

S2. Ambient PM concentrations and brake temperatures

Table S2. Average disc brake temperature before ($T_{disc, before}$) and after ($T_{disc, after}$) each round of sampling and average $PM_{2.5}$ and PM_{10} ambient concentrations during on-road sampling for the test vehicles

	$T_{disc,before}$(°C)	$T_{disc,after}$(°C)	Ambient $PM_{2.5}$ (μg/m^3)	Ambient PM_{10} (μg/m^3)
Sentra	77	115	6	11
Accord	75	117	7	14
Suburban	77	118	7	12

S3. DustTrak collocation test results

Table S3. Results from DustTrak $PM_{2.5}$ collocation tests before and after sampling

Vehicle	Dataset	R^2	Intercept	Slope	Slope p-Value
Sentra	Before	0.92	-0.21	1.07	<0.001
	After	0.93	0.14	1.04	<0.001
Accord	Before	0.89	0.32	1.08	<0.001
	After	0.91	0.11	1.12	<0.001
Suburban	Before	0.95	0.12	1.06	<0.001
	After	0.91	-0.03	1.09	<0.001

Table S4. Results from DustTrak PM_{10} collocation tests before and after sampling

Vehicle	Dataset	R^2	Intercept	Slope	Slope p-Value
Sentra	Before	0.90	-0.12	1.10	<0.001
	After	0.93	0.13	1.07	<0.001
Accord	Before	0.94	0.14	1.11	<0.001
	After	0.88	-0.08	1.04	<0.001
Suburban	Before	0.92	0.18	1.05	<0.001
	After	0.89	0.12	1.03	<0.001

Supplementary information for Chapter 4

Table S5. Detailed description of the sampling sites including 24 locations in summer (September 2019) and 26 locations in winter (February 2020)

Type	Description	Season	Number of sampling Locations*	Cities included in sampling	Annual average daily traffic (AADT)	Average relative humidity
Urban Traffic	Near-roadway and urban locations near major roads and intersections with high traffic volume	Summer	6	Compton, Long Beach, Los Angeles	50,400 ± 32,000	60%
		Winter	7	Compton, Long Beach, Los Angeles		
Urban Community	Urban residential locations and suburban areas with moderate traffic	Summer	13	Chino Hills, Hawthorne, Pasadena, La Miranda, Los Angeles, Santa Monica	18,100 ± 17,700	61%
		Winter	15	Altadena, El Monte, Gardena, Lakewood, Los Angeles, Rancho Palos Verdes, Torrance, West Covina, Whittier		
Urban Background	Residential sites far from traffic in more secluded areas	Summer	3	Artesia, Bell Canyon, Los Angeles	7,400 ± 6,900	55%
		Winter	2	Los Angeles		
Desert	Located inland, far from the ports, in desert-dominated environment	Summer	2	Riverside, San Bernardino	N/A	39%
		Winter	2	Palmdale, Riverside		

***Four sites repeated between summer and winter**

S4. Sample analysis

PM collected on PUF and Teflon filter substrates was completely solubilized using an automated microwave-assisted acid digestion protocol (Milestone Ethos Easy with SK15 rotor), which has been discussed in detail in the previous studies (Dillner et al., 2007; Herner et al., 2006; Lough et al., 2005). For collected Teflon filter samples, a mixture of ultra-high purity acids (16 M HNO_3, 1.50 mL; 12 M HCL, 0.50 mL; and 28 M HF, 0.20 mL) was used to solubilize the PM (Herner et al., 2006). For the PUF samples (coarse fraction), the microwave chemistry used a mixture of acids and hydrogen peroxide (16 M HNO_3, 1.50 mL;12 M HCL, 0.38 mL;28M HF, 0.10; and 30% H_2O_2, 0.50 mL) to bring PM and PUF into complete solution (Dillner et al., 2007). The microwave digests were diluted to 15.0 ml (fine fraction) or 30.0 ml (coarse fraction) for SF-ICP-MS analysis. Included in each digestion batch of 33 samples were five method blanks, five Certified Reference Material (CRM) (National Institute of Standards and Technology (NIST); Urban Particulate Material-2x, San Joaquin Soil, Marine Sediment, Auto Catalyst), and two spiked blanks as previously detailed (Lough et al., 2005; Pakbin et al., 2011).

The overall uncertainty of each reported analytical measurement was estimated by error propagation of the three primary sources of uncertainty: (a) SF-ICP-MS measurement - from the standard deviation of quadruplicate measurements on each sample, (b) method blank subtraction – from the standard deviation of multiple blanks, and (c) digestion recovery - long term running precision of replicate measurements NIST CRMs (Lough et al., 2005; Pakbin et al., 2011).

The effect of relative humidity (RH) on $PM_{2.5}$ and $PM_{2.5-10}$ concentrations have been previously reported (Lou et al., 2017). As shown in Table S5, while RH at the urban traffic (60%), urban community (61%), and urban background (55%) locations were generally similar, RH values at the desert locations (39%) were lower than other sites. At the urban sites, the effect of RH on $PM_{2.5}$

and $PM_{2.5-10}$ mass concentrations is expected to be minimal due to the limited variation in RH. While RH could have an impact on the measured concentrations at the desert sites, the $PM_{2.5}$ and $PM_{2.5-10}$ concentration values were not adjusted for RH since only a small fraction of the samples (4 out of 50 samples) were collected at the desert locations. In addition, all samples were conditioned at the RH of 40±3% and the temperature of 21±1.5 ºC before the chemical speciation analysis in the lab to minimize the effect of relative humidity.

Table S6. Method detection limits (MDLs) for the measured elements

Symbol	Element	MDL (ng/m^3)	% of values below MDL	Symbol	Element	MDL (ng/m^3)	% of values below MDL
Li	Lithium	3.5E-02	0	Mo	Molybdenum	5.5E-02	2
Na	Sodium	1.4E+00	0	Pd	Palladium	2.5E-03	2
Mg	Magnesium	3.5E-01	0	Cd	Cadmium	3.0E-03	0
Al	Aluminum	9.0E-01	0	Sb	Antimony	8.5E-03	0
P	Phosphorus	2.9E-01	0	Cs	Cesium	4.0E-04	0
S	Sulfur	1.5E+00	0	Ba	Barium	2.5E-02	0
K	Potassium	6.5E-01	0	La	Lanthanum	5.5E-03	0
Ca	Calcium	1.5E+00	0	Ce	Cerium	5.5E-03	0
Ti	Titanium	1.9E-01	0	Pr	Praseodymium	1.5E-04	0
V	Vanadium	2.5E-03	0	Nd	Neodymium	6.0E-04	0
Cr	Chromium	7.0E-02	0	Sm	Samarium	2.5E-04	0
Mn	Manganese	3.0E-02	0	Eu	Europium	4.0E-04	0
Fe	Iron	2.0E-01	0	Dy	Dysprosium	2.5E-04	0
Co	Cobalt	2.5E-03	0	Ho	Holmium	4.5E-04	6
Ni	Nickel	2.2E-01	14	Yb	Ytterbium	4.5E-04	0
Cu	Copper	9.5E-02	0	Lu	Lutetium	2.0E-04	6
Zn	Zinc	4.8E-01	0	Hf	Hafnium	5.0E-03	0
Rb	Rubidium	7.5E-03	0	Ta	Tantalum	2.0E-03	0
Sr	Strontium	7.0E-02	0	Pb	Lead	2.9E-03	0
Y	Yttrium	2.5E-03	0	Th	Thorium	7.5E-04	0
Zr	Zirconium	1.6E-03	0	U	Uranium	2.5E-03	2
Nb	Niobium	2.0E-03	0				

Table S7 shows the criteria for classifying PM elements based on roadside enrichment (RE). Elements that consistently showed strong roadside enrichments (REs>20%) with traffic volume across different pairs of sampling locations were categorized as Type I elements. The RE for Type II elements were always positive, indicating an impact from traffic. However, the REs of Type II elements were not consistently strong (20% or higher), at least between one pair of the sampling sites, and therefore, these elements may originate from other anthropogenic sources as well as traffic. The RE for Type III elements were negative between at least one pair of the sampling sites, and elements in this category were not consistently impacted by traffic.

Table S7. Criteria for classifying PM elements based on roadside enrichment (RE)

	Enrichment with traffic	**Urban Community vs. Urban Background**	**Urban Traffic vs. Urban Background**	**Urban Traffic vs. Urban Community**
Type I	Strong	RE>20% for all pairs		
Type II	Weak	Positive RE with RE<20% for at least one pair		
Type III	Inconsistent	RE<0 for at least one pair		

Table S8. Average absolute concentrations of metals and trace elements in $PM_{2.5}$ and $PM_{2.5-10}$ at different sampling sites (ng/m^3)

	$PM_{2.5}$				$PM_{2.5-10}$			
	Urban traffic	Urban community	Urban background	Desert	Urban traffic	Urban community	Urban background	Desert
PM mass	10.9±1.3	8.9±2.1	6.8±2.7	10.5±2.6	9.6±0.8	8.3±2.0	7.4±3.7	12.4±3.8
Na	550.1±147.4	480.5±152.3	354.6±249.1	296.7±105.4	621.1±136	614.2±257	367±145.5	344.2±108.8
S	535.4±80.8	483.8±101.6	349.2±155.3	375.3±105.1	116±13.8	108.1±30.4	66.9±19.8	99±32.9
Fe	251.3±73.3	163.5±75.1	126.4±60	302±78.3	361.6±70.3	269.5±73.9	254.7±118.9	464.6±144.9
Ca	127.5±22	100.3±33.4	110.4±78.9	264.4±77.3	288.9±49.8	238.7±58.9	264.9±155.8	521.4±150.4
Al	114.7±26.1	93±38.8	104.8±57.4	240.7±62.9	298.4±46.5	266±63	307±172.1	541.9±136.2
Mg	90.2±13.1	73.3±22.1	64.7±42	91.6±27.7	144.7±17.4	135.1±30	120±61.3	176.9±53.2
K	87.6±15.7	79.1±26.1	64.9±29	141.7±19	126.2±16.4	114.8±22.9	118.3±58.7	232.2±74.9
Ba	25.7±9.4	14.9±8.3	7.8±3.6	16.5±4.6	26.2±9.3	16.5±7.3	10±3.7	17.1±6.5
Ti	18.4±5.8	12.6±4.9	10.7±5.4	22.3±5.9	27.3±4	22.2±5.9	23±12.2	37.3±12.8
Cu	12.8±4.2	7.5±3.3	3.8±1.6	6.7±2.6	12.1±3.2	7.5±2.4	4.1±1.2	5.5±2.3
Zn	11.5±3.6	8.7±4.4	4.6±2.1	11.8±4.9	9.2±2.1	6±2.2	4.6±2.3	7.8±3.1
P	7.1±1	6.1±2.2	5.5±2.7	16±7.2	11.3±2.5	10.3±3.4	11.1±5.2	28.6±16
Zr	5.8±2.2	3.2±1.5	1.7±0.8	2.6±0.9	5.5±2	3.3±1.2	1.8±0.8	2.4±1.1
Mn	4.1±1.4	2.9±1.3	2.4±1.3	5.9±1.4	4.8±0.6	3.9±0.9	4.7±3.1	8.7±2.9
Sb	3.4±1.1	2.3±1.1	1±0.4	2.7±1.3	2.2±0.8	1.3±0.6	0.6±0.3	1.2±0.7
Sr	2.6±0.8	1.7±0.6	1.2±0.6	2.6±0.4	3.1±0.6	2.4±0.6	2.1±0.9	3.9±0.8
Cr	2.0±0.4	1.4±0.5	0.8±0.3	1.5±0.2	1.1±0.2	0.8±0.2	0.6±0.2	1.1±0.5
Pb	2.2±0.8	1.9±1.9	1.2±0.6	2.4±0.8	0.9±0.3	0.7±0.6	0.6±0.4	0.8±0.3
Co	0.09±0.03	0.03±0.06	0.06±0.03	0.03±0.05	0.11±0.02	0.02±0.09	0.09±0.02	0.02±0.09
Mo	0.9±0.4	0.5±0.2	0.2±0.1	0.3±0.1	0.5±0.2	0.2±0.1	0.1±0.1	0.2±0.1
V	0.7±0.4	0.5±0.2	0.4±0.3	0.7±0.3	0.6±0.1	0.5±0.1	0.5±0.3	0.9±0.3
Ni	0.7±0.2	0.5±0.3	0.3±0.1	0.5±0.2	0.6±0.2	0.4±0.2	0.3±0.2	0.4±0.2
Li	0.42±0.20	0.27±0.14	0.20±0.10	0.61±0.42	0.23±0.03	0.21±0.04	0.21±0.08	0.39±0.09
Ce	0.3±0.1	0.2±0.1	0.2±0.1	0.3±0.1	0.5±0.1	0.3±0.1	0.3±0.1	0.6±0.1
Rb	0.2±0.1	0.2±0.1	0.2±0.1	0.5±0.1	0.4±0.1	0.4±0.1	0.4±0.2	0.9±0.2
La	0.2±0.1	0.2±0.1	0.1±0.1	0.2±0.1	0.4±0.4	0.2±0.1	0.2±0.1	0.3±0.1
Hf	0.13±0.05	0.08±0.03	0.04±0.02	0.06±0.02	0.11±0.03	0.03±0.07	0.07±0.02	0.02±0.04
Cd	0.058±0.029	0.047±0.032	0.025±0.013	0.056±0.021	0.021±0.011	0.013±0.003	0.010±0.005	0.015±0.006
Y	0.064±0.012	0.045±0.016	0.040±0.024	0.079±0.024	0.123±0.017	0.101±0.023	0.098±0.051	0.172±0.054
Nd	0.059±0.014	0.045±0.019	0.046±0.024	0.096±0.026	0.124±0.020	0.106±0.029	0.116±0.061	0.193±0.052
Nb	0.041±0.010	0.029±0.011	0.025±0.011	0.056±0.016	0.082±0.019	0.064±0.020	0.062±0.029	0.113±0.019
Pd	0.030±0.009	0.019±0.008	0.012±0.005	0.022±0.005	0.029±0.011	0.021±0.010	0.016±0.008	0.027±0.013
Pr	0.018±0.004	0.013±0.006	0.013±0.007	0.027±0.008	0.036±0.006	0.030±0.008	0.031±0.016	0.054±0.015
Th	0.020±0.004	0.016±0.006	0.018±0.009	0.041±0.012	0.048±0.007	0.041±0.009	0.045±0.021	0.088±0.023
Cs	0.015±0.004	0.013±0.005	0.015±0.006	0.039±0.008	0.022±0.003	0.020±0.004	0.021±0.008	0.039±0.010
Sm	0.009±0.002	0.007±0.003	0.008±0.004	0.016±0.004	0.020±0.003	0.018±0.004	0.021±0.012	0.034±0.009
Eu	0.008±0.002	0.005±0.002	0.004±0.002	0.008±0.002	0.013±0.004	0.009±0.003	0.008±0.004	0.013±0.004
Dy	0.007±0.002	0.006±0.002	0.006±0.003	0.013±0.003	0.016±0.003	0.014±0.003	0.016±0.008	0.026±0.007
Ho	0.002±0.001	0.001±0.001	0.001±0.001	0.003±0.001	0.003±0.001	0.003±0.001	0.003±0.002	0.005±0.001
Yb	0.006±0.002	0.004±0.002	0.004±0.002	0.008±0.002	0.010±0.002	0.008±0.002	0.009±0.001	0.014±0.001
Lu	0.001±0.001	0.001±0.001	0.001±0.001	0.001±0.001	0.002±0.001	0.001±0.001	0.001±0.001	0.002±0.001
Ta	0.003±0.001	0.002±0.001	0.002±0.001	0.004±0.001	0.006±0.002	0.005±0.002	0.004±0.001	0.009±0.002
U	0.011±0.002	0.009±0.003	0.008±0.004	0.019±0.007	0.017±0.003	0.015±0.004	0.015±0.006	0.027±0.009

Average concentration ±s standard deviation (ng/m^3)

Table S9. Average normalized concentrations of metals and trace elements in $PM_{2.5}$ and $PM_{2.5-10}$ at different sampling sites (μg/g)

	$PM_{2.5}$				$PM_{2.5-10}$			
	Urban traffic	Urban community	Urban background	Desert	Urban traffic	Urban community	Urban background	Desert
Na	28078.3±5774	48553.8±16616.5	57801.8±24526.8	51243.9±15915.5	27567.9±2491.3	52220.1±7323.9	78505.7±36421.8	64859.4±15190.3
S	35863.1±4092.3	51142±7268.3	58044.6±21031.4	49758.1±10163.9	8075.4±1514.8	9872.6±1912.5	13565.4±4006	12102.8±1569.1
Fe	28737.2±1256.2	17587.5±2661.7	18359.4±6861.2	22729.1±5151.1	37374.1±3106.2	34845.2±2703.2	34854.8±16272.6	37406.2±5712.7
Ca	25176.3±3059.3	14429.4±5054.8	11415.7±3169.1	11680.5±1586	42367.1±2950.4	34717.9±5087	30801±13133.3	29915.1±4093.9
Al	23577.3±4511.8	14014.5±3709.5	10480.2±3619.4	10455.9±1881.5	45171.3±5767.1	40608.1±3846.9	35085.9±18712.9	30967.7±3955.9
Mg	8734±1193.2	8595±2604.9	8514.4±2689.2	8298±1118	14311.1±478.1	16209.3±891.9	17535.7±7482.4	15081±1826.4
K	14253.4±3159.9	9052.9±1520.1	9810.1±7589.9	8015.4±987	18743.4±886.1	15995.2±1053	15202.9±8309.6	13107.8±1366.1
Ba	1568.2±167.4	1102.8±265.2	1625.3±672.6	2318.4±716.9	1387.5±333.5	1475.4±455	2099.2±1084.1	2695.1±887.5
Ti	2147.1±304.5	1485.4±234	1438.3±532.9	1665.3±412	2971.7±337.2	3115.1±353.3	2871.3±1290.7	2839.5±347.9
Cu	614.4±147.4	557.9±98.4	843.5±286.6	1165.3±330.9	426.5±120.6	625.4±196.7	968±484.3	1252.7±327.9
Zn	1081.8±293.6	647.5±125.7	964.2±374.2	1038.1±228.5	612.1±163.3	631.7±125.5	753.7±277	946.6±180.5
P	1480.3±417	781.8±157.2	703.8±267	652.8±100.3	2132.9±635	1546.4±379.4	1326.9±653.9	1187.4±286.5
Zr	242.7±44.2	238.4±73.7	368.3±156.1	525.1±184.4	187.9±64.2	271.9±122.2	444.4±308.6	569.9±202.1
Mn	569.1±46	334.7±63.6	323.3±113.2	372.2±90.2	699.9±94	605.5±100.1	505±223.9	495.2±52.7
Sb	245.3±86.7	146.6±28.7	247.9±84.6	310.3±80.1	91.9±42.7	99.7±43	169.6±92.3	229.1±79.2
Sr	255.3±38.1	165.5±30.8	211.7±158.6	232.3±60.1	331.6±46.8	294±41.6	315.9±158.8	318.3±52
Pb	223.7±36.9	170.1±48.8	211.6±162.3	196.6±65.8	65±20.1	79.8±24.3	82.5±50.3	91.2±26.7
Cr	147.4±21.8	128.5±15.8	183.1±175.8	184.7±31.8	82.4±17.5	80.6±7.8	95.5±28.5	115.7±16.1
Mo	30.1±8.8	30±3.6	52.3±14.8	85±35.6	12.2±3.9	17.3±5.4	28.6±11.8	50±24.4
Ni	48.7±6.1	41.7±5.2	62.6±27.6	66.8±17.9	32.4±16.7	48.7±28.3	51.3±25.2	61.6±22.6
V	69.1±19.3	66±27.4	58.1±19.9	66.4±34.1	71.1±9.7	72.5±14.2	62.3±24.6	59.5±14.3
Li	78.6±82.5	28.9±7.9	30.6±13.8	38.3±17.7	32.3±4.2	28.7±3.1	27.5±15.1	24.6±2.8
Ce	31.6±4.4	21.2±3.3	22.9±7.8	31±9	47.1±7.8	43.2±2.4	45±21.5	49.5±13.6
La	14.8±2.1	14.9±4.8	17.4±9	23.3±16.2	23±4.1	23.9±3.4	26.4±12.4	38.3±40.9
Rb	44±8.4	25.4±5.3	21±12.3	18.7±3.1	71.6±6.6	57.3±4.3	51.5±27.5	44.9±5.5
Hf	5.5±1	5.7±1.4	8.4±3.3	12.1±3.8	4.3±0.8	5.5±2.1	8.8±5.5	11.5±3.5
Co	10.5±0.4	6.9±1	7±2.6	7.9±1.5	12.4±1.2	12.4±1.8	11.4±4.7	11.7±1.8
Y	7.3±0.6	5.3±1.6	4.9±1.3	5.8±0.7	13.8±2	13.1±0.9	13.1±5.8	12.7±1.5
Nd	9.21±1.23	6.28±1.33	5.07±1.82	5.39±1.02	15.98±2.54	15.57±0.97	13.85±6.85	12.9±1.78
Cd	5.46±1.71	3.55±1.24	6.62±11.37	5.15±2.16	1.16±0.38	1.33±0.15	1.72±1.19	2.16±0.95
Nb	5.5±1.21	3.59±0.41	3.33±1.23	3.69±0.69	9.84±2.32	8.52±0.71	8.54±5.19	8.43±1.6
Pd	2.08±0.09	1.6±0.3	2.21±1.1	2.73±0.6	2.28±0.89	2.26±1.04	2.78±1.88	3.03±1.1
Th	3.96±0.68	2.43±0.72	1.77±0.63	1.85±0.33	7.39±1.58	6.15±0.78	5.52±3.17	4.95±0.55
Pr	2.56±0.38	1.73±0.38	1.48±0.5	1.64±0.28	4.48±0.83	4.23±0.21	3.92±1.9	3.77±0.49
Cs	3.77±0.28	2.18±0.52	1.54±0.81	1.36±0.37	3.21±0.29	3±0.41	2.77±1.88	2.32±0.31
U	1.83±0.52	1.17±0.33	1±0.34	0.99±0.2	2.16±0.54	2.08±0.45	2±0.98	1.77±0.3
Sm	1.58±0.22	1.07±0.25	0.8±0.32	0.77±0.14	2.85±0.49	2.76±0.28	2.34±1.32	2.08±0.32
Eu	0.75±0.02	0.48±0.07	0.53±0.19	0.71±0.15	1.1±0.19	1.05±0.18	1.16±0.62	1.3±0.38
Dy	1.23±0.14	0.81±0.21	0.64±0.23	0.66±0.13	2.15±0.19	2.13±0.17	1.85±0.95	1.68±0.24
Yb	0.72±0.04	0.5±0.11	0.45±0.15	0.53±0.13	1.15±0.05	1.14±0.02	1.11±0.59	1.06±0.16
Ta	0.42±0.07	0.27±0.04	0.26±0.11	0.26±0.04	0.9±0.52	0.64±0.22	0.63±0.5	0.61±0.24
Ho	0.24±0.02	0.16±0.04	0.13±0.04	0.14±0.02	0.43±0.03	0.42±0.02	0.37±0.19	0.35±0.04
Lu	0.11±0	0.07±0.02	0.07±0.02	0.09±0.02	0.17±0.01	0.17±0	0.19±0.2	0.17±0.03

Average concentration ±s standard deviation (μg/g)

Table S10. Elemental concentrations of selected traffic elements in the collected samples

Table S10a. Selected $PM_{2.5}$ elemental concentrations (ng/m^3)

Sample	Sampling Location	Ba	Cr	Cu	Mo	Pd	Sb	Zn	Zr
1	Urban Traffic	19.105	1.493	8.067	0.563	0.027	2.131	9.197	3.608
2	Urban Traffic	16.565	1.546	9.181	0.669	0.023	3.093	8.726	3.771
3	Urban Traffic	30.497	1.959	15.237	0.646	0.031	3.690	11.530	7.838
4	Urban Traffic	13.347	2.383	7.890	0.488	0.017	2.686	6.624	3.060
5	Urban Traffic	32.198	1.955	17.050	0.811	0.036	3.467	12.801	8.224
6	Urban Traffic	27.276	2.179	15.009	0.781	0.028	2.910	11.159	7.342
7	Urban Traffic	30.085	2.881	14.418	1.382	0.039	4.999	18.671	5.254
8	Urban Traffic	40.339	2.176	19.516	1.462	0.037	4.663	16.293	8.896
9	Urban Traffic	40.656	2.681	17.033	1.780	0.051	5.685	16.246	7.574
10	Urban Traffic	33.416	1.815	16.152	0.597	0.036	3.816	12.063	8.174
11	Urban Traffic	19.505	1.579	11.113	0.451	0.024	2.404	7.745	4.620
12	Urban Traffic	20.211	2.079	10.744	1.121	0.025	3.529	11.525	4.166
13	Urban Traffic	11.127	1.517	5.473	1.489	0.018	1.563	7.340	2.567
14	Urban Community	18.001	1.631	8.694	0.661	0.023	2.740	10.559	3.932
15	Urban Community	12.730	1.358	6.193	0.453	0.018	2.637	10.461	2.528
16	Urban Community	18.315	1.175	9.670	0.366	0.023	2.246	6.590	4.292
17	Urban Community	10.585	1.318	6.497	0.400	0.014	1.866	5.120	2.729
18	Urban Community	8.944	1.462	5.323	0.457	0.013	1.510	5.316	2.042
19	Urban Community	28.317	1.820	13.376	0.874	0.031	3.745	17.894	5.602
20	Urban Community	7.689	0.916	5.044	0.349	0.011	1.621	7.130	2.020
21	Urban Community	5.116	2.138	3.112	0.152	0.014	0.670	3.931	1.705
22	Urban Community	5.693	0.939	4.149	0.265	0.009	0.959	4.704	1.623
23	Urban Community	18.332	1.586	8.844	0.521	0.022	2.708	9.357	4.118
24	Urban Community	12.804	1.856	6.821	0.593	0.019	2.366	8.731	2.609
25	Urban Community	2.918	0.212	2.691	0.278	0.006	0.793	2.703	0.792
26	Urban Community	15.281	1.456	8.747	0.375	0.021	2.348	7.626	4.104
27	Urban Community	15.925	1.413	8.786	0.494	0.021	2.380	7.843	4.073
28	Urban Community	16.978	1.311	9.881	0.403	0.021	1.997	8.877	4.404
29	Urban Community	12.387	1.783	6.823	0.472	0.015	2.002	8.240	2.624
30	Urban Community	6.469	0.914	3.737	0.377	0.010	1.079	3.843	1.409
31	Urban Community	11.863	1.524	5.310	0.443	0.017	2.692	9.668	2.403
32	Urban Community	11.848	1.567	6.188	0.317	0.014	2.242	8.277	2.569
33	Urban Community	31.563	2.234	13.119	0.806	0.034	4.757	19.701	5.392
34	Urban Community	30.995	1.746	11.568	0.735	0.034	3.489	14.285	5.255
35	Urban Community	1.579	0.220	1.776	0.087	0.003	0.356	1.466	0.555
36	Urban Community	26.892	2.143	12.057	0.695	0.031	4.203	15.726	4.709
37	Urban Community	13.209	1.195	7.100	0.362	0.020	1.659	6.929	3.763
38	Urban Community	11.526	1.115	5.609	0.334	0.016	1.564	7.638	2.533
39	Urban Community	8.286	1.010	4.869	0.408	0.013	1.212	4.129	2.042
40	Urban Community	23.854	1.613	10.962	0.816	0.029	4.247	12.979	4.915
41	Urban Community	29.081	2.173	14.017	0.646	0.035	3.276	13.701	6.054
42	Urban Background	10.125	1.099	4.761	0.273	0.017	1.154	6.764	1.754
43	Urban Background	5.866	0.801	3.212	0.175	0.009	0.833	3.072	1.239
44	Urban Background	1.736	0.340	1.058	0.061	0.002	0.289	1.222	0.396
45	Urban Background	10.119	0.959	5.221	0.260	0.014	1.333	5.177	2.658
46	Urban Background	11.270	0.977	4.938	0.259	0.014	1.386	6.582	2.232
47	Desert	17.770	1.612	6.917	0.330	0.024	2.739	11.492	2.837
48	Desert	17.047	1.496	7.251	0.390	0.024	2.690	12.490	2.817
49	Desert	9.222	1.098	2.634	0.111	0.013	0.878	4.669	1.141
50	Desert	21.846	1.766	9.938	0.497	0.026	4.540	18.364	3.679

Table S10b. Selected $PM_{2.5-10}$ elemental concentrations (ng/m^3)

Sample	Sampling Location	Ba	Cr	Cu	Mo	Pd	Sb	Zn	Zr
1	Urban Traffic	17.537	0.978	7.779	0.312	0.019	1.355	6.644	3.181
2	Urban Traffic	18.455	1.019	10.268	0.544	0.020	1.667	8.108	3.920
3	Urban Traffic	31.985	1.279	14.524	0.380	0.032	2.831	9.184	7.690
4	Urban Traffic	15.988	0.905	10.516	0.354	0.014	1.407	6.534	4.176
5	Urban Traffic	32.600	1.190	15.633	0.474	0.038	2.833	10.150	7.974
6	Urban Traffic	28.380	1.033	13.916	0.497	0.032	2.557	8.927	7.095
7	Urban Traffic	27.802	1.177	10.178	0.363	0.034	2.287	9.599	4.729
8	Urban Traffic	35.466	1.255	15.183	1.037	0.039	3.183	11.747	7.142
9	Urban Traffic	38.023	1.504	13.368	0.462	0.046	2.978	12.356	6.270
10	Urban Traffic	42.559	1.351	17.721	0.381	0.053	3.582	12.521	8.670
11	Urban Traffic	19.188	0.930	10.808	0.274	0.019	1.450	8.015	3.879
12	Urban Traffic	20.632	1.161	11.404	0.963	0.020	1.795	9.216	3.950
13	Urban Traffic	11.406	0.749	5.680	0.234	0.017	0.939	6.018	2.719
14	Urban Community	23.658	0.902	9.099	0.285	0.030	1.997	7.204	4.547
15	Urban Community	11.385	0.713	5.501	0.181	0.014	0.926	5.235	2.200
16	Urban Community	17.279	0.886	9.211	0.230	0.017	1.502	7.620	3.980
17	Urban Community	11.750	0.731	7.460	0.232	0.010	0.934	4.722	3.043
18	Urban Community	13.598	0.839	8.531	0.351	0.015	1.129	5.990	3.350
19	Urban Community	36.286	1.160	14.220	0.518	0.043	2.835	11.469	6.541
20	Urban Community	15.344	0.756	6.090	0.155	0.022	1.201	5.740	3.053
21	Urban Community	6.639	0.231	3.225	0.072	0.011	0.553	1.894	1.930
22	Urban Community	16.499	0.904	8.895	0.367	0.017	1.393	7.745	3.160
23	Urban Community	19.839	0.698	8.300	0.258	0.024	1.684	6.314	4.113
24	Urban Community	7.462	0.526	4.290	0.121	0.010	0.519	3.635	1.639
25	Urban Community	7.205	0.451	4.170	0.147	0.010	0.570	3.062	1.521
26	Urban Community	24.252	0.801	9.290	0.234	0.031	1.909	6.772	4.739
27	Urban Community	18.842	0.753	8.366	0.229	0.023	1.483	5.399	4.121
28	Urban Community	13.721	0.747	8.062	0.222	0.014	1.161	6.009	3.390
29	Urban Community	14.330	0.762	7.822	0.319	0.014	1.186	7.655	3.041
30	Urban Community	8.648	0.742	5.365	0.221	0.011	0.717	3.749	1.877
31	Urban Community	11.329	0.562	4.246	0.115	0.022	0.897	4.099	1.918
32	Urban Community	13.016	0.775	6.662	0.192	0.015	1.049	5.397	2.593
33	Urban Community	24.541	1.167	8.332	0.228	0.034	1.843	9.426	3.659
34	Urban Community	27.589	0.918	8.862	0.222	0.033	1.984	6.808	4.348
35	Urban Community	7.119	0.576	3.875	0.104	0.009	0.395	3.197	1.566
36	Urban Community	23.119	1.071	7.907	0.207	0.035	1.599	9.520	3.450
37	Urban Community	14.695	0.652	7.081	0.181	0.022	1.125	4.591	3.644
38	Urban Community	13.685	0.570	5.978	0.150	0.021	1.029	5.121	2.619
39	Urban Community	10.231	0.658	6.299	0.237	0.013	0.904	4.300	2.363
40	Urban Community	23.833	0.880	10.109	0.253	0.038	2.150	7.738	4.645
41	Urban Community	26.662	0.906	11.588	0.335	0.036	2.524	8.581	5.727
42	Urban Background	12.380	0.979	4.191	0.111	0.020	0.567	8.679	1.462
43	Urban Background	6.874	0.504	3.332	0.098	0.009	0.400	2.874	1.193
44	Urban Background	4.542	0.276	2.197	0.069	0.005	0.325	2.193	0.831
45	Urban Background	11.642	0.507	5.394	0.140	0.022	0.993	3.611	2.925
46	Urban Background	14.728	0.592	5.159	0.133	0.025	0.932	5.640	2.356
47	Desert	17.957	1.560	6.467	0.171	0.022	1.030	8.864	2.470
48	Desert	15.607	1.095	5.989	0.175	0.021	1.136	9.925	2.347
49	Desert	8.334	0.340	1.673	0.046	0.016	0.347	2.549	0.810
50	Desert	26.651	1.328	7.989	0.242	0.050	2.217	10.015	3.998

Table S11. Roadside enrichments (REs) of (a) $PM_{2.5}$ elements, and (b) $PM_{2.5-10}$ elements

Table S11a. $PM_{2.5}$ RE			
Type I	UC vs. UB	UT vs. UB	UT vs. UC
Li	26%	**52%**	35%
Cr	**41%**	**59%**	30%
Fe	23%	**50%**	35%
Ni	**49%**	**62%**	26%
Cu	**49%**	**70%**	**41%**
Zn	**48%**	**60%**	25%
Sr	30%	**53%**	33%
Zr	**49%**	**71%**	**44%**
Mo	**56%**	**78%**	**50%**
Pd	40%	**62%**	37%
Cd	**47%**	**58%**	21%
Sb	**56%**	**71%**	34%
Ba	**47%**	**70%**	**42%**
La	31%	**57%**	38%
Ce	27%	**55%**	39%
Eu	28%	**55%**	38%
Hf	**47%**	**70%**	**44%**
Type II	UC vs UB.	UT vs. UB	UT vs. UC
Na	26%	36%	13%
Mg	12%	28%	19%
P	9%	22%	14%
S	28%	35%	10%
K	18%	26%	10%
Ti	15%	**42%**	32%
V	12%	40%	31%
Mn	15%	**41%**	30%
Co	19%	**44%**	29%
Y	10%	37%	30%
Nb	12%	37%	29%
Pr	4%	30%	27%
Yb	7%	37%	32%
Lu	15%	**45%**	35%
Ta	16%	37%	25%
Pb	38%	**44%**	11%
U	8%	25%	19%
Type III	UC vs UB.	UT vs. UB	UT vs. UC
Al	-13%	9%	19%
Ca	-10%	13%	21%
Rb	-4%	11%	15%
Cs	-15%	0%	13%
Nd	-2%	22%	24%
Sm	-14%	6%	18%
Dy	-7%	17%	23%
Ho	-3%	23%	25%
Th	-14%	12%	23%

REs> 40% are bolded

UT: Urban traffic, UC: Urban community, UB: Urban background

Table S11b. $PM_{2.5-10}$ RE			
Type I	UC vs UB.	UT vs. UB	UT vs. UC
Cr	25%	**49%**	32%
Cu	**46%**	**66%**	38%
Zn	24%	**50%**	34%
Zr	**47%**	**68%**	40%
Mo	**52%**	**77%**	**53%**
Pd	24%	**45%**	28%
Cd	24%	**54%**	39%
Sb	**52%**	**71%**	**40%**
Ba	39%	**62%**	37%
Hf	**46%**	**68%**	**40%**
Type II	UC vs UB.	UT vs. UB	UT vs. UC
Na	**40%**	**41%**	1%
Mg	11%	17%	7%
S	38%	**42%**	7%
Fe	5%	30%	25%
Ni	18%	**44%**	32%
Sr	12%	31%	21%
Y	3%	20%	18%
Nb	4%	24%	21%
La	17%	**53%**	**43%**
Ce	10%	34%	26%
Eu	13%	39%	29%
Lu	5%	24%	20%
Ta	9%	29%	22%
Pb	12%	31%	21%
U	4%	14%	10%
Type III	UC vs UB.	UT vs. UB	UT vs. UC
Li	0%	13%	13%
Al	-15%	-3%	11%
P	-8%	2%	10%
K	-3%	6%	9%
Ca	-11%	8%	17%
Ti	-4%	16%	19%
V	-13%	3%	15%
Mn	-20%	2%	18%
Co	-5%	17%	21%
Rb	-9%	1%	9%
Cs	-6%	4%	9%
Pr	-4%	14%	17%
Nd	-9%	7%	15%
Sm	-19%	-5%	12%
Dy	-13%	2%	13%
Ho	-11%	7%	16%
Yb	-2%	16%	18%
Th	-8%	6%	13%

REs> 40% are bolded

UT: Urban traffic, UC: Urban community, UB: Urban background

Table S12. Varimax normalized principal component loadings (a) $PM_{2.5}$, and (b) $PM_{2.5-10}$

Table S12a. Varimax normalized principal component loadings in $PM_{2.5}$

	Principal component loadings			
	Mineral dust	Traffic	Marine aerosol	Industrial
Rb	**0.97**	0.08	0.01	0.14
Th	**0.97**	0.17	0.07	0.02
Sm	**0.97**	0.21	0.03	0.07
Al	**0.96**	0.19	0.03	0.08
Ca	**0.95**	0.15	0.13	0.06
Dy	**0.94**	0.32	0.05	0.04
P	**0.91**	0.06	0.14	0.12
Nd	**0.91**	0.38	0.07	0.09
Ho	**0.90**	0.39	0.10	0.04
U	**0.90**	0.17	0.09	-0.11
Cs	**0.90**	0.14	-0.27	0.08
Pr	**0.86**	0.45	0.11	0.13
Nb	**0.81**	0.52	0.06	0.11
Ta	**0.78**	0.35	0.20	0.18
Yb	**0.78**	0.60	0.07	-0.01
Y	**0.76**	0.48	0.37	0.05
K	**0.76**	0.33	0.04	0.36
Mn	**0.76**	0.53	0.09	0.32
Ti	**0.72**	0.58	0.14	0.19
Fe	0.69	0.69	0.07	0.16
Co	0.62	0.42	0.23	0.40
Zr	0.15	**0.97**	0.01	-0.10
Hf	0.16	**0.97**	0.05	-0.12
Cu	0.20	**0.97**	0.09	0.00
Ba	0.29	**0.94**	0.06	0.09
Pd	0.34	**0.88**	0.17	0.18
Sb	0.32	**0.82**	0.16	0.33
Eu	0.58	**0.78**	0.13	0.07
Zn	0.43	**0.74**	0.09	0.41
Sr	0.49	**0.74**	0.15	0.23
Cr	0.21	**0.74**	0.25	0.35
Mo	0.00	**0.73**	0.44	0.30
Lu	0.68	**0.72**	0.06	-0.04
Cd	0.21	0.65	-0.22	0.61
Ce	0.51	0.63	0.30	0.19
Pb	0.27	0.53	-0.13	0.45
Li	0.35	0.51	-0.30	-0.13
Ni	0.15	0.50	0.41	0.41
Na	-0.14	-0.01	**0.94**	-0.01
S	-0.01	0.17	**0.92**	0.02
V	0.33	-0.04	**0.80**	0.18
Mg	0.51	0.28	**0.72**	0.01
La	0.07	0.13	0.69	-0.13
% of variance	41.67	30.92	10.61	4.77
Cumulative %	41.67	72.59	83.20	87.97
Eigenvalue	17.92	13.30	4.56	2.05

Bold: loadings larger than 0.7, Underlined: loadings between 0.5 and 0.7

Table S12b. Varimax normalized principal component loadings in $PM_{2.5-10}$

	Principal component loadings		
	Mineral dust	Traffic	Marine aerosol
Al	**0.99**	0.05	0.08
Rb	**0.98**	0.10	0.00
Sm	**0.98**	0.04	0.08
Dy	**0.98**	0.12	0.09
Mn	**0.96**	0.07	0.15
Nd	**0.96**	0.21	0.07
Ho	**0.96**	0.24	0.07
Th	**0.95**	0.14	0.01
K	**0.95**	0.03	0.21
Cs	**0.93**	0.20	-0.05
Pr	**0.93**	0.29	0.07
Li	**0.93**	0.25	0.06
Ti	**0.90**	0.30	0.17
Yb	**0.90**	0.38	0.08
Y	**0.89**	0.37	0.16
Ca	**0.89**	0.30	0.03
P	**0.88**	-0.07	0.13
Co	**0.87**	0.25	0.29
U	**0.87**	0.08	0.16
V	**0.86**	-0.15	0.43
Lu	**0.82**	0.48	0.02
Fe	**0.80**	0.57	0.09
Nb	**0.77**	0.56	-0.12
Sr	**0.72**	0.62	0.11
Ce	**0.70**	0.50	0.15
Sb	0.06	**0.99**	0.03
Ba	0.18	**0.97**	-0.01
Zr	-0.04	**0.97**	0.03
Cu	0.00	**0.94**	0.19
Hf	-0.04	**0.93**	0.11
Pd	0.28	**0.88**	-0.18
Zn	0.48	**0.83**	0.18
Eu	0.54	**0.82**	-0.09
Cr	0.55	**0.72**	0.31
Mo	-0.07	**0.70**	0.35
Cd	0.37	0.55	0.31
Pb	0.47	0.50	-0.01
Ta	0.43	0.45	-0.18
Na	-0.22	0.02	**0.89**
S	0.04	0.34	**0.78**
Ni	0.30	0.11	**0.73**
Mg	0.61	0.07	**0.72**
La	0.25	-0.04	0.33
% of variance	51.68	25.60	8.27
Cumulative %	51.68	77.28	85.55
Eigenvalue	22.22	11.01	3.56

Bold: loadings larger than 0.7, Underlined: loadings between 0.5 and 0.7

Table S13. Results of multiple linear regression analysis for mass concentrations of (a) $PM_{2.5}$ and (b) $PM_{2.5-10}$

(a) $PM_{2.5}$

	Unstandardized coefficients	Standardized coefficients	t	Sig.	R^2
	B	Beta			
Constant	9.35		33.71	<0.001	0.76
Traffic	1.44	0.60	8.53	<0.001	
Mineral dust	1.19	0.49	7.07	<0.001	
Marine aerosol	0.94	0.39	5.60	<0.001	
Industrial	0.43	0.18	2.57	0.014	

(b) $PM_{2.5-10}$

	Unstandardized coefficients	Standardized coefficients	t	Sig.	R^2
	B	Beta			
Constant	8.91		64.91	<0.001	0.86
Mineral dust	2.01	0.78	14.50	<0.001	
Marine aerosol	0.97	0.38	6.98	<0.001	
Traffic	0.85	0.33	6.15	<0.001	

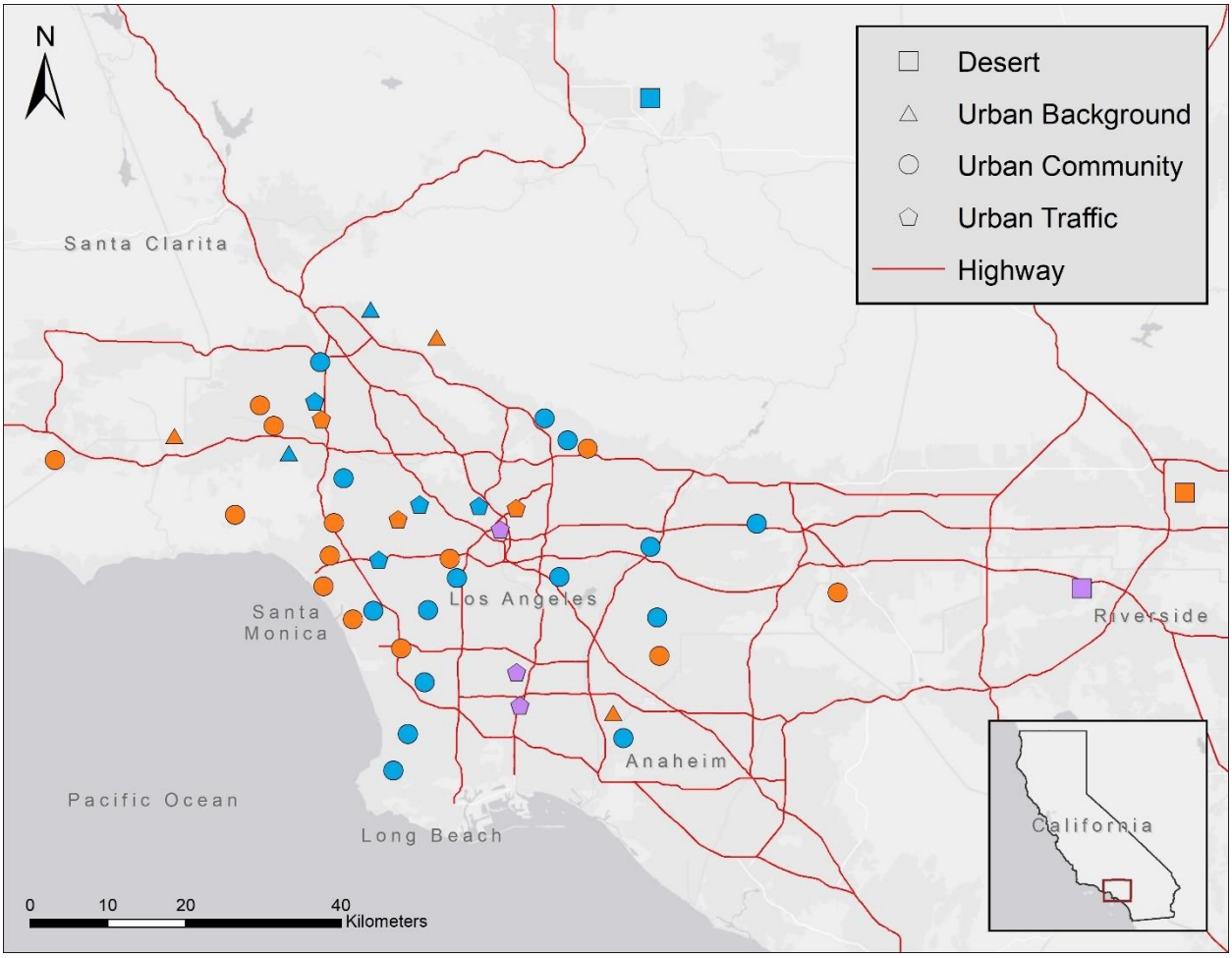

Figure S1. Location of the sampling sites in the Greater Los Angeles area for summer (orange), winter (blue), and repeated samples in summer and winter (purple)

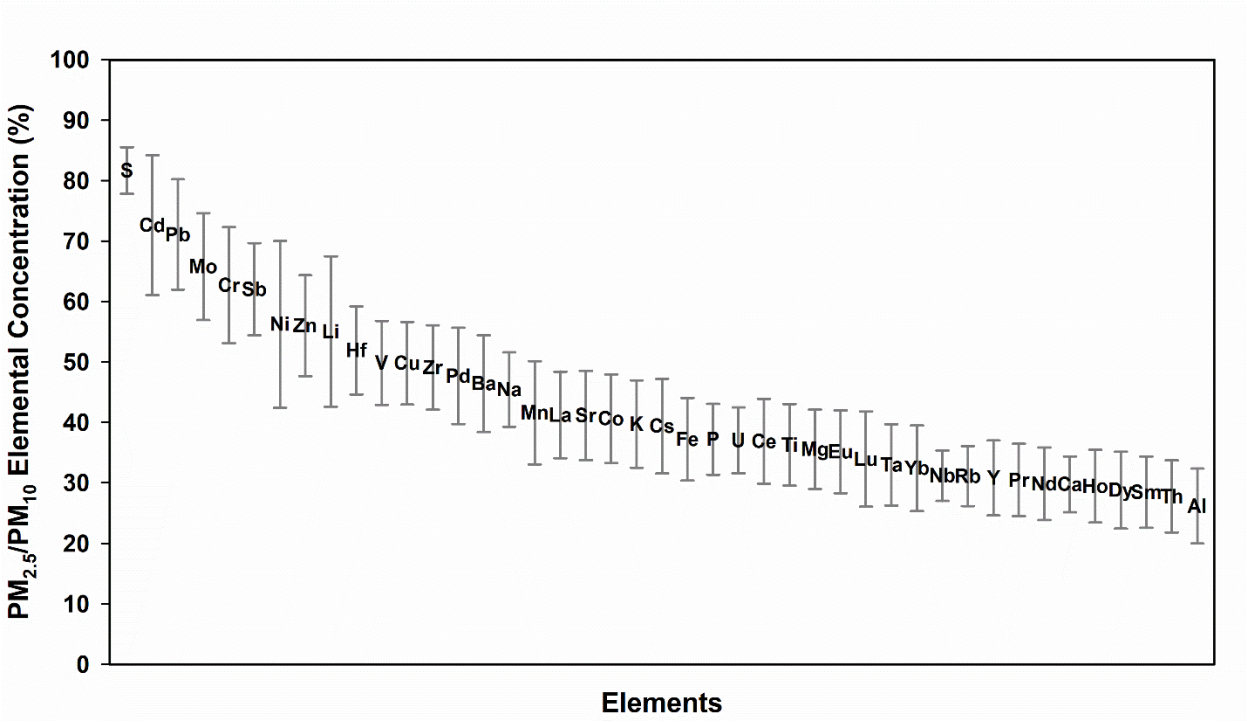

Figure S2. Percentage of metals and trace elements in PM_{10} that is confined in $PM_{2.5}$. Symbol of the chemical elements represent the average values, and error bars show the standard deviation across all of the sampling sites.

Figure S3 shows average crustal enrichment factors (EFs) for selected elements and trace metals in both fine and coarse particles across the sampling sites. The calculated EFs were generally higher in $PM_{2.5}$ than $PM_{2.5-10}$, presumably because of the different physical and chemical processes that selectively enhanced these elements in smaller particles. This is in agreement with the findings of previous studies that reported higher EFs in $PM_{2.5}$ compared to $PM_{2.5-10}$ (Arhami et al., 2009). Pd, Sb, and S were shown to have the largest average EFs among $PM_{2.5}$ and $PM_{2.5-10}$ elements. Some of the traffic tracers including Mo, and Zn as well elements such as Cd and Li also showed substantial average EF values (EF>5) in $PM_{2.5}$ and $PM_{2.5-10}$. Other traffic tracers such as Ba, Cr, Pb, and Zr showed high EFs only in $PM_{2.5}$. In contrast to traffic tracers, crustal elements such as Ca, K, Mg were shown to have low EFs (EF<5) in fine and coarse particles, indicating a lack of major anthropogenic sources for these elements.

Previously, Sb, S, Cd, Mo, and Zn were reported to have the largest EF values in $PM_{2.5}$ and $PM_{2.5-10}$ (Arhami et al., 2009). Other studies have reported high EF values for Cu and Zn (Birmili et al., 2006; Cheung et al., 2011). More recent studies reported very high EF values for Pd (10^3 <average EF< 10^4) in $PM_{2.5}$ and PM_{10} (Das and Chellam, 2020). While a wide range of sampling sites with diverse local emission sources were covered in this study, our findings are in reasonable agreement with the results of the previous studies.

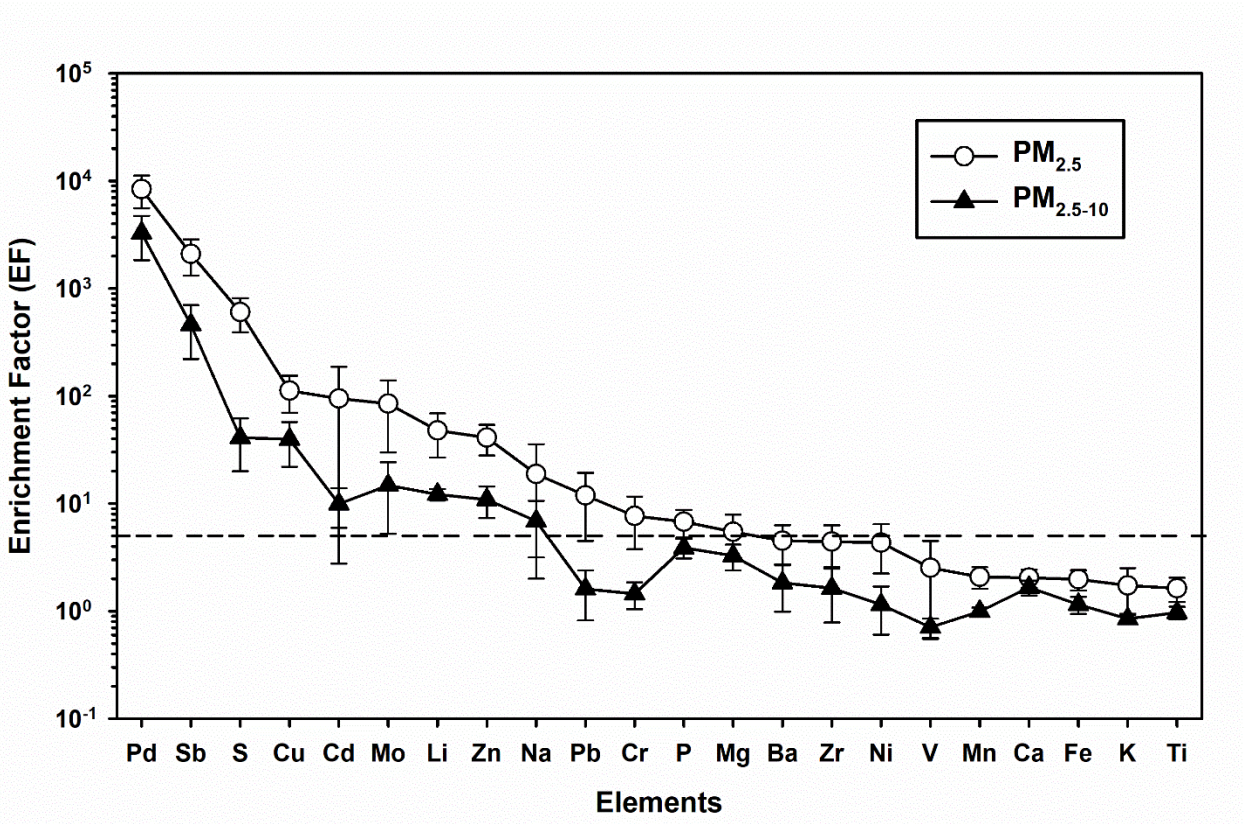

Figure S3. Crustal enrichment factors (EFs) for selected elements. The horizontal line represents anthropogenic EF threshold (EF=5).

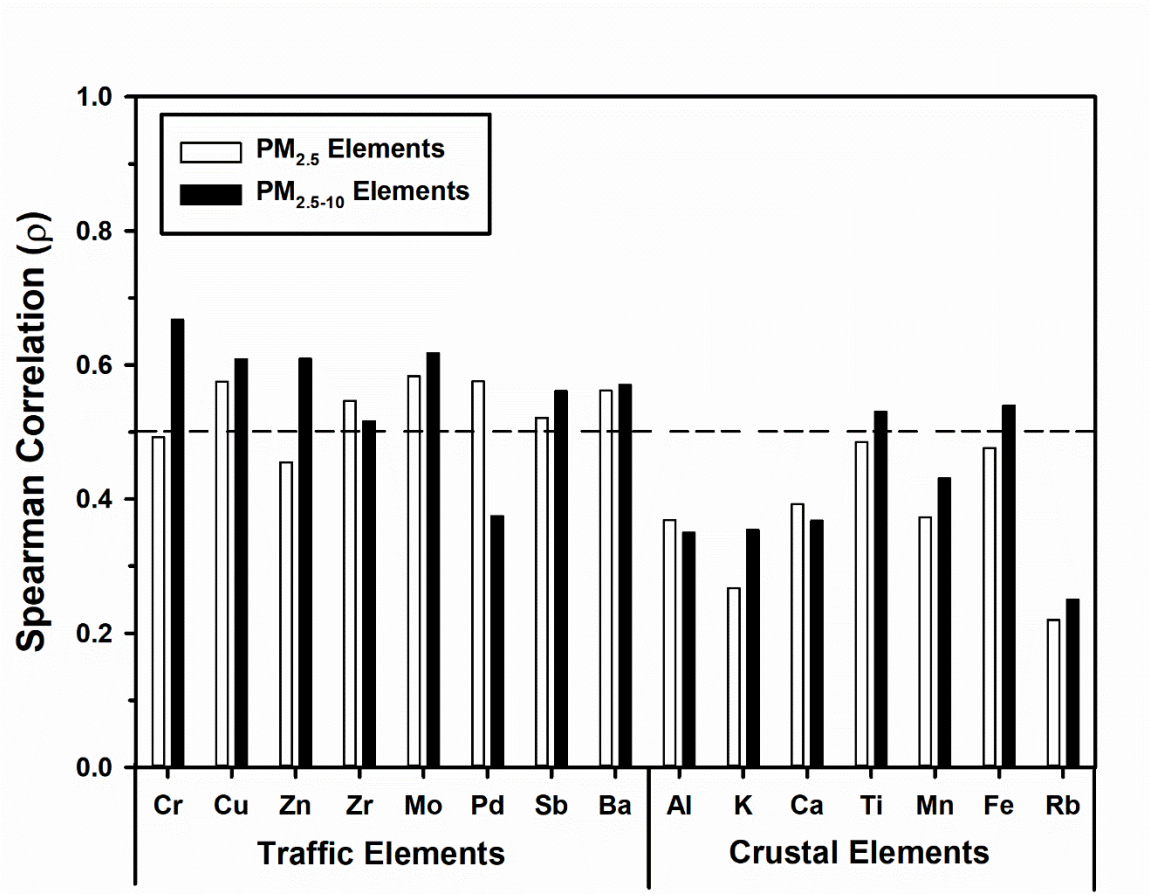

Figure S4. Spearman correlation coefficients of selected $PM_{2.5}$ and $PM_{2.5-10}$ traffic and crustal elements with the annual average daily traffic (AADT)

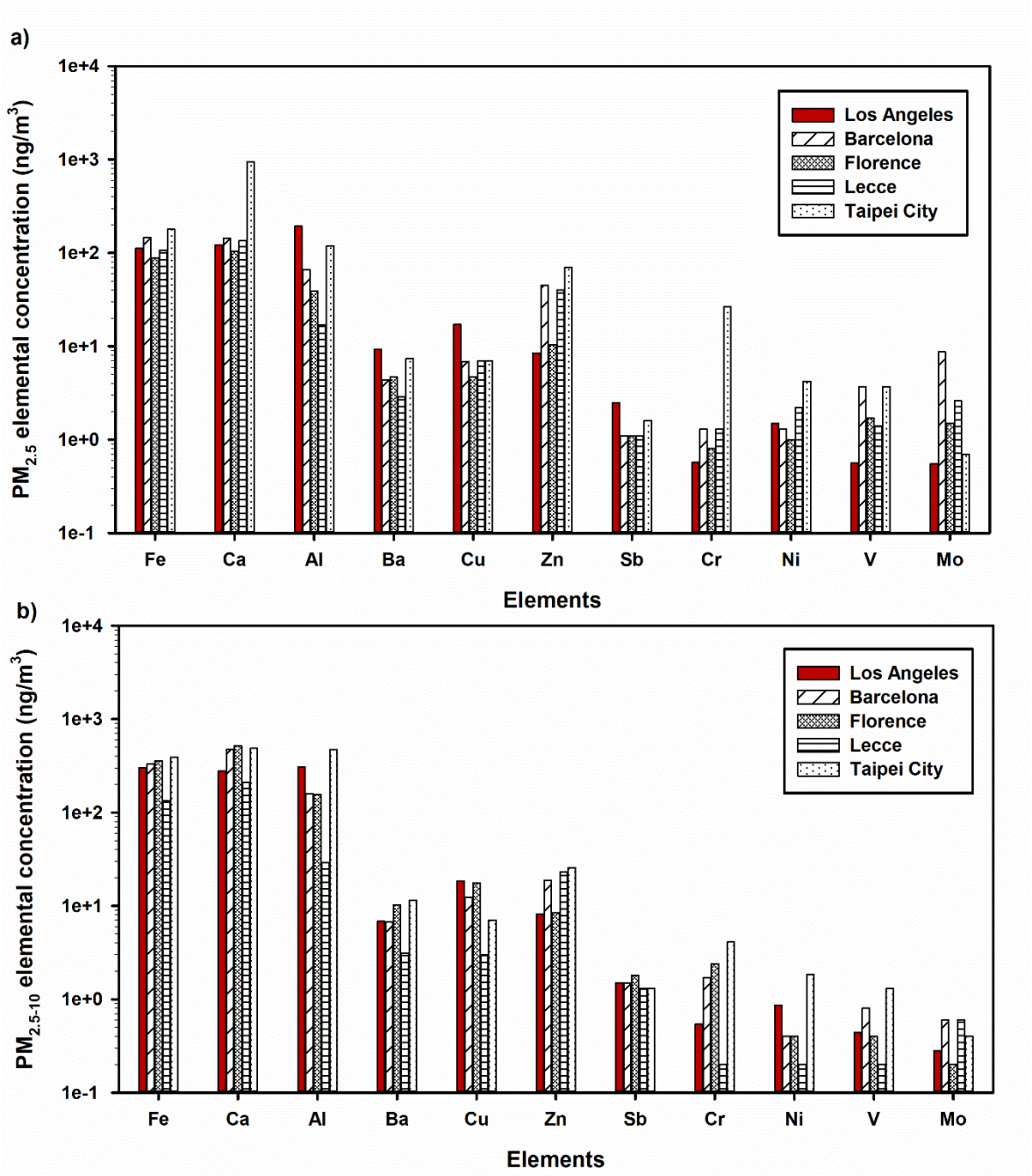

Figure S5. Concentrations of selected elements in Los Angeles (current study), Barcelona (Fulvio Amato et al., 2016), Florence (Fulvio Amato et al., 2016), Lecce (Perrone et al., 2019), Taipei city (Hsu et al., 2019) (a) $PM_{2.5}$ elemental concentrations, (b) $PM_{2.5-10}$ elemental concentrations

The normalized concentrations of selected elements based on the reported values by Habre et al. (2020) are shown in Figure S6. In both the current and previous studies, two-week integrated samples were collected in both warm and cold times of the year, and the chemical speciation analysis was performed at Wisconsin State Laboratory of Hygiene (WSLH) through Sector Field Inductively Coupled Plasma Mass Spectrometry (SF-ICP-MS) using similar filter and Polyurethane foam (PUF) substrates. The sampling locations of the previous studies were also bounded to a similar area in Southern California, covering coastal, urban, and suburban locations with various emission sources, including traffic, industrial, and combustion sources. Therefore, we expect the comparison between the elemental composition of the two studies to be meaningful.

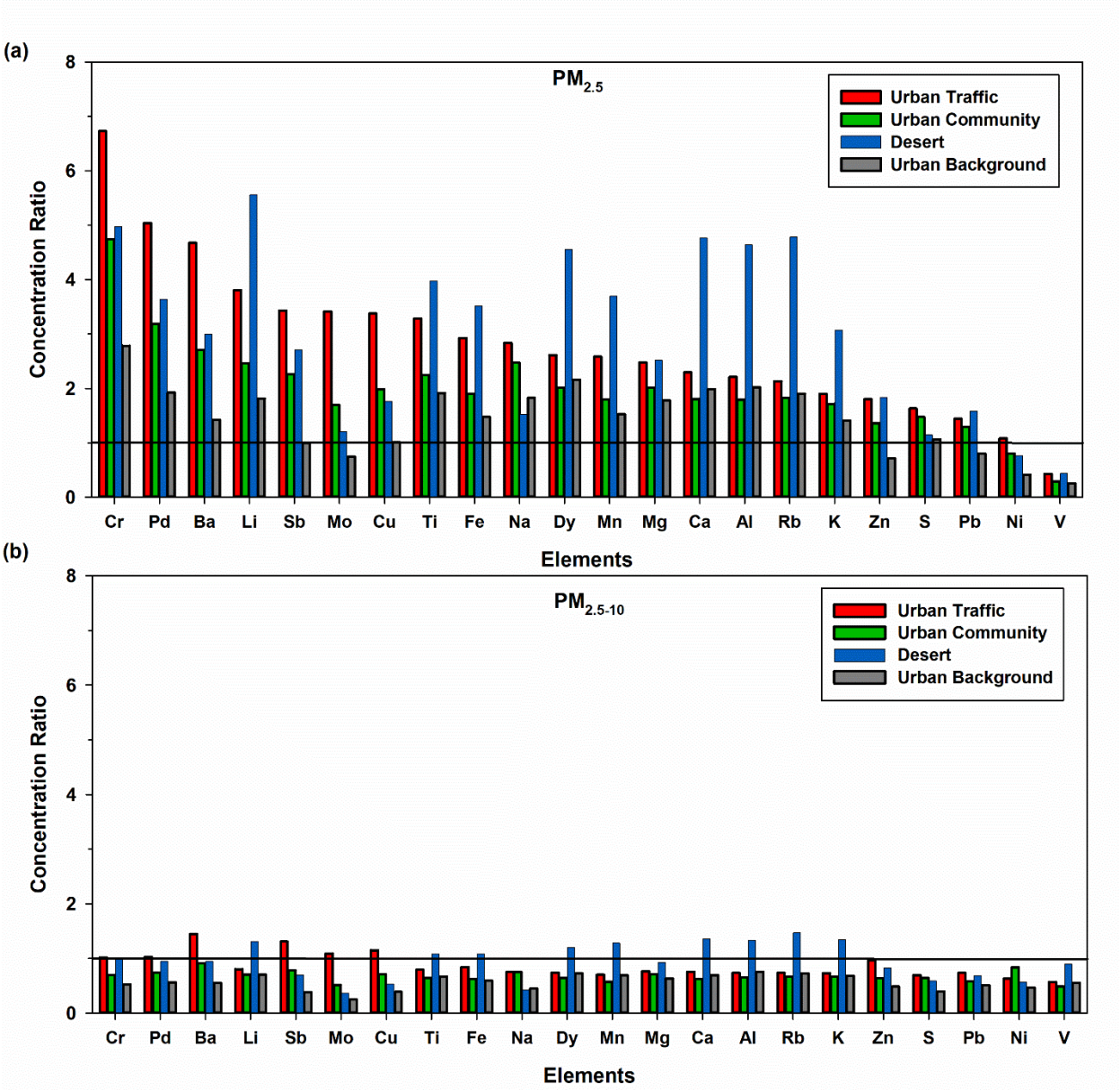

Figure S6. Concentration ratios of selected elements between this study and a previous study of Southern California communities in 2008-2009 (Habre et al. (2020)) (a) $PM_{2.5}$ elements (b) $PM_{2.5-10}$ elements

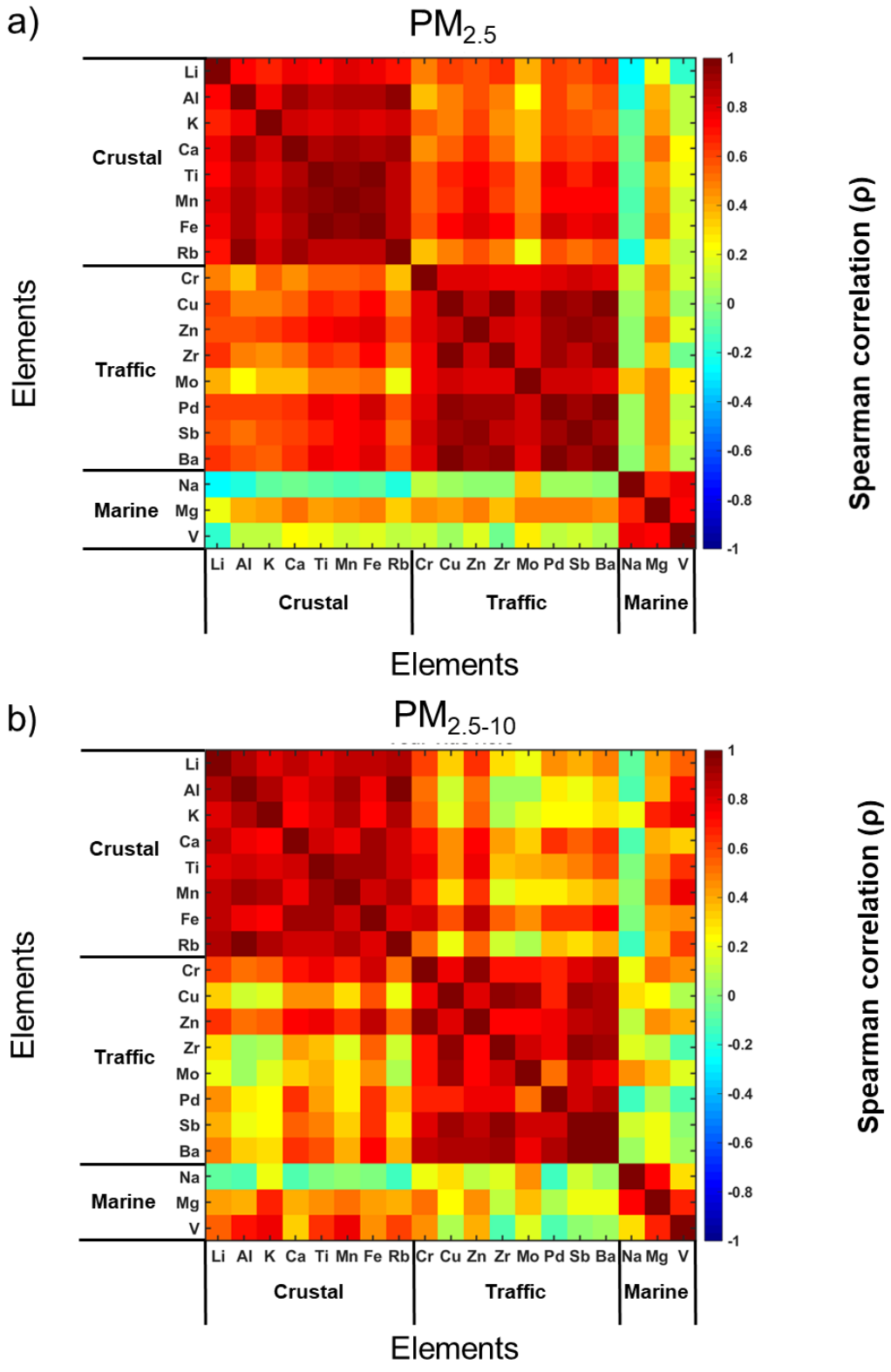

Figure S7. Spearman correlation matrix for selected trace elements representing marine, traffic, and crustal sources (a) $PM_{2.5}$, (b) $PM_{2.5-10}$

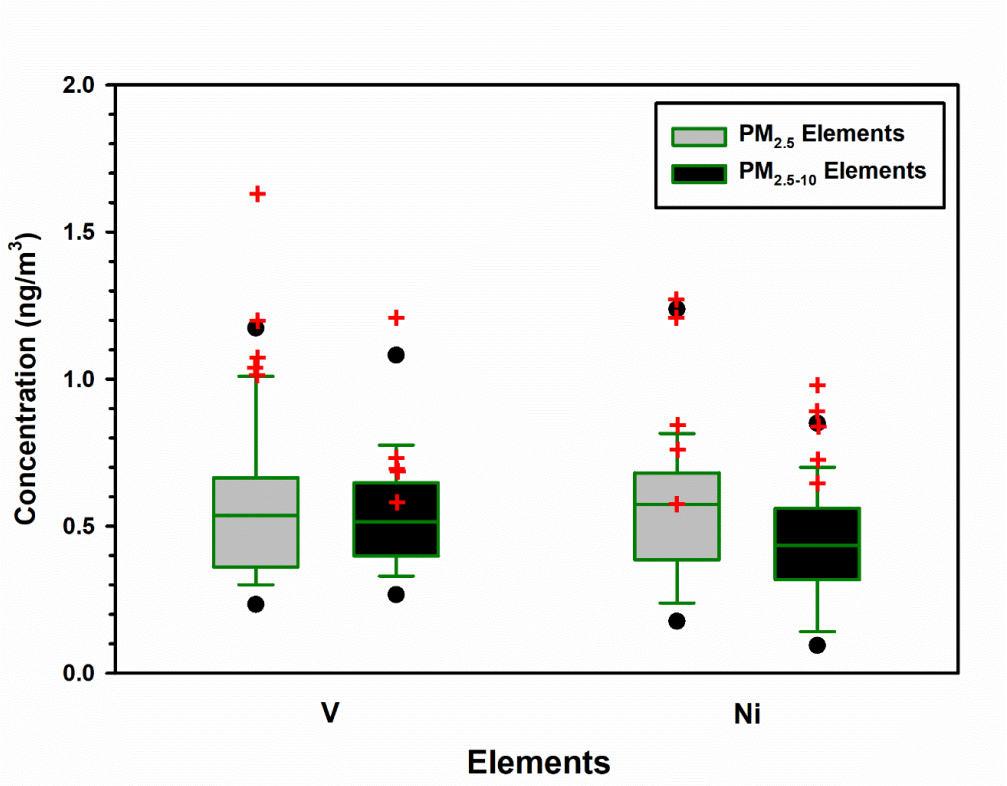

Figure S8. The distribution of $PM_{2.5}$ and $PM_{2.5-10}$ concentrations of V and Ni. The red marks denote the elemental concentrations of V and Ni at the sampling locations within 8 miles of Ports of Long Beach and Los Angeles

To assess the performance of the model at different sampling locations, an analysis was performed on model residual values. Mean absolute percentage error (MAPE) was calculated based on Eq (S1) (Bai et al., 2019):

$$MAPE = \frac{100}{n} \sum_{t}^{n} \left| \frac{A_t - F_t}{A_t} \right| \quad \text{(S1)}$$

Where *n* is the number of samples, and A_t and F_t are the observed and predicted values.

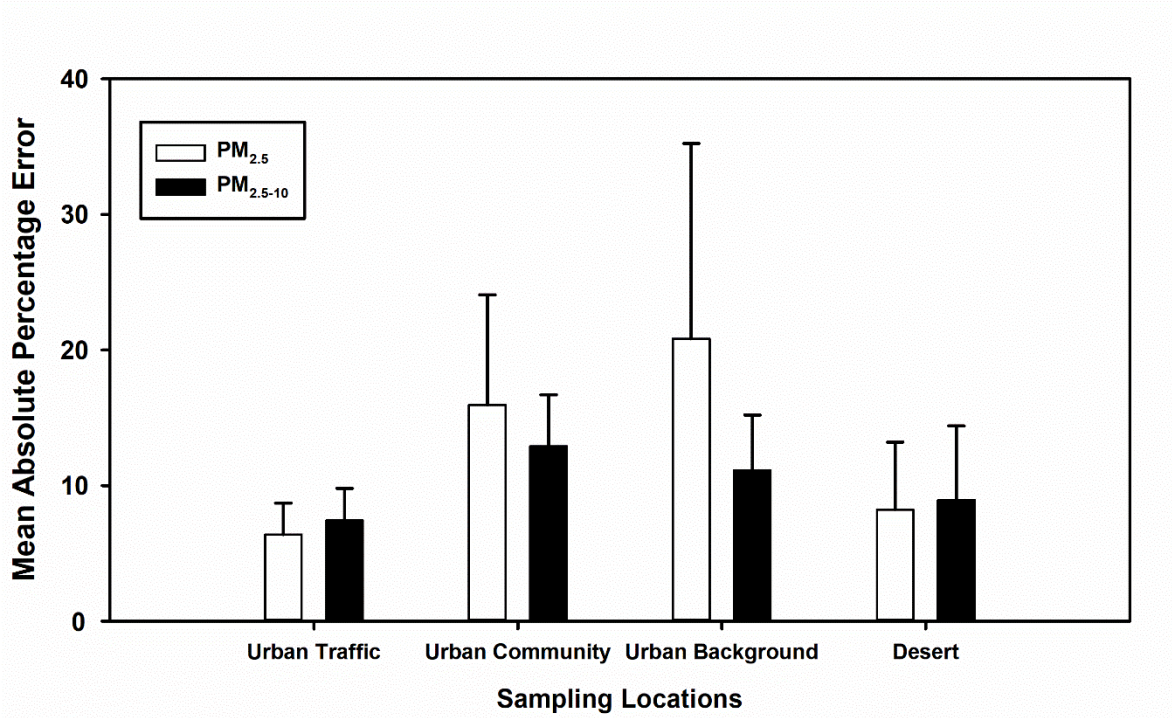

Figure S9. Mean absolute percentage error (MAPE) at various sampling locations

References

Aatmeeyata, Kaul, D.S., Sharma, M., 2009. Traffic generated non-exhaust particulate emissions from concrete pavement: A mass and particle size study for two-wheelers and small cars. Atmos. Environ. 43, 5691–5697. https://doi.org/10.1016/j.atmosenv.2009.07.032

Aatmeeyata, Sharma, M., 2010a. Polycyclic aromatic hydrocarbons, elemental and organic carbon emissions from tire-wear. Sci. Total Environ. 408, 4563–4568. https://doi.org/10.1016/j.scitotenv.2010.06.011

Aatmeeyata, Sharma, M., 2010b. Contribution of Traffic-Generated Nonexhaust PAHs, Elemental Carbon, and Organic Carbon Emission to Air and Urban Runoff Pollution. J. Environ. Eng. 136, 1447–1450. https://doi.org/10.1061/(asce)ee.1943-7870.0000274

Abrams, J.Y., Weber, R.J., Klein, M., Sarnat, S.E., Chang, H.H., Strickland, M.J., Verma, V., Fang, T., Bates, J.T., Mulholland, J.A., Russell, A.G., Tolbert, P.E., 2017. Erratum: Associations between Ambient Fine Particulate Oxidative Potential and Cardiorespiratory Emergency Department Visits. Environ. Health Perspect. 125, 129001. https://doi.org/10.1289/EHP3048

Abu-Allaban, M., Gillies, J.A., Gertler, A.W., Clayton, R., Proffitt, D., 2003. Tailpipe, resuspended road dust, and brake-wear emission factors from on-road vehicles. Atmos. Environ. 37, 5283–5293. https://doi.org/10.1016/j.atmosenv.2003.05.005

Alemani, M., Nosko, O., Metinoz, I., Olofsson, U., 2016. A study on emission of airborne wear particles from car brake friction pairs. SAE Int. J. Mater. Manuf. 9, 147–157. https://doi.org/10.4271/2015-01-2665

Alemani, M., Wahlström, J., Olofsson, U., 2018. On the influence of car brake system

parameters on particulate matter emissions. Wear 396–397, 67–74. https://doi.org/10.1016/j.wear.2017.11.011

Almeida, S.M., Manousakas, M., Diapouli, E., Kertesz, Z., Samek, L., Hristova, E., Šega, K., Alvarez, R.P., Belis, C.A., Eleftheriadis, K., Albania, Civici, N., Radic, R., Vukic, L., Hristova, E., Veleva, B., Šega, K., Bešlic, I., Davila, S., Godec, R., Manousakas, M., Diapouli, E., Vratolis, S., Eleftheriadis, K., Kertesz, Z., Belis, C.A., Bernatonis, M., Djukanovic, G., Jancic, D., Samek, L., Furman, L., Stegowski, Z., Almeida, S.M., Galinha, C., Balan, V., Nikolovska, L., Stefanovska, A., Radenkovic, M., Kneževic, J., Banu Oztas, N., Cantay, E., Turchenko, D. V., Abdullaev, S., Padilla Alvarez, R., Karydas, A.G., 2020. Ambient particulate matter source apportionment using receptor modelling in European and Central Asia urban areas. Environ. Pollut. 266. https://doi.org/10.1016/j.envpol.2020.115199

Altuwayjiri, A., Pirhadi, M., Taghvaee, S., Sioutas, C., 2021. Long-Term trends in the contribution of PM2.5sources to organic carbon (OC) in the Los Angeles basin and the effect of PM emission regulations. Faraday Discuss. 226, 74–99. https://doi.org/10.1039/d0fd00074d

Alves, C., Evtyugina, M., Vicente, A., Conca, E., Amato, F., 2021. Organic profiles of brake wear particles. Atmos. Res. 255. https://doi.org/10.1016/j.atmosres.2021.105557

Alves, C.A., Vicente, A.M.P., Calvo, A.I., Baumgardner, D., Amato, F., Querol, X., Pio, C., Gustafsson, M., 2020. Physical and chemical properties of non-exhaust particles generated from wear between pavements and tyres. Atmos. Environ. 224, 117252. https://doi.org/10.1016/j.atmosenv.2019.117252

Amato, Fulvio, Alastuey, A., Karanasiou, A., Lucarelli, F., Nava, S., Calzolai, G., Severi, M., Becagli, S., Gianelle, V.L., Colombi, C., Alves, C., Custódio, D., Nunes, T., Cerqueira, M., Pio, C., Eleftheriadis, K., Diapouli, E., Reche, C., Minguillón, M.C., Manousakas, M.I., Maggos, T., Vratolis, S., Harrison, R.M., Querol, X., 2016. AIRUSE-LIFE+: A harmonized PM speciation and source apportionment in five southern European cities. Atmos. Chem. Phys. 16, 3289–3309. https://doi.org/10.5194/acp-16-3289-2016

Amato, F., Favez, O., Pandolfi, M., Alastuey, A., Querol, X., Moukhtar, S., Bruge, B., Verlhac, S., Orza, J.A.G., Bonnaire, N., Le Priol, T., Petit, J.F., Sciare, J., 2016. Traffic induced particle resuspension in Paris: Emission factors and source contributions. Atmos. Environ. 129, 114–124. https://doi.org/10.1016/j.atmosenv.2016.01.022

Amato, F., Pandolfi, M., Moreno, T., Furger, M., Pey, J., Alastuey, A., Bukowiecki, N., Prevot, A.S.H., Baltensperger, U., Querol, X., 2011a. Sources and variability of inhalable road dust particles in three European cities. Atmos. Environ. 45, 6777–6787. https://doi.org/10.1016/J.ATMOSENV.2011.06.003

Amato, F., Pandolfi, M., Viana, M., Querol, X., Alastuey, A., Moreno, T., 2009. Spatial and chemical patterns of PM10 in road dust deposited in urban environment. Atmos. Environ. 43, 1650–1659. https://doi.org/10.1016/j.atmosenv.2008.12.009

Amato, F., Viana, M., Richard, A., Furger, M., Prévôt, A.S.H., Nava, S., Lucarelli, F., Bukowiecki, N., Alastuey, A., Reche, C., Moreno, T., Pandolfi, M., Pey, J., Querol, X., 2011b. Size and time-resolved roadside enrichment of atmospheric particulate pollutants. Atmos. Chem. Phys. 11, 2917–2931. https://doi.org/10.5194/acp-11-2917-2011

André Nel, 2005. Air Pollution – Related Illness : Effects of Particles. Science (80-.). 308, 804–

806.

Apeagyei, E., Bank, M.S., Spengler, J.D., 2011. Distribution of heavy metals in road dust along an urban-rural gradient in Massachusetts. Atmos. Environ. 45, 2310–2323. https://doi.org/10.1016/J.ATMOSENV.2010.11.015

Araujo, J.A., Nel, A.E., 2009. Particulate matter and atherosclerosis: Role of particle size, composition and oxidative stress. Part. Fibre Toxicol. 6, 1–19. https://doi.org/10.1186/1743-8977-6-24

Arhami, M., Sillanpää, M., Hu, S., Olson, M.R., Schauer, J.J., Sioutas, C., 2009. Size-segregated inorganic and organic components of PM in the communities of the Los Angeles Harbor. Aerosol Sci. Technol. 43, 145–160. https://doi.org/10.1080/02786820802534757

Armstrong, B., Hutchinson, E., Unwin, J., Fletcher, T., 2004. Lung cancer risk after exposure to polycyclic aromatic hydrocarbons: A review and meta-analysis. Environ. Health Perspect. 112, 970–978. https://doi.org/10.1289/ehp.6895

Auffan, M., Tella, M., Liu, W., Pariat, A., Cabié, M., Borschneck, D., Angeletti, B., Landrot, G., Mouneyrac, C., Giambérini, L., Rose, J., 2017. Structural and physical-chemical behavior of a CeO2 nanoparticle based diesel additive during combustion and environmental release. Environ. Sci. Nano 4, 1974–1980. https://doi.org/10.1039/c7en00494j

Axsen, J., Wolinetz, M., 2018. Reaching 30% plug-in vehicle sales by 2030: Modeling incentive and sales mandate strategies in Canada. Transp. Res. Part D Transp. Environ. 65, 596–617. https://doi.org/10.1016/j.trd.2018.09.012

Badaloni, C., Cesaroni, G., Cerza, F., Davoli, M., Brunekreef, B., Forastiere, F., 2017. Effects of

long-term exposure to particulate matter and metal components on mortality in the Rome longitudinal study. Environ. Int. 109, 146–154. https://doi.org/10.1016/j.envint.2017.09.005

Baensch-Baltruschat, B., Kocher, B., Kochleus, C., Stock, F., Reifferscheid, G., 2021. Tyre and road wear particles - A calculation of generation, transport and release to water and soil with special regard to German roads. Sci. Total Environ. 752, 141939. https://doi.org/10.1016/j.scitotenv.2020.141939

Baensch-Baltruschat, B., Kocher, B., Stock, F., Reifferscheid, G., 2020. Tyre and road wear particles (TRWP) - A review of generation, properties, emissions, human health risk, ecotoxicity, and fate in the environment. Sci. Total Environ. 733, 137823. https://doi.org/10.1016/j.scitotenv.2020.137823

Bai, L., Su, X., Zhao, D., Zhang, Y., Cheng, Q., Zhang, H., Wang, S., Xie, M., Su, H., 2018. Exposure to traffic-related air pollution and acute bronchitis in children: Season and age as modifiers. J. Epidemiol. Community Health 72, 426–433. https://doi.org/10.1136/jech-2017-209948

Bai, Y., Zeng, B., Li, C., Zhang, J., 2019. An ensemble long short-term memory neural network for hourly PM2.5 concentration forecasting. Chemosphere 222, 286–294. https://doi.org/10.1016/j.chemosphere.2019.01.121

Barkenbus, J.N., 2020. ProspectsBarkenbus, J. N. (2020). Prospects for electric vehicles. Applied Sciences (Switzerland), 12(14), 1–13. https://doi.org/10.3390/su12145813 for electric vehicles. Appl. Sci. 12, 1–13.

Basagaña, X., Jacquemin, B., Karanasiou, A., Ostro, B., Querol, X., Agis, D., Alessandrini, E., Alguacil, J., Artiñano, B., Catrambone, M., De La Rosa, J.D., Díaz, J., Faustini, A., Ferrari,

S., Forastiere, F., Katsouyanni, K., Linares, C., Perrino, C., Ranzi, A., Ricciardelli, I., Samoli, E., Zauli-Sajani, S., Sunyer, J., Stafoggia, M., Angelini, P., Berti, G., Bisanti, L., Cadum, E., Chiusolo, M., Davoli, M., De'Donato, F., Demaria, M., Gandini, M., Grosa, M., Pandolfi, P., Pelosini, R., Pietrodangelo, A., Pizzi, L., Poluzzi, V., Priod, G., Randi, G., Rowinski, M., Scarinzi, C., Stivanello, E., Dimakopoulou, K., Elefteriadis, K., Kelessis, A., Maggos, T., Michalopoulos, N., Pateraki, S., Petrakakis, M., Rodopoulou, S., Sypsa, V., Barrera-Gómez, J., Fernandez, R., Perez, N., Pey, J., Salvador, P., Sanchez, A.M., Tobias, A., Bidondo, M., Declercq, C., Le Tertre, A., Lozano, P., Medina, S., Pascal, L., Pascal, M., 2015. Short-term effects of particulate matter constituents on daily hospitalizations and mortality in five South-European cities: Results from the MED-PARTICLES project. Environ. Int. 75, 151–158. https://doi.org/10.1016/j.envint.2014.11.011

Basu, R., Harris, M., Sie, L., Malig, B., Broadwin, R., Green, R., 2014. Effects of fine particulate matter and its constituents on low birth weight among full-term infants in California. Environ. Res. 128, 42–51. https://doi.org/10.1016/j.envres.2013.10.008

Bates, J.T., Fang, T., Verma, V., Zeng, L., Weber, R.J., Tolbert, P.E., Abrams, J.Y., Sarnat, S.E., Klein, M., Mulholland, J.A., Russell, A.G., 2019. Review of Acellular Assays of Ambient Particulate Matter Oxidative Potential: Methods and Relationships with Composition, Sources, and Health Effects. Environ. Sci. Technol. 53, 4003–4019. https://doi.org/10.1021/acs.est.8b03430

Bates, J.T., Weber, R.J., Abrams, J., Verma, V., Fang, T., Klein, M., Strickland, M.J., Sarnat, S.E., Chang, H.H., Mulholland, J.A., Tolbert, P.E., Russell, A.G., 2015. Reactive Oxygen Species Generation Linked to Sources of Atmospheric Particulate Matter and Cardiorespiratory Effects. Environ. Sci. Technol. 49, 13605–13612.

https://doi.org/10.1021/acs.est.5b02967

Beddows, D.C.S., Harrison, R.M., 2021. PM10 and PM2.5 emission factors for non-exhaust particles from road vehicles: Dependence upon vehicle mass and implications for battery electric vehicles. Atmos. Environ. 244, 117886. https://doi.org/10.1016/j.atmosenv.2020.117886

Beelen, R., Hoek, G., van den Brandt, P.A., Goldbohm, R.A., Fischer, P., Schouten, L.J., Jerrett, M., Hughes, E., Armstrong, B., Brunekreef, B., 2008. Long-term effects of traffic-related air pollution on mortality in a Dutch cohort (NLCS-AIR study). Environ. Health Perspect. 116, 196–202. https://doi.org/10.1289/ehp.10767

Beji, A., Deboudt, K., Khardi, S., Muresan, B., Flament, P., Fourmentin, M., Lumière, L., 2020. Non-exhaust particle emissions under various driving conditions: Implications for sustainable mobility. Transp. Res. Part D Transp. Environ. 81, 102290. https://doi.org/10.1016/j.trd.2020.102290

Birmili, W., Allen, A.G., Bary, F., Harrison, R.M., 2006. Trace metal concentrations and water solubility in size-fractionated atmospheric particles and influence of road traffic. Environ. Sci. Technol. 40, 1144–1153. https://doi.org/10.1021/es0486925

Boonyatumanond, R., Murakami, M., Wattayakorn, G., Togo, A., Takada, H., 2007. Sources of polycyclic aromatic hydrocarbons (PAHs) in street dust in a tropical Asian mega-city, Bangkok, Thailand. Sci. Total Environ. 384, 420–432. https://doi.org/10.1016/j.scitotenv.2007.06.046

Bortey-Sam, N., Ikenaka, Y., Akoto, O., Nakayama, S.M.M., Asante, K.A., Baidoo, E., Obirikorang, C., Saengtienchai, A., Isoda, N., Nimako, C., Mizukawa, H., Ishizuka, M.,

2017. Oxidative stress and respiratory symptoms due to human exposure to polycyclic aromatic hydrocarbons (PAHs) in Kumasi, Ghana. Environ. Pollut. 228, 311–320. https://doi.org/10.1016/j.envpol.2017.05.036

Boucher, J., Friot, D., 2017. Primary Microplastics in the Oceans, Marine Environmental Research.

Bozlaker, A., Spada, N.J., Fraser, M.P., Chellam, S., 2014. Elemental characterization of PM2.5 and PM10 emitted from light duty vehicles in the Washburn Tunnel of Houston, Texas: Release of rhodium, palladium, and platinum. Environ. Sci. Technol. 48, 54–62. https://doi.org/10.1021/es4031003

Brauer, M., Lencar, C., Tamburic, L., Koehoorn, M., Demers, P., Karr, C., 2008. A cohort study of traffic-related air pollution impacts on birth outcomes. Environ. Health Perspect. 116, 680–686. https://doi.org/10.1289/ehp.10952

Bu, X., Xie, Z., Liu, J., Wei, L., Wang, X., Chen, M., Ren, H., 2021. Global PM2.5-attributable health burden from 1990 to 2017: Estimates from the Global Burden of disease study 2017. Environ. Res. 197, 111123. https://doi.org/10.1016/j.envres.2021.111123

Buekers, J., Van Holderbeke, M., Bierkens, J., Int Panis, L., 2014. Health and environmental benefits related to electric vehicle introduction in EU countries. Transp. Res. Part D Transp. Environ. 33, 26–38. https://doi.org/10.1016/j.trd.2014.09.002

Bukowiecki, N., Lienemann, P., Hill, M., Figi, R., Richard, A., Furger, M., Rickers, K., Falkenberg, G., Zhao, Y., Cliff, S.S., Prevot, A.S.H., Baltensperger, U., Buchmann, B., Gehrig, R., 2009. Real-World Emission Factors for Antimony and Other Brake Wear Related Trace Elements: Size-Segregated Values for Light and Heavy Duty Vehicles.

Environ. Sci. Technol. 43, 8072–8078. https://doi.org/10.1021/es9006096

Bukowiecki, N., Lienemann, P., Hill, M., Furger, M., Richard, A., Amato, F., Prévôt, A.S.H., Baltensperger, U., Buchmann, B., Gehrig, R., 2010. PM10 emission factors for non-exhaust particles generated by road traffic in an urban street canyon and along a freeway in Switzerland. Atmos. Environ. 44, 2330–2340. https://doi.org/10.1016/j.atmosenv.2010.03.039

Burchart-Korol, D., Jursova, S., Folęga, P., Korol, J., Pustejovska, P., Blaut, A., 2018. Environmental life cycle assessment of electric vehicles in Poland and the Czech Republic. J. Clean. Prod. 202, 476–487. https://doi.org/10.1016/j.jclepro.2018.08.145

Burnett, R., Chen, H., Szyszkowicz, M., Fann, N., Hubbell, B., Pope, C.A., Apte, J.S., Brauer, M., Cohen, A., Weichenthal, S., Coggins, J., Di, Q., Brunekreef, B., Frostad, J., Lim, S.S., Kan, H., Walker, K.D., Thurston, G.D., Hayes, R.B., Lim, C.C., Turner, M.C., Jerrett, M., Krewski, D., Gapstur, S.M., Diver, W.R., Ostro, B., Goldberg, D., Crouse, D.L., Martin, R. V, Peters, P., Pinault, L., Tjepkema, M., Van Donkelaar, A., Villeneuve, P.J., Miller, A.B., Yin, P., Zhou, M., Wang, L., Janssen, N.A.H., Marra, M., Atkinson, R.W., Tsang, H., Thach, T.Q., Cannon, J.B., Allen, R.T., Hart, J.E., Laden, F., Cesaroni, G., Forastiere, F., Weinmayr, G., Jaensch, A., Nagel, G., Concin, H., Spadaro, J. V, 2018. Global estimates of mortality associated with longterm exposure to outdoor fine particulate matter. Proc. Natl. Acad. Sci. U. S. A. 115, 9592–9597. https://doi.org/10.1073/pnas.1803222115

Cakmak, S., Hebbern, C., Vanos, J., Crouse, D.L., Tjepkema, M., 2019. Exposure to traffic and mortality risk in the 1991–2011 Canadian Census Health and Environment Cohort (CanCHEC). Environ. Int. 124, 16–24. https://doi.org/10.1016/j.envint.2018.12.045

Calas, A., Uzu, G., Kelly, F.J., Houdier, S., Martins, J.M.F., Thomas, F., Molton, F., Charron, A., Dunster, C., Oliete, A., Jacob, V., Besombes, J.L., Chevrier, F., Jaffrezo, J.L., 2018. Comparison between five acellular oxidative potential measurement assays performed with detailed chemistry on PM10 samples from the city of Chamonix (France). Atmos. Chem. Phys. 18, 7863–7875. https://doi.org/10.5194/acp-18-7863-2018

California Energy Commission, 2021. ZEV and Infrastructure Stats Data [WWW Document]. URL https://www.energy.ca.gov/files/zev-and-infrastructure-stats-data

Cesari, D., Amato, F., Pandolfi, M., Alastuey, A., Querol, X., Contini, D., 2016. An inter-comparison of PM10 source apportionment using PCA and PMF receptor models in three European sites. Environ. Sci. Pollut. Res. 23, 15133–15148. https://doi.org/10.1007/s11356-016-6599-z

Chandra Verma, P., Menapace, L., Bonfanti, A., Ciudin, R., Gialanella, S., Straffelini, G., 2015. Braking pad-disc system: Wear mechanisms and formation of wear fragments. Wear 322–323, 251–258. https://doi.org/10.1016/j.wear.2014.11.019

Chang, X. dong, Huang, H. bo, Jiao, R. nan, Liu, J. peng, 2020. Experimental investigation on the characteristics of tire wear particles under different non-vehicle operating parameters. Tribol. Int. 150, 106354. https://doi.org/10.1016/j.triboint.2020.106354

Chen, R., Jia, B., Tian, Y., Feng, Y., 2021. Source-specific health risk assessment of PM2.5-bound heavy metals based on high time-resolved measurement in a Chinese megacity: insights into seasonal and diurnal variations. Ecotoxicol. Environ. Saf. 216, 112167. https://doi.org/10.1016/j.ecoenv.2021.112167

Cheung, K., Daher, N., Kam, W., Shafer, M.M., Ning, Z., Schauer, J.J., Sioutas, C., 2011.

Spatial and temporal variation of chemical composition and mass closure of ambient coarse particulate matter (PM10-2.5) in the Los Angeles area. Atmos. Environ. 45, 2651–2662. https://doi.org/10.1016/j.atmosenv.2011.02.066

Cheung, K., Shafer, M.M., Schauer, J.J., Sioutas, C., 2012. Historical trends in the mass and chemical species concentrations of coarse particulate matter in the Los Angeles basin and relation to sources and air quality regulations. J. Air Waste Manag. Assoc. 62, 541–556. https://doi.org/10.1080/10962247.2012.661382

Chow, J.C., Watson, J.G., Fujita, E.M., Lu, Z., Lawson, D.R., Ashbaugh, L.L., 1994. Temporal and spatial variations of PM2.5 and PM10 aerosol in the Southern California air quality study. Atmos. Environ. 28, 2061–2080. https://doi.org/10.1016/1352-2310(94)90474-X

Chung, A., Chang, D.P.Y., Kleeman, M.J., Perry, K.D., Cahill, T.A., Dutcher, D., McDougall, E.M., Stroud, K., 2001. Comparison of real-time instruments used to monitor airborne particulate matter. J. Air Waste Manag. Assoc. 51, 109–120. https://doi.org/10.1080/10473289.2001.10464254

Crobeddu, B., Aragao-Santiago, L., Bui, L.C., Boland, S., Baeza Squiban, A., 2017. Oxidative potential of particulate matter 2.5 as predictive indicator of cellular stress. Environ. Pollut. 230, 125–133. https://doi.org/10.1016/j.envpol.2017.06.051

Crosignani, P., Nanni, A., Pepe, N., Pozzi, C., Silibello, C., Poggio, A., Conte, M., 2021. The effect of non-compliance of diesel vehicle emissions with euro limits on mortality in the city of Milan. Atmosphere (Basel). 12, 1–11. https://doi.org/10.3390/atmos12030342

Dahl, A., Gharibi, A., Swietlicki, E., Gudmundsson, A., Bohgard, M., Ljungman, A., Blomqvist, G., Gustafsson, M., 2006. Traffic-generated emissions of ultrafine particles from pavement–

tire interface. Atmos. Environ. 40, 1314–1323. https://doi.org/10.1016/J.ATMOSENV.2005.10.029

Dall'Osto, M., Beddows, D.C.S., Gietl, J.K., Olatunbosun, O.A., Yang, X., Harrison, R.M., 2014. Characteristics of tyre dust in polluted air: Studies by single particle mass spectrometry (ATOFMS). Atmos. Environ. 94, 224–230. https://doi.org/10.1016/j.atmosenv.2014.05.026

Das, S., Chellam, S., 2020. Estimating light-duty vehicles' contributions to ambient PM2.5 and PM10 at a near-highway urban elementary school via elemental characterization emphasizing rhodium, palladium, and platinum. Sci. Total Environ. 747, 141268. https://doi.org/10.1016/j.scitotenv.2020.141268

de Souza, L.L.P., Lora, E.E.S., Palacio, J.C.E., Rocha, M.H., Renó, M.L.G., Venturini, O.J., 2018. Comparative environmental life cycle assessment of conventional vehicles with different fuel options, plug-in hybrid and electric vehicles for a sustainable transportation system in Brazil. J. Clean. Prod. 203, 444–468. https://doi.org/10.1016/j.jclepro.2018.08.236

Delogu, M., Zanchi, L., Dattilo, C.A., Pierini, M., 2017. Innovative composites and hybrid materials for electric vehicles lightweight design in a sustainability perspective. Mater. Today Commun. 13, 192–209. https://doi.org/10.1016/j.mtcomm.2017.09.012

Denby, B.R., Kupiainen, K.J., Gustafsson, M., 2018. Review of Road Dust Emissions, Non-Exhaust Emissions. Elsevier Inc. https://doi.org/10.1016/b978-0-12-811770-5.00009-1

Depaolini, A., Bianchi, G., Fornai, D., Cardelli, A., Badalassi, M., Cardelli, C., Davoli, E., 2017. Physical and chemical characterization of representative samples of recycled rubber from

end-of-life tires. Chemosphere 184, 1320–1326. https://doi.org/10.1016/j.chemosphere.2017.06.093

Diekmann, A., Giese, U., Schaumann, I., 2019. Polycyclic aromatic hydrocarbons in consumer goods made from recycled rubber material: A review. Chemosphere 220, 1163–1178. https://doi.org/10.1016/j.chemosphere.2018.12.111

Dillner, A.M., Shafer, M.M., Schauer, J.J., 2007. A Novel Method Using Polyurethane Foam (PUF) Substrates to Determine Trace Element Concentrations in Size-Segregated Atmospheric Particulate Matter on Short Time Scales. Aerosol Sci. Technol. 41, 75–85. https://doi.org/10.1080/02786820601113282

Duong, T.T.T., Lee, B.K., 2011. Determining contamination level of heavy metals in road dust from busy traffic areas with different characteristics. J. Environ. Manage. 92, 554–562. https://doi.org/10.1016/j.jenvman.2010.09.010

Eeftens, M., Tsai, M.Y., Ampe, C., Anwander, B., Beelen, R., Bellander, T., Cesaroni, G., Cirach, M., Cyrys, J., de Hoogh, K., De Nazelle, A., de Vocht, F., Declercq, C., Dedele, A., Eriksen, K., Galassi, C., Gražulevičiene, R., Grivas, G., Heinrich, J., Hoffmann, B., Iakovides, M., Ineichen, A., Katsouyanni, K., Korek, M., Krämer, U., Kuhlbusch, T., Lanki, T., Madsen, C., Meliefste, K., Mölter, A., Mosler, G., Nieuwenhuijsen, M., Oldenwening, M., Pennanen, A., Probst-Hensch, N., Quass, U., Raaschou-Nielsen, O., Ranzi, A., Stephanou, E., Sugiri, D., Udvardy, O., Vaskövi, É., Weinmayr, G., Brunekreef, B., Hoek, G., 2012. Spatial variation of PM2.5, PM10, PM2.5 absorbance and PMcoarse concentrations between and within 20 European study areas and the relationship with NO2 - Results of the ESCAPE project. Atmos. Environ. 62, 303–317.

https://doi.org/10.1016/j.atmosenv.2012.08.038

Eriksson, M., Bergman, F., Jacobson, S., 2002. On the nature of tribological contact in automotive brakes. Wear 252, 26–36. https://doi.org/10.1016/S0043-1648(01)00849-3

Essl, C., Golubkov, A.W., Gasser, E., Nachtnebel, M., Zankel, A., Ewert, E., Fuchs, A., 2020. Comprehensive hazard analysis of failing automotive lithium-ion batteries in overtemperature experiments. Batteries 6. https://doi.org/10.3390/batteries6020030

European Environment Agency, 2019. Airbase - The European Air Quality Database.

Fan, Z., Meng, Q., Weisel, C., Laumbach, R., Ohman-Strickland, P., Shalat, S., Hernandez, M.Z., Black, K., 2009. Acute exposure to elevated PM2.5 generated by traffic and cardiopulmonary health effects in healthy older adults. J. Expo. Sci. Environ. Epidemiol. 19, 525–533. https://doi.org/10.1038/jes.2008.46

Fang, T., Lakey, P.S.J., Weber, R.J., Shiraiwa, M., 2019. Oxidative Potential of Particulate Matter and Generation of Reactive Oxygen Species in Epithelial Lining Fluid. Environ. Sci. Technol. 53, 12784–12792. https://doi.org/10.1021/acs.est.9b03823

Farahani, V.J., Soleimanian, E., Pirhadi, M., Sioutas, C., 2021. Long-term trends in concentrations and sources of PM2.5–bound metals and elements in central Los Angeles. Atmos. Environ. 253, 118361. https://doi.org/10.1016/j.atmosenv.2021.118361

Farrow, K., Oueslati, W., 2020. Non-exhaust emissions from road transport Causes, consequences and policy responses.

Farwick zum Hagen, F.H., Mathissen, M., Grabiec, T., Hennicke, T., Rettig, M., Grochowicz, J., Vogt, R., Benter, T., 2019a. Study of Brake Wear Particle Emissions: Impact of Braking

and Cruising Conditions. Environ. Sci. Technol. 53, 5143–5150. https://doi.org/10.1021/acs.est.8b07142

Farwick zum Hagen, F.H., Mathissen, M., Grabiec, T., Hennicke, T., Rettig, M., Grochowicz, J., Vogt, R., Benter, T., 2019b. On-road vehicle measurements of brake wear particle emissions. Atmos. Environ. 217, 116943. https://doi.org/10.1016/j.atmosenv.2019.116943

Fernandes, Y., Bry, A., de Persis, S., 2018. Identification and quantification of gases emitted during abuse tests by overcharge of a commercial Li-ion battery. J. Power Sources 389, 106–119. https://doi.org/10.1016/j.jpowsour.2018.03.034

Figi, R., Nagel, O., Tuchschmid, M., Lienemann, P., Gfeller, U., Bukowiecki, N., 2010. Quantitative analysis of heavy metals in automotive brake linings: A comparison between wet-chemistry based analysis and in-situ screening with a handheld X-ray fluorescence spectrometer. Anal. Chim. Acta 676, 46–52. https://doi.org/10.1016/J.ACA.2010.07.031

Filip, P., 2013. Friction brakes for automative and aircraft. Encycl. Tribol. https://doi.org/https://doi.org/10.1007/978-0-387-92897-5_172

Foitzik, M.J., Unrau, H.J., Gauterin, F., Dörnhöfer, J., Koch, T., 2018. Investigation of ultra fine particulate matter emission of rubber tires. Wear 394–395, 87–95. https://doi.org/10.1016/j.wear.2017.09.023

Forouzanfar, M.H., Alexander, L., Bachman, V.F., Biryukov, S., Brauer, M., Casey, D., Coates, M.M., Delwiche, K., Estep, K., Frostad, J.J., Astha, K.C., Kyu, H.H., Moradi-Lakeh, M., Ng, M., Slepak, E., Thomas, B.A., Wagner, J., Achoki, T., Atkinson, C., Barber, R.M., Cooperrider, K., Dandona, L., Dicker, D., Flaxman, A.D., Fleming, T.D., Foreman, K.J., Gakidou, E., Hay, S.I., Heuton, K.R., Iannarone, M.L., Ku, T., Larson, H.J., Lim, S.S.,

Lopez, A.D., Lozano, R., MacIntyre, M.F., Margono, C., McLain, A., Mokdad, A.H., Mullany, E.C., Murray, C.J.L., Naghavi, M., Nguyen, G., Pain, A.W., Richardson, L., Robinson, M., Sandar, L., Stephens, N., Temesgen, A.M., Thomson, B., Vos, T., Wan, X., Wang, H., Wurtz, B., Ebel, B.E., Ellenbogen, R.G., Wright, J.L., Alfonso-Cristancho, R., Anderson, B.O., Jensen, P.N., Quistberg, D.A., Riederer, A., Vavilala, M.S., Zunt, J.R., Anderson, H.R., Pourmalek, F., Gotay, C.C., Burnett, R., Shin, H.H., Weichenthal, S., Cohen, A., Knudsen, A., Aasvang, G., Kinge, J.M., Skirbekk, V., Vollset, S., Abbafati, C., Abbasoglu Ozgoren, A., Çavlin, A., Kucuk Bicer, B., Abd-Allah, F., Abera, S.F., Melaku, Y.A., Aboyans, V., Abraham, B., Puthenpurakal Abraham, J., Abraham, J.P., Thorne-Lyman, A.L., Ding, E.L., Fahimi, S., Khatibzadeh, S., Wagner, G.R., Bukhman, G., Campos-Nonato, I.R., Feigl, A.B., Salomon, J.A., Benzian, H., Abubakar, I., Abu-Rmeileh, N.M.E., Aburto, T.C., Avila, M.A., Barquera, S., Barrientos-Gutierrez, T., Campuzano, J.C., Cantoral, A.J., Contreras, A.G., Cuevas-Nasu, L., De, V., García-Guerra, F.A., Gomez Dantes, H., Gonzalez de Cosio, T., González-Castell, D., Heredia-Pi, I.B., Hernandez, L., Jauregui, A., Medina, C., Mejia-Rodriguez, F., Montañez Hernandez, J.C., Pedraza, L.S., Pedroza, A., Quezada, A.D., Salvo, D., Sanchez, L.M., Sánchez-Pimienta, T.G., Servan-Mori, E.E., Shamah Levy, T., Téllez Rojo, M.M., Villalpando, S., Adelekan, A., Adofo, K., Adou, A.K., Adsuar, J.C., Fra Paleo, U., Afshin, A., Micha, R., Mozaffarian, D., Shahraz, S., Shangguan, S., Singh, G.M., Agardh, E.E., Al Khabouri, M.J., Al Lami, F.H., Alam, S., Naheed, A., Alasfoor, D., Albittar, M.I., Alegretti, M.A., Cavalleri, F., Aleman, A. V., Colistro, V., Alemu, Z.A., Alhabib, S., Chen, Z., Gething, P., Ali, R., Bennett, D.A., Briggs, A.D.M., Rahimi, K., Scarborough, P., Simard, E.P., Ali, M.K., Argeseanu Cunningham, S., Liu, Y., Narayan, K.M.V., Omer, S.B., Alla, F., Guillemin, F., Allebeck, P., Roy, N.,

Kivipelto, M., Weiderpass, E., Fereshtehnejad, S., Havmoeller, R., Sindi, S., Allen, P.J., Alsharif, U., Endres, M., Nolte, S., Papachristou, C., Alvarez, E., Alvis-Guzman, N., Paternina Caicedo, A.J., Amankwaa, A.A., Amare, A.T., Hoek, H.W., Gansevoort, R.T., Yenesew, M., Ameh, E.A., Ameli, O., Amini, H., Tanner, M., Ammar, W., Harb, H.L., Antonio, C.A.T., Faraon, E.A., Panelo, C.A., Anwari, P., Arnlöv, J., Larsson, A., Arsic Arsenijevic, V.S., Artaman, A., Asghar, R.J., Assadi, R., Atkins, L.S., Awuah, B., Laryea, D.O., Badawi, A., Bahit, M.C., Bakfalouni, T., Balakrishnan, K., Balalla, S., Feigin, V.L., Te Ao, B.J., Balu, R., Dandona, R., Goenka, S., Kumar, G., Murthy, K.S., Reddy, K., Banerjee, A., Barker-Collo, S.L., del Pozo-Cruz, B., Barregard, L., Barrero, L.H., Basto-Abreu, A.C., Batis Ruvalcaba, C., de Castro, E.F., Lopez, N., Texcalac, J.L., Basu, A., Gaffikin, L., Basu, S., Basulaiman, M.O., Memish, Z.A., Beardsley, J., Bedi, N., Bekele, T., Bell, M.L., Huang, J.J., Benjet, C., Borges, G., Gutiérrez, R.A., Orozco, R., Trasande, L., Hagan, H., Bernabé, E., Wolfe, C.D.A., Beyene, T.J., Bhala, N., Derrett, S., Bhalla, A., Jha, V., Bhutta, Z.A., Nisar, M.I., Bikbov, B., Bin Abdulhak, A.A., Vijayakumar, L., Chiang, P.P., Blore, J.D., Brooks, P.M., Lakshmana Balaji, A., Colquhoun, S.M., Weintraub, R.G., Blyth, F.M., Meretoja, A., Bohensky, M.A., Bora Basara, B., Yentür, G.K., Kose, M.R., Pekericli, A., Uzun, S.B., Bornstein, N.M., Bose, D., Boufous, S., Degenhardt, L., Bourne, R.R., Brainin, M., Brazinova, A., Majdan, M., Breitborde, N.J., Schöttker, B., Brenner, H., Broday, D.M., Lunevicius, R., Bruce, N.G., Dherani, M.K., Pope, D., Brugha, T.S., Brunekreef, B., Kromhout, H., Buchbinder, R., Gabbe, B., Gibney, K.B., Thrift, A.G., Bui, L.N., Nguyen, N.T., Bulloch, A.G., Patten, S.B., Tonelli, M., Wang, J., Burch, M., Burney, P.G.J., Jarvis, D.L., Rodriguez, A., Rushton, L., Soljak, M., Williams, T.N., Caravanos, J., Nash, D., Cárdenas, R., Cardis, E., Nieuwenhuijsen, M.J., Rojas-Rueda, D., Carpenter,

D.O., Leung, R., Caso, V., Castañeda-Orjuela, C.A., Castro, R.E., Catalá-López, F., Chadha, V.K., Chang, J., Scott, J.G., Hoy, D.G., Knibbs, L.D., Charlson, F.J., Erskine, H.E., Ferrari, A.J., Gouda, H.N., Veerman, L.J., Whiteford, H.A., Chen, W., Zou, X., Chen, H., London, S.J., Jiang, Y., Takahashi, K., Chimed-Ochir, O., Chowdhury, R., Powles, J., Christophi, C.A., Chuang, T., Chugh, S.S., Cirillo, M., Claßen, T.K.D., Kraemer, A., Tobollik, M., Colomar, M., Cooper, C., Cooper, L.T., Coresh, J., Matsushita, K., Tran, B.X., Courville, K.J., Criqui, M.H., Stein, M.B., Damsere-Derry, J., Danawi, H., Refaat, A.H., Dargan, P.I., Davis, A., Fay, D.F.J., Schmidt, J.C., Davitoiu, D. V., Dayama, A., DeLeo, D., de Lima, G., Machado, V.M.P., Nogueira, J.R., Teixeira, C.M., Dellavalle, R.P., Deribe, K., Mekonnen, W., Des Jarlais, D.C., Dessalegn, M., deVeber, G.A., Lindsay, M.P., Hu, H., Devries, K.M., McKee, M., Pearce, N., Stöckl, H., Tillmann, T., Watts, C.H., Dharmaratne, S.D., Dokova, K., Dorsey, E.R., Driscoll, T.R., Marks, G.B., Leigh, J., Duan, L., Li, Y., Liu, S., Ma, J., Wang, L., Ye, P., Zhou, M., Liang, X., Durrani, A.M., Elshrek, Y.M., Ermakov, S.P., Soshnikov, S., Eshrati, B., Farzadfar, F., Esteghamati, A., Hafezi-Nejad, N., Sheikhbahaei, S., Sepanlou, S.G., Heydarpour, P., Sahraian, M., Rahimi-Movaghar, V., Ferri, C.P., Foigt, N., Franklin, R.C., Gamkrelidze, A., Khonelidze, I., Sturua, L., Gankpé, F.G., Gasana, E., Sabin, N., Geleijnse, J.M., Gessner, B.D., Gillum, R.F., Ginawi, I.A.M., Giroud, M., Giussani, G., Goginashvili, K., Gona, P., Goto, A., Guerrant, R.L., Terkawi, A.S., Gugnani, H.C., Gunnell, D., Gupta, R., Hagstromer, M., Halasa, Y.A., Idrisov, B.T., Hamadeh, R.R., Hammami, M., Hankey, G.J., Hao, Y., Zheng, Y., Haregu, T., van de Vijver, S., Haro, J., Hedayati, M.T., Hijar, M., Hoffman, H.J., Mensah, G.A., Sampson, U.K., Hornberger, J.C., Hosgood, H., Hsairi, M., Hu, G., Huang, C., Hubbell, B.J., Huiart, L., Racapé, L., Husseini, A., Iburg, K.M., Ikeda, N., Innos, K.,

Inoue, M., Kawakami, N., Shibuya, K., Islami, F., Ismayilova, S., Jacobsen, K.H., Jansen, H.A., Jassal, S.K., Jayaraman, S., Jeemon, P., Prabhakaran, D., Jiang, F., Jiang, G., Phillips, M.R., Jonas, J.B., Juel, K., She, J., Kan, H., Kany Roseline, S.S., Karam, N.E., Karch, A., Karema, C.K., Karthikeyan, G., Paul, V.K., Satpathy, M., Tandon, N., Kaul, A., Kazi, D.S., Kemp, A.H., Lotufo, P.A., Polanczyk, G. V., Santos, I.S., Kengne, A.P., Matzopoulos, R., Parry, C.D., Sliwa, K., Mayosi, B.M., Stein, D.J., Keren, A., Khader, Y.S., Ali Hassan Khalifa, S.E., Khan, E.A., Khang, Y., Kieling, C., Kim, D., Kim, S., Kim, Y., Kimokoti, R.W., Kinfu, Y., Kissela, B.M., Kokubo, Y., Kosen, S., Warouw, T.S., Kravchenko, M., Varakin, Y.Y., Krishnaswami, S., Kuate Defo, B., Kuipers, E.J., Polinder, S., Kulkarni, C., Kulkarni, V.S., Kwan, G.F., Lai, T., Lalloo, R., Lallukka, T., Shiri, R., Lam, H., Lan, Q., Lansingh, V.C., Lavados, P.M., Lawrynowicz, A.E., Leasher, J.L., Lee, J., Yoon, S., Levi, M., Liang, J., Wang, Y., Zhu, J., Lipshultz, S.E., Lloyd, B.K., Room, R., Logroscino, G., Lortet-Tieulent, J., Ma, S., Phua, H.P., Magis-Rodriguez, C., Mahdi, A.A., Malekzadeh, R., Mangalam, S., Mapoma, C.C., Masiye, F., Marape, M., Marcenes, W., Meaney, P.A., Margolis, D.J., Silberberg, D.H., Martin, R. V., Marzan, M.B., Mashal, M.T., Mason-Jones, A.J., Mazorodze, T.T., McKay, A.C., Mehndiratta, M., Meltzer, M., Mendoza, W., Apolinary Mhimbira, F., Miller, T.R., Mills, E.J., Mishra, S., Mohamed Ibrahim, N., Mohammad, K.A., Mola, G.L., Monasta, L., Montico, M., Ronfani, L., Moore, A.R., Morawska, L., Norman, R.E., Mori, R., Tsilimbaris, M., Moschandreas, J., Moturi, W.N., Werdecker, A., Mueller, U.O., Westerman, R., Mukaigawara, M., Nahas, Z., Naidoo, K.S., Naldi, L., Nand, D., Nangia, V., Neal, B., Nejjari, C., Neupane, S.P., Newton, C.R., Ngalesoni, F.N., Ngirabega, J.D., Nolla, J.M., Vollset, S.E., Norheim, O.F., Norrving, B., Nyakarahuka, L., Oh, I., Ohkubo, T., Olusanya, B.O., Opio, J.N., Pagcatipunan, R.S.,

Pandian, J.D., Park, E., Seedat, S., Pavlin, B.I., Pejin Stokic, L., Pereira, D.M., Perez-Padilla, R., Perez-Ruiz, F., Perico, N., Remuzzi, G., Trillini, M., Perry, S.A.L., Pervaiz, A., Pesudovs, K., Peterson, C.B., Petzold, M., Plass, D., Poenaru, D., Pond, C.D., Pope, C., Popova, S., Rehm, J., Prasad, N.M., Qato, D.M., Rafay, A., Rana, S.M., Ur Rahman, S., Raju, M., Rakovac, I., Rao, M., Razavi, H., Ribeiro, A.L., Velasquez-Melendez, G., Riccio, P.M., Sposato, L.A., Roca, A., Romieu, I., Straif, K., Ruhago, G.M., Sunguya, B.F., Sacco, R.L., Saha, S., Sahathevan, R., Sanabria, J.R., Sanchez-Riera, L., Sapkota, A., Saunders, J.E., Soneji, S., Sawhney, M., Saylan, M.I., Schneider, I.J.C., Schwebel, D.C., Singh, J.A., Serdar, B., Shaddick, G., Shinohara, Y., Shishani, K., Shiue, I., Sigfusdottir, I.D., Singh, A., Søreide, K., Sreeramareddy, C.T., Stapelberg, N.J.C., Stathopoulou, V., Steckling, N., Stroumpoulis, K., Swaminathan, S., Swaroop, M., Yano, Y., Sykes, B.L., Tabb, K.M., Talongwa, R.T., Tanne, D., Tavakkoli, M., Thackway, S. V., Thurston, G.D., Topouzis, F., Towbin, J.A., Toyoshima, H., Traebert, J., Trujillo, U., Tsala Dimbuene, Z., Tuzcu, E., Uchendu, U.S., Ukwaja, K.N., Van Dingenen, R., van Gool, C.H., van Os, J., Vasankari, T.J., Vasconcelos, A.N., Violante, F.S., Victorovich Vlassov, V., Waller, S.G., Wallin, M.T., Wang, W., Wessells, K., Wilkinson, J.D., Williams, H.C., Woldeyohannes, S.M., Wong, J.Q., Woolf, A.D., Xu, G., Yan, L.L., Yang, G., Yip, P., Yonemoto, N., Younis, M.Z., Younoussi, Z., Yu, C., Zaki, M.E., Zhao, Y., Zhu, S., 2015. Global, regional, and national comparative risk assessment of 79 behavioural, environmental and occupational, and metabolic risks or clusters of risks in 188 countries, 1990-2013: A systematic analysis for the Global Burden of Disease Study 2013. Lancet 386, 2287–2323. https://doi.org/10.1016/S0140-6736(15)00128-2

Franklin, M., Koutrakis, P., Schwartz, P., 2008. The role of particle composition on the

association between PM2.5 and mortality. Epidemiology 19, 680–9.

Gadd, J., Kennedy, P., 2000. Preliminary examination of organic compounds present in tyres, brake pads and road bitumen in New Zealand. Rep. - Kingett Mitchell Ltd Resour. Environ. Consult. 1–23.

Gao, D., J. Godri Pollitt, K., A. Mulholland, J., G. Russell, A., J. Weber, R., 2020a. Characterization and comparison of PM2.5 oxidative potential assessed by two acellular assays. Atmos. Chem. Phys. 20, 5197–5210. https://doi.org/10.5194/acp-20-5197-2020

Gao, D., Ripley, S., Weichenthal, S., Godri Pollitt, K.J., 2020b. Ambient particulate matter oxidative potential: Chemical determinants, associated health effects, and strategies for risk management. Free Radic. Biol. Med. 151, 7–25. https://doi.org/10.1016/j.freeradbiomed.2020.04.028

Gao, Y., Nelson, E.D., Field, M.P., Ding, Q., Li, H., Sherrell, R.M., Gigliotti, C.L., Van Ry, D.A., Glenn, T.R., Eisenreich, S.J., 2002. Characterization of atmospheric trace elements on PM2.5 particulate matter over the New York-New Jersey harbor estuary. Atmos. Environ. 36, 1077–1086. https://doi.org/10.1016/S1352-2310(01)00381-8

Garg, B.D., Cadle, S.H., Mulawa, P.A., Groblicki, P.J., Laroo, C., Parr, G.A., 2000. Brake wear particulate matter emissions. Environ. Sci. Technol. 34, 4463–4469. https://doi.org/10.1021/es001108h

Gharibvand, L., Shavlik, D., Ghamsary, M., Beeson, W.L., Soret, S., Knutsen, R., Knutsen, S.F., 2017. The association between ambient fine particulate air pollution and lung cancer incidence: Results from the AHSMOG-2 study. Environ. Health Perspect. 125, 378–384. https://doi.org/10.1289/EHP124

Gianini, M.F.D., Piot, C., Herich, H., Besombes, J.L., Jaffrezo, J.L., Hueglin, C., 2013. Source apportionment of PM10, organic carbon and elemental carbon at Swiss sites: An intercomparison of different approaches. Sci. Total Environ. 454–455, 99–108. https://doi.org/10.1016/j.scitotenv.2013.02.043

Gietl, J.K., Lawrence, R., Thorpe, A.J., Harrison, R.M., 2010. Identification of brake wear particles and derivation of a quantitative tracer for brake dust at a major road. Atmos. Environ. 44, 141–146. https://doi.org/10.1016/j.atmosenv.2009.10.016

Gill, L.W., Ring, P., Casey, B., Higgins, N.M.P., Johnston, P.M., 2017. Long term heavy metal removal by a constructed wetland treating rainfall runoff from a motorway. Sci. Total Environ. 601–602, 32–44. https://doi.org/10.1016/j.scitotenv.2017.05.182

Golubkov, A.W., Planteu, R., Krohn, P., Rasch, B., Brunnsteiner, B., Thaler, A., Hacker, V., 2018. Thermal runaway of large automotive Li-ion batteries. RSC Adv. 8, 40172–40186. https://doi.org/10.1039/C8RA06458J

Golubkov, A.W., Scheikl, S., Planteu, R., Voitic, G., Wiltsche, H., Stangl, C., Fauler, G., Thaler, A., Hacker, V., 2015. Thermal runaway of commercial 18650 Li-ion batteries with LFP and NCA cathodes - Impact of state of charge and overcharge. RSC Adv. 5, 57171–57186. https://doi.org/10.1039/c5ra05897j

Gramstat, S., Mertens, T., Waninger, R., Lugovyy, D., 2020. Impacts on brake particle emission testing. Atmosphere (Basel). 11. https://doi.org/10.3390/atmos11101132

Grieshop, A.P., Lipsky, E.M., Pekney, N.J., Takahama, S., Robinson, A.L., 2006. Fine particle emission factors from vehicles in a highway tunnel: Effects of fleet composition and season. Atmos. Environ. 40, 287–298. https://doi.org/10.1016/j.atmosenv.2006.03.064

Grigoratos, T., 2018. Regulation on Brake/Tire Composition. Non-Exhaust Emiss. 89–100. https://doi.org/10.1016/b978-0-12-811770-5.00004-2

Grigoratos, T., Gustafsson, M., Eriksson, O., Martini, G., 2018. Experimental investigation of tread wear and particle emission from tyres with different treadwear marking. Atmos. Environ. 182, 200–212. https://doi.org/10.1016/j.atmosenv.2018.03.049

Grigoratos, T., Martini, G., 2015. Brake wear particle emissions: a review. Environ. Sci. Pollut. Res. 22, 2491–2504. https://doi.org/10.1007/s11356-014-3696-8

Grigoratos, T., Martini, G., 2014. Non-exhaust Traffic Related Emissions. Brake and tyre wear PM, JRC Science and Policy Reports. Luxemburg. https://doi.org/10.2790/22000

Gualtieri, M., Mantecca, P., Cetta, F., Camatini, M., 2008. Organic compounds in tire particle induce reactive oxygen species and heat-shock proteins in the human alveolar cell line A549. Environ. Int. 34, 437–442. https://doi.org/10.1016/j.envint.2007.09.010

Gustafsson, M., Blomqvist, G., Gudmundsson, A., Dahl, A., Swietlicki, E., Bohgard, M., Lindbom, J., Ljungman, A., 2008. Properties and toxicological effects of particles from the interaction between tyres, road pavement and winter traction material. Sci. Total Environ. 393, 226–240. https://doi.org/10.1016/J.SCITOTENV.2007.12.030

Gustafsson, M., Eriksson, O., 2015. Emission of inhalable particles from studded tyre wear of road pavements : a comparative study.

Habre, R., Girguis, M., Urman, R., Fruin, S., Lurmann, F., Shafer, M., Gorski, P., Franklin, M., McConnell, R., Avol, E., Gilliland, F., 2020. Contribution of Tailpipe and Non-tailpipe Traffic Sources to Quasi-Ultrafine, Fine and Coarse Particulate Matter in Southern

California. J. Air Waste Manage. Assoc. 0. https://doi.org/10.1080/10962247.2020.1826366

Hadei, M., Naddafi, K., 2020. Cardiovascular effects of airborne particulate matter: A review of rodent model studies. Chemosphere 242. https://doi.org/10.1016/j.chemosphere.2019.125204

Hagino, H., Oyama, M., Sasaki, S., 2016. Laboratory testing of airborne brake wear particle emissions using a dynamometer system under urban city driving cycles. Atmos. Environ. 131, 269–278. https://doi.org/10.1016/j.atmosenv.2016.02.014

Hagino, H., Oyama, M., Sasaki, S., 2015. Airborne brake wear particle emission due to braking and accelerating. Wear 334–335, 44–48. https://doi.org/10.1016/j.wear.2015.04.012

Hakimzadeh, M., Soleimanian, E., Mousavi, A., Borgini, A., De Marco, C., Ruprecht, A.A., Sioutas, C., 2020. The impact of biomass burning on the oxidative potential of PM2.5 in the metropolitan area of Milan. Atmos. Environ. 224, 117328. https://doi.org/10.1016/j.atmosenv.2020.117328

Hall, T.J., 2017. A Comparison of Braking Behavior between an IC Engine and Pure Electric Vehicle in Los Angeles City Driving Conditions. SAE Tech. Pap. Part F1301. https://doi.org/10.4271/2017-01-2518

Hannan, M.A., Hoque, M.M., Hussain, A., Yusof, Y., Ker, P.J., 2018. State-of-the-Art and Energy Management System of Lithium-Ion Batteries in Electric Vehicle Applications: Issues and Recommendations. IEEE Access 6, 19362–19378. https://doi.org/10.1109/ACCESS.2018.2817655

Harrison, R.M., Jones, A.M., Gietl, J., Yin, J., Green, D.C., 2012. Estimation of the contributions

of brake dust, tire wear, and resuspension to nonexhaust traffic particles derived from atmospheric measurements. Environ. Sci. Technol. 46, 6523–6529. https://doi.org/10.1021/es300894r

Harrison, R.M., Tilling, R., Harrad, S., Jarvis, K., 2003. A study of trace metals and polycyclic aromatic hydrocarbons in the roadside environment 37, 2391–2402. https://doi.org/10.1016/S1352-2310(03)00122-5

Hartmann, N.B., Hüffer, T., Thompson, R.C., Hassellöv, M., Verschoor, A., Daugaard, A.E., Rist, S., Karlsson, T., Brennholt, N., Cole, M., Herrling, M.P., Hess, M.C., Ivleva, N.P., Lusher, A.L., Wagner, M., 2019. Are We Speaking the Same Language? Recommendations for a Definition and Categorization Framework for Plastic Debris. Environ. Sci. Technol. 53, 1039–1047. https://doi.org/10.1021/acs.est.8b05297

Hasheminassab, S., Daher, N., Saffari, A., Wang, D., Ostro, B.D., Sioutas, C., 2014. Spatial and temporal variability of sources of ambient fine particulate matter (PM2.5) in California. Atmos. Chem. Phys. 14, 12085–12097. https://doi.org/10.5194/acp-14-12085-2014

Hasheminassab, S., Sowlat, M.H., Pakbin, P., Katzenstein, A., Low, J., Polidori, A., 2020. High time-resolution and time-integrated measurements of particulate metals and elements in an environmental justice community within the Los Angeles Basin: Spatio-temporal trends and source apportionment. Atmos. Environ. X 7, 100089. https://doi.org/10.1016/j.aeaoa.2020.100089

Henderson, S.B., Beckerman, B., Jerrett, M., Brauer, M., 2007. Application of land use regression to estimate long-term concentrations of traffic-related nitrogen oxides and fine particulate matter. Environ. Sci. Technol. 41, 2422–2428.

https://doi.org/10.1021/es0606780

Herner, J.D., Green, P.G., Kleeman, M.J., 2006. Measuring the trace elemental composition of size-resolved airborne particles. Environ. Sci. Technol. 40, 1925–1933. https://doi.org/10.1021/es052315q

Heydari, S., Tainio, M., Woodcock, J., de Nazelle, A., 2020. Estimating traffic contribution to particulate matter concentration in urban areas using a multilevel Bayesian meta-regression approach. Environ. Int. 141, 105800. https://doi.org/10.1016/j.envint.2020.105800

Hinds, W.C., 1999. Aerosol technology: properties, behavior, and measurement of airborne particles., 2nd ed. Wiley, New York.

Hjortenkrans, D.S.T., Bergbäck, B.G., Häggerud, A. V., 2008. Response to comment on "Metal emissions from brake linings and tires: Case studies of Stockholm, Sweden 1995/1998 and 2005." Environ. Sci. Technol. 42, 2710. https://doi.org/10.1021/es7028069

Hsu, C.Y., Chiang, H.C., Chen, M.J., Yang, T.T., Wu, Y.S., Chen, Y.C., 2019. Impacts of hazardous metals and PAHs in fine and coarse particles with long-range transports in Taipei City. Environ. Pollut. 250, 934–943. https://doi.org/10.1016/j.envpol.2019.04.038

Hu, S., Polidori, A., Arhami, M., Shafer, M.M., Schauer, J.J., Cho, A., Sioutas, C., 2008. Redox activity and chemical speciation of size fractioned PM in the communities of the Los Angeles-Long Beach harbor. Atmos. Chem. Phys. 8, 6439–6451. https://doi.org/10.5194/acp-8-6439-2008

Huang, B.F., Chang, Y.C., Han, A.L., Hsu, H.T., 2018. Metal composition of ambient PM2.5 influences the pulmonary function of schoolchildren: A case study of school located nearby

of an electric arc furnace factory. Toxicol. Ind. Health 34, 253–261. https://doi.org/10.1177/0748233717754173

Huang, P., Wang, Q., Li, K., Ping, P., Sun, J., 2015. The combustion behavior of large scale lithium titanate battery. Sci. Rep. 5, 1–12. https://doi.org/10.1038/srep07788

Hüffer, T., Wagner, S., Reemtsma, T., Hofmann, T., 2019. Sorption of organic substances to tire wear materials: Similarities and differences with other types of microplastic. TrAC - Trends Anal. Chem. 113, 392–401. https://doi.org/10.1016/j.trac.2018.11.029

Hulskotte, J.H.J., Roskam, G.D., Denier van der Gon, H.A.C., 2014. Elemental composition of current automotive braking materials and derived air emission factors. Atmos. Environ. 99, 436–445. https://doi.org/10.1016/j.atmosenv.2014.10.007

Hussain, S., Abdul Hamid, M.K., Mat Lazim, A.R., Abu Bakar, A.R., 2014. Brake wear particle size and shape analysis of non-asbestos organic (NAO) and semi metallic brake pad. J. Teknol. 71, 129–134. https://doi.org/10.11113/jt.v71.3731

Hussein, T., Johansson, C., Karlsson, H., Hansson, H.C., 2008. Factors affecting non-tailpipe aerosol particle emissions from paved roads: On-road measurements in Stockholm, Sweden. Atmos. Environ. 42, 688–702. https://doi.org/10.1016/j.atmosenv.2007.09.064

IEA, 2021. Global EV Outlook 2021.

Iijima, A., Sato, K., Yano, K., Kato, M., Kozawa, K., Furuta, N., 2008. Emission factor for antimony in brake abrasion dusts as one of the major atmospheric antimony sources. Environ. Sci. Technol. 42, 2937–2942. https://doi.org/10.1021/es702137g

Iijima, A., Sato, K., Yano, K., Tago, H., Kato, M., Kimura, H., Furuta, N., 2007. Particle size

and composition distribution analysis of automotive brake abrasion dusts for the evaluation of antimony sources of airborne particulate matter. Atmos. Environ. 41, 4908–4919. https://doi.org/10.1016/j.atmosenv.2007.02.005

Jan Kole, P., Löhr, A.J., Van Belleghem, F.G.A.J., Ragas, A.M.J., 2017. Wear and tear of tyres: A stealthy source of microplastics in the environment. Int. J. Environ. Res. Public Health 14. https://doi.org/10.3390/ijerph14101265

Janssen, N.A.H., Strak, M., Yang, A., Hellack, B., Kelly, F.J., Kuhlbusch, T.A.J., Harrison, R.M., Brunekreef, B., Cassee, F.R., Steenhof, M., Hoek, G., 2015. Associations between three specific a-cellular measures of the oxidative potential of particulate matter and markers of acute airway and nasal inflammation in healthy volunteers. Occup. Environ. Med. 72, 49–56. https://doi.org/10.1136/oemed-2014-102303

Järlskog, I., Strömvall, A.M., Magnusson, K., Galfi, H., Björklund, K., Polukarova, M., Garção, R., Markiewicz, A., Aronsson, M., Gustafsson, M., Norin, M., Blom, L., Andersson-Sköld, Y., 2021. Traffic-related microplastic particles, metals, and organic pollutants in an urban area under reconstruction. Sci. Total Environ. 774. https://doi.org/10.1016/j.scitotenv.2021.145503

Jeong, C.H., Traub, A., Huang, A., Hilker, N., Wang, J.M., Herod, D., Dabek-Zlotorzynska, E., Celo, V., Evans, G.J., 2020. Long-term analysis of PM2.5 from 2004 to 2017 in Toronto: Composition, sources, and oxidative potential. Environ. Pollut. 263, 114652. https://doi.org/10.1016/j.envpol.2020.114652

Jeong, C.H., Wang, J.M., Hilker, N., Debosz, J., Sofowote, U., Su, Y., Noble, M., Healy, R.M., Munoz, T., Dabek-Zlotorzynska, E., Celo, V., White, L., Audette, C., Herod, D., Evans,

G.J., 2019. Temporal and spatial variability of traffic-related PM2.5 sources: Comparison of exhaust and non-exhaust emissions. Atmos. Environ. 198, 55–69. https://doi.org/10.1016/j.atmosenv.2018.10.038

Jerrett, M., Burnett, R.T., Ma, R., Arden Pope, C., Krewski, D., Newbold, K.B., Thurston, G., Shi, Y., Finkelstein, N., Calle, E.E., Thun, M.J., 2005. Spatial analysis of air pollution and mortality in Los Angeles. Epidemiology 16, 727–736. https://doi.org/10.1097/01.ede.0000181630.15826.7d

Jerrett, M., Shankardass, K., Berhane, K., Gauderman, W.J., Künzli, N., Avol, E., Gilliland, F., Lurmann, F., Molitor, J.N., Molitor, J.T., Thomas, D.C., Peters, J., McConnell, R., 2008. Traffic-related air pollution and asthma onset in children: A prospective cohort study with individual exposure measurement. Environ. Health Perspect. 116, 1433–1438. https://doi.org/10.1289/ehp.10968

Karagulian, F., Belis, C.A., Dora, C.F.C., Prüss-Ustün, A.M., Bonjour, S., Adair-Rohani, H., Amann, M., 2015. Contributions to cities' ambient particulate matter (PM): A systematic review of local source contributions at global level. Atmos. Environ. 120, 475–483. https://doi.org/10.1016/j.atmosenv.2015.08.087

Kim, B.M., Teffera, S., Zeldin, M.D., 2000. Characterization of PM25 and PM10 in the South Coast Air Basin of Southern California: Part 1-Spatial Variations. J. Air Waste Manag. Assoc. 50, 2034–2044. https://doi.org/10.1080/10473289.2000.10464242

Kim, G., Lee, S., 2018. Characteristics of Tire Wear Particles Generated by a Tire Simulator under Various Driving Conditions. Environ. Sci. Technol. 52, 12153–12161. https://doi.org/10.1021/acs.est.8b03459

Kitahara, K.I., Nakata, H., 2020. Plastic additives as tracers of microplastic sources in Japanese road dusts. Sci. Total Environ. 736, 139694. https://doi.org/10.1016/j.scitotenv.2020.139694

Klöckner, P., Seiwert, B., Weyrauch, S., Escher, B.I., Reemtsma, T., Wagner, S., 2021. Comprehensive characterization of tire and road wear particles in highway tunnel road dust by use of size and density fractionation. Chemosphere 279. https://doi.org/10.1016/j.chemosphere.2021.130530

Kovochich, M., Liong, M., Parker, J.A., Oh, S.C., Lee, J.P., Xi, L., Kreider, M.L., Unice, K.M., 2021. Chemical mapping of tire and road wear particles for single particle analysis. Sci. Total Environ. 757, 144085. https://doi.org/10.1016/j.scitotenv.2020.144085

Kramer, A.L., Dorn, S., Perez, A., Roper, C., Titaley, I.A., Cayton, K., Cook, R.P., Cheong, P.H.Y., Massey Simonich, S.L., 2021. Assessing the oxidative potential of PAHs in ambient PM2.5 using the DTT consumption assay. Environ. Pollut. 285, 117411. https://doi.org/10.1016/j.envpol.2021.117411

Kreider, M.L., Panko, J.M., McAtee, B.L., Sweet, L.I., Finley, B.L., 2010. Physical and chemical characterization of tire-related particles: Comparison of particles generated using different methodologies. Sci. Total Environ. 408, 652–659. https://doi.org/10.1016/j.scitotenv.2009.10.016

Kukutschová, J., Filip, P., 2018. Review of Brake Wear Emissions. Non-Exhaust Emiss. 123–146. https://doi.org/10.1016/b978-0-12-811770-5.00006-6

Kukutschová, J., Moravec, P., Tomášek, V., Matějka, V., Smolík, J., Schwarz, J., Seidlerová, J., Šafářová, K., Filip, P., 2011. On airborne nano/micro-sized wear particles released from

low-metallic automotive brakes. Environ. Pollut. 159, 998–1006. https://doi.org/10.1016/j.envpol.2010.11.036

Kumar, P., Pirjola, L., Ketzel, M., Harrison, R.M., 2013. Nanoparticle emissions from 11 non-vehicle exhaust sources - A review. Atmos. Environ. https://doi.org/10.1016/j.atmosenv.2012.11.011

Kumar, V.V., Kumaran, S.S., 2019. Friction material composite: Types of brake friction material formulations and effects of various ingredients on brake performance-a review. Mater. Res. Express 6. https://doi.org/10.1088/2053-1591/ab2404

Kupiainen, K.J., Tervahattu, H., Räisänen, M., Mäkelä, T., Aurela, M., Hillamo, R., 2005. Size and composition of airborne particles from pavement wear, tires, and traction sanding. Environ. Sci. Technol. 39, 699–706. https://doi.org/10.1021/es035419e

Kwak, J.H., Kim, H., Lee, J., Lee, S., 2013. Characterization of non-exhaust coarse and fine particles from on-road driving and laboratory measurements. Sci. Total Environ. 458–460, 273–282. https://doi.org/10.1016/j.scitotenv.2013.04.040

Lai, X., Wang, S., Wang, H., Zheng, Y., Feng, X., 2021. Investigation of thermal runaway propagation characteristics of lithium-ion battery modules under different trigger modes. Int. J. Heat Mass Transf. 171, 121080. https://doi.org/10.1016/j.ijheatmasstransfer.2021.121080

Larsen, R.K., Baker, J.E., 2003. Source apportionment of polycyclic aromatic hydrocarbons in the urban atmosphere: A comparison of three methods. Environ. Sci. Technol. 37, 1873–1881. https://doi.org/10.1021/es0206184

Larsson, F., Andersson, P., Mellander, B.E., 2016. Lithium-ion battery aspects on fires in electrified vehicles on the basis of experimental abuse tests. Batteries 2, 1–13. https://doi.org/10.3390/batteries2020009

Lassen, C., Hansen, S.F., Magnusson, K., Hartmann, N.B., Rehne Jensen, P., Nielsen, T.G., Brinch, A., 2015. Microplastics: Occurrence , effects and sources of releases to the environment in Denmark, Environmental project No. 1793. Strandgade.

Lawrence, S., Sokhi, R., Ravindra, K., Mao, H., Prain, H.D., Bull, I.D., 2013. Source apportionment of traffic emissions of particulate matter using tunnel measurements. Atmos. Environ. 77, 548–557. https://doi.org/10.1016/j.atmosenv.2013.03.040

Le Tertre, A., Medina, Samoli, Forsberg, Michelozzi, Boumghar, Vonk, Bellini, Atkinson, Ayres, Sunyer, Schwartz, Katsouyanni, 2002. cardiovascular diseases in eight European cities. J. Epidemol Community Heath 56, 773–779.

Lee, S.E., Llaneras, E., Klauer, S.G., Sudweeks, J., 2007. Analyses of Rear-End Crashes and Near-Crashes in the 100-Car Naturalistic Driving Study to Support Rear-Signaling Countermeasure Development. U.S. Department of Transportation National Highway Traffic Safety Administration. Washington, D.C.

Lee, S.J., Demokritou, P., Koutrakis, P., Delgado-Saborit, J.M., 2006. Development and evaluation of personal respirable particulate sampler (PRPS). Atmos. Environ. 40, 212–224. https://doi.org/10.1016/j.atmosenv.2005.08.041

Li, W., Yang, X., Wang, S., Xiao, J., Hou, Q., 2021. Research and prospect of ceramics for automotive disc-brakes. Ceram. Int. 47, 10442–10463. https://doi.org/10.1016/j.ceramint.2020.12.206

Li, W., Yang, X., Wang, S., Xiao, J., Hou, Q., 2020. Comprehensive analysis on the performance and material of automobile brake discs. Metals (Basel). 10. https://doi.org/10.3390/met10030377

Liang, J., Feng, C., Zeng, G., Zhong, M., Gao, X., Li, Xiaodong, He, X., Li, Xin, Fang, Y., Mo, D., 2017. Atmospheric deposition of mercury and cadmium impacts on topsoil in a typical coal mine city, Lianyuan, China. Chemosphere 189, 198–205. https://doi.org/10.1016/j.chemosphere.2017.09.046

Liati, A., Schreiber, D., Lugovyy, D., Gramstat, S., Dimopoulos Eggenschwiler, P., 2019. Airborne particulate matter emissions from vehicle brakes in micro- and nano-scales: Morphology and chemistry by electron microscopy. Atmos. Environ. 212, 281–289. https://doi.org/10.1016/j.atmosenv.2019.05.037

Lin, Y.C., Tsai, C.J., Wu, Y.C., Zhang, R., Chi, K.H., Huang, Y.T., Lin, S.H., Hsu, S.C., 2015. Characteristics of trace metals in traffic-derived particles in Hsuehshan Tunnel, Taiwan: Size distribution, potential source, and fingerprinting metal ratio. Atmos. Chem. Phys. 15, 4117–4130. https://doi.org/10.5194/acp-15-4117-2015

Liu, Q., Lu, Z., Xiong, Y., Huang, F., Zhou, J., Schauer, J.J., 2020. Oxidative potential of ambient PM2.5 in Wuhan and its comparisons with eight areas of China. Sci. Total Environ. 701, 134844. https://doi.org/10.1016/j.scitotenv.2019.134844

Liu, W.J., Xu, Y.S., Liu, W.X., Liu, Q.Y., Yu, S.Y., Liu, Y., Wang, X., Tao, S., 2018. Oxidative potential of ambient PM2.5 in the coastal cities of the Bohai Sea, northern China: Seasonal variation and source apportionment. Environ. Pollut. 236, 514–528. https://doi.org/10.1016/j.envpol.2018.01.116

Llompart, M., Sanchez-Prado, L., Pablo Lamas, J., Garcia-Jares, C., Roca, E., Dagnac, T., 2013. Hazardous organic chemicals in rubber recycled tire playgrounds and pavers. Chemosphere 90, 423–431. https://doi.org/10.1016/j.chemosphere.2012.07.053

Lou, C., Liu, H., Li, Y., Peng, Y., Wang, J., Dai, L., 2017. Relationships of relative humidity with PM2.5 and PM10 in the Yangtze River Delta, China. Environ. Monit. Assess. 189. https://doi.org/10.1007/s10661-017-6281-z

Lough, G.C., Schauer, J.J., Park, J.S., Shafer, M.M., Deminter, J.T., Weinstein, J.P., 2005. Emissions of metals associated with motor vehicle roadways. Environ. Sci. Technol. 39, 826–836. https://doi.org/10.1021/es048715f

Lovett, C., Sowlat, M.H., Saliba, N.A., Shihadeh, A.L., Sioutas, C., 2018. Oxidative potential of ambient particulate matter in Beirut during Saharan and Arabian dust events. Atmos. Environ. 188, 34–42. https://doi.org/10.1016/j.atmosenv.2018.06.016

Luhana, L., Sokhi, R., Warner, L., Mao, H., Boulter, P., McCrae, I., Wright, J., Osborn, D., 2004. Characterisation of Exhaust Particulate Emissions from Road Vehicles - Measurement of non-exhaust particulate matter. Characterisation Exhaust Part. Emiss. from Road Veh.

Magari, S.R., Schwartz, J., Williams, P.L., Hauser, R., Smith, T.J., Christiani, D.C., 2002. The Association of Particulate Air Metal Concentrations with Heart Rate Variability. Environ. Health Perspect. 110.

Malachova, K., Kukutschova, J., Rybkova, Z., Sezimova, H., Placha, D., Cabanova, K., Filip, P., 2016. Toxicity and mutagenicity of low-metallic automotive brake pad materials. Ecotoxicol. Environ. Saf. 131, 37–44. https://doi.org/10.1016/j.ecoenv.2016.05.003

Markiewicz, A., Björklund, K., Eriksson, E., Kalmykova, Y., Strömvall, A.M., Siopi, A., 2017. Emissions of organic pollutants from traffic and roads: Priority pollutants selection and substance flow analysis. Sci. Total Environ. 580, 1162–1174. https://doi.org/10.1016/j.scitotenv.2016.12.074

Marris, C.R., Kompella, S.N., Miller, M.R., Incardona, J.P., Brette, F., Hancox, J.C., Sørhus, E., Shiels, H.A., 2020. Polyaromatic hydrocarbons in pollution: a heart-breaking matter. J. Physiol. 598, 227–247. https://doi.org/10.1113/JP278885

Mathissen, M., Grigoratos, T., Lahde, T., Vogt, R., 2019. Brake Wear Particle Emissions of a Passenger Car Measured on a Chassis Dynamometer. Atmosphere (Basel). 10, 556. https://doi.org/10.3390/atmos10090556

Mathissen, M., Grochowicz, J., Schmidt, C., Vogt, R., Farwick zum Hagen, F.H., Grabiec, T., Steven, H., Grigoratos, T., 2018. A novel real-world braking cycle for studying brake wear particle emissions. Wear 414–415, 219–226. https://doi.org/10.1016/j.wear.2018.07.020

Mathissen, M., Scheer, V., Kirchner, U., Vogt, R., Benter, T., 2012. Non-exhaust PM emission measurements of a light duty vehicle with a mobile trailer. Atmos. Environ. 59, 232–242. https://doi.org/10.1016/j.atmosenv.2012.05.020

Mathissen, M., Scheer, V., Vogt, R., Benter, T., 2011. Investigation on the potential generation of ultrafine particles from the tire-road interface. Atmos. Environ. 45, 6172–6179. https://doi.org/10.1016/j.atmosenv.2011.08.032

Maurya, A.K., Bokare, P.S., 2012. Study of Deceleration Behaviour of Different Vehicle Types. Int. J. Traffic Transp. Eng. 2, 253–270. https://doi.org/10.7708/ijtte.2012.2(3).07

Menapace, C., Leonardi, M., Secchi, M., Bonfanti, A., Gialanella, S., Straffelini, G., 2019. Thermal behavior of a phenolic resin for brake pad manufacturing. J. Therm. Anal. Calorim. 137, 759–766. https://doi.org/10.1007/s10973-019-08004-2

Miao, Y., Hynan, P., Von Jouanne, A., Yokochi, A., 2019. Current li-ion battery technologies in electric vehicles and opportunities for advancements. Energies 12, 1–20. https://doi.org/10.3390/en12061074

Milani, M., Pucillo, F.P., Ballerini, M., Camatini, M., Gualtieri, M., Martino, S., 2004. First evidence of tyre debris characterization at the nanoscale by focused ion beam. Mater. Charact. 52, 283–288. https://doi.org/10.1016/j.matchar.2004.06.001

Miller, D.M., Buettner, G.R., Aust, S.D., 1990. Transition metals as catalysts of "autoxidation" reactions. Free Radic. Biol. Med. 8, 95–108. https://doi.org/10.1016/0891-5849(90)90148-C

Miller, M.R., 2020. Oxidative stress and the cardiovascular effects of air pollution. Free Radic. Biol. Med. 151, 69–87. https://doi.org/10.1016/j.freeradbiomed.2020.01.004

Mleczek, P., Borowiak, K., Budka, A., Szostek, M., Niedzielski, P., 2021. Possible sources of rare earth elements near different classes of road in Poland and their phytoextraction to herbaceous plant species. Environ. Res. 193. https://doi.org/10.1016/j.envres.2020.110580

Moawad, a., Sharer, P., Rousseau, a., 2011. Light-Duty Vehicle Fuel Consumption Displacement Potential up to 2045. Energy 510p.

Morillas, H., Gredilla, A., Gallego-Cartagena, E., Upasen, S., Maguregui, M., Madariaga, J.M., 2020a. PM10 spatial distribution and metals speciation study in the Bilbao metropolitan area during the 2017–2018 period. Chemosphere 259.

https://doi.org/10.1016/j.chemosphere.2020.127482

Morillas, H., Maguregui, M., Gallego-Cartagena, E., Marcaida, I., Carral, N., Madariaga, J.M., 2020b. The influence of marine environment on the conservation state of Built Heritage: An overview study. Sci. Total Environ. 745, 140899. https://doi.org/10.1016/j.scitotenv.2020.140899

Morillas, H., Marcaida, I., Maguregui, M., Upasen, S., Gallego-Cartagena, E., Madariaga, J.M., 2019. Identification of metals and metalloids as hazardous elements in PM2.5 and PM10 collected in a coastal environment affected by diffuse contamination. J. Clean. Prod. 226, 369–378. https://doi.org/10.1016/j.jclepro.2019.04.063

Motallebi, N., Taylor, C.A., Croes, B.E., 2003. Particulate matter in california: Part 2—Spatial, Temporal, and Compositional Patterns of PM2.5, PM10–2.5, and PM10. J. Air Waste Manag. Assoc. 53, 1517–1530. https://doi.org/10.1080/10473289.2003.10466323

Mousavi, A., Sowlat, M.H., Hasheminassab, S., Polidori, A., Shafer, M.M., Schauer, J.J., Sioutas, C., 2019. Impact of emissions from the Ports of Los Angeles and Long Beach on the oxidative potential of ambient PM0.25 measured across the Los Angeles County. Sci. Total Environ. 651, 638–647. https://doi.org/10.1016/j.scitotenv.2018.09.155

Mousavi, A., Sowlat, M.H., Sioutas, C., 2018. Diurnal and seasonal trends and source apportionment of redox-active metals in Los Angeles using a novel online metal monitor and Positive Matrix Factorization (PMF). Atmos. Environ. 174, 15–24. https://doi.org/10.1016/j.atmosenv.2017.11.034

Mukhtar, A., Limbeck, A., 2013. Recent developments in assessment of bio-accessible trace metal fractions in airborne particulate matter: A review. Anal. Chim. Acta 774, 11–25.

https://doi.org/10.1016/j.aca.2013.02.008

NAEI, 2018. Road transport emission factor.

Niemann, H., Winner, H., Asbach, C., Kaminski, H., Frentz, G., Milczarek, R., 2020. Influence of disc temperature on ultrafine, fine, and coarse particle emissions of passenger car disc brakes with organic and inorganic pad binder materials. Atmosphere (Basel). 11. https://doi.org/10.3390/atmos11101060

Norris, G., Duvall, R., Brown, S., Bai, S., 2014. EPA Positive Matrix Factorization (PMF) 5.0 Fundamentals and User Guide.

Nosko, O., Olofsson, U., 2017. Quantification of ultrafine airborne particulate matter generated by the wear of car brake materials. Wear 374–375, 92–96. https://doi.org/10.1016/j.wear.2017.01.003

Oliveira, C., Pio, C., Caseiro, A., Santos, P., Nunes, T., Mao, H., Luahana, L., Sokhi, R., 2010. Road traffic impact on urban atmospheric aerosol loading at Oporto, Portugal. Atmos. Environ. 44, 3147–3158. https://doi.org/10.1016/j.atmosenv.2010.05.027

Olofsson, U., Tu, M., Nosko, O., Lyu, Y., Dizdar, S., 2018. A pin-on-disc study of airborne wear particle emissions from studded tyre on concrete road contacts. Wear 410–411, 165–172. https://doi.org/10.1016/j.wear.2018.06.012

Orach, J., Rider, C.F., Carlsten, C., 2021. Concentration-dependent health effects of air pollution in controlled human exposures. Environ. Int. 150, 106424. https://doi.org/10.1016/j.envint.2021.106424

Oroumiyeh, F., Jerrett, M., Del Rosario, I., Lipsitt, J., Liu, J., Paulson, S.E., Ritz, B., Schauer,

J.J., Shafer, M.M., Shen, J., Weichenthal, S., Banerjee, S., Zhu, Y., 2022. Elemental composition of fine and coarse particles across the greater Los Angeles area: Spatial variation and contributing sources. Environ. Pollut. 292, 118356. https://doi.org/10.1016/j.envpol.2021.118356

Oroumiyeh, F., Zhu, Y., 2021. Brake and tire particles measured from on-road vehicles : Effects of vehicle mass and braking intensity. Atmos. Environ. X 12, 100121. https://doi.org/10.1016/j.aeaoa.2021.100121

Ostro, B., Feng, W.Y., Broadwin, R., Green, S., Lipsett, M., 2007. The effects of components of fine particulate air pollution on mortality in California: Results from CALFINE. Environ. Health Perspect. 115, 13–19. https://doi.org/10.1289/ehp.9281

Ostro, B., Hu, J., Goldberg, D., Reynolds, P., Hertz, A., Bernstein, L., Kleeman, M.J., 2015. Associations of mortality with long-term exposures to fine and ultrafine particles, species and sources: Results from the California teachers study Cohort. Environ. Health Perspect. 123, 549–556. https://doi.org/10.1289/ehp.1408565

Ostro, B., Lipsett, M., Reynolds, P., Goldberg, D., Hertz, A., Garcia, C., Henderson, K.D., Bernstein, L., 2010. Long-term exposure to constituents of fine particulate air pollution and mortality: Results from the California Teachers Study. Environ. Health Perspect. 118, 363–369. https://doi.org/10.1289/ehp.0901181

Owusu, P.A., Sarkodie, S.A., 2020. Global estimation of mortality, disability-adjusted life years and welfare cost from exposure to ambient air pollution. Sci. Total Environ. 742, 140636. https://doi.org/10.1016/j.scitotenv.2020.140636

Pacyna, J.M., Pacyna, E.G., 2001. An assessment of global and regional emissions of trace

metals to the atmosphere from anthropogenic sources worldwide. Environ. Rev. 9, 269–298. https://doi.org/10.1139/er-9-4-269

Padoan, E., Amato, F., 2018. Chapter 2 - Vehicle Non-Exhaust Emissions: Impact on Air Quality, in: Amato, F.B.T.-N.-E.E. (Ed.), . Academic Press, pp. 21–65. https://doi.org/https://doi.org/10.1016/B978-0-12-811770-5.00002-9

Pakbin, P., Ning, Z., Shafer, M.M., Schauer, J.J., Sioutas, C., 2011. Seasonal and Spatial Coarse Particle Elemental Concentrations in the Los Angeles Area. Aerosol Sci. Technol. 45, 949–963. https://doi.org/10.1080/02786826.2011.571309

Panko, J., Kreider, M., Unice, K., 2018. Review of Tire Wear Emissions. Non-Exhaust Emiss. 147–160. https://doi.org/10.1016/b978-0-12-811770-5.00007-8

Panko, J., McAtee, B., Kreider, M., Gustafsson, M., Blomqvist, G., Gudmundsson, A., Sweet, L., Finley, B., 2009. Physio-chemical analysis of airborne tire wear particles, in: Toxicology Letters. p. S205. https://doi.org/10.1016/j.toxlet.2009.06.621

Panko, J.M., Chu, J., Kreider, M.L., Unice, K.M., 2013. Measurement of airborne concentrations of tire and road wear particles in urban and rural areas of France, Japan, and the United States. Atmos. Environ. 72, 192–199. https://doi.org/10.1016/j.atmosenv.2013.01.040

Pant, P., Harrison, R.M., 2013. Estimation of the contribution of road traffic emissions to particulate matter concentrations from field measurements: A review. Atmos. Environ. 77, 78–97. https://doi.org/10.1016/j.atmosenv.2013.04.028

Park, I., Kim, H., Lee, S., 2018. Characteristics of tire wear particles generated in a laboratory simulation of tire/road contact conditions. J. Aerosol Sci. 124, 30–40.

https://doi.org/10.1016/j.jaerosci.2018.07.005

Park, I., Lee, J., Lee, S., 2017. Laboratory study of the generation of nanoparticles from tire tread. Aerosol Sci. Technol. 51, 188–197. https://doi.org/10.1080/02786826.2016.1248757

Park, J., Joo, B., Seo, H., Song, W., Lee, J.J., Lee, W.K., Jang, H., 2021. Analysis of wear induced particle emissions from brake pads during the worldwide harmonized light vehicles test procedure (WLTP). Wear 466–467, 203539. https://doi.org/10.1016/j.wear.2020.203539

Park, J., Park, E.H., Schauer, J.J., Yi, S.M., Heo, J., 2018. Reactive oxygen species (ROS) activity of ambient fine particles (PM2.5) measured in Seoul, Korea. Environ. Int. 117, 276–283. https://doi.org/10.1016/j.envint.2018.05.018

Pedersen, M., Giorgis-Allemand, L., Bernard, C., Aguilera, I., Andersen, A.-M.N., Ballester, F., Beelen, R.M.J., Chatzi, L., Cirach, M., Danileviciute, A., Dedele, A., Eijsden, M. van, Estarlich, M., Fernández-Somoano, A., Fernández, M.F., Forastiere, F., Gehring, U., Grazuleviciene, R., Gruzieva, O., Heude, B., Hoek, G., Hoogh, K. de, van den Hooven, E.H., Håberg, S.E., Jaddoe, V.W. V, Klümper, C., Korek, M., Krämer, U., Lerchundi, A., Lepeule, J., Nafstad, P., Nystad, W., Patelarou, E., Porta, D., Postma, D., Raaschou-Nielsen, O., Rudnai, P., Sunyer, J., Stephanou, E., Sørensen, M., Thiering, E., Tuffnell, D., Varró, M.J., Vrijkotte, T.G.M., Wijga, A., Wilhelm, M., Wright, J., Nieuwenhuijsen, M.J., Pershagen, G., Brunekreef, B., Kogevinas, M., Slama, R., 2013. Ambient air pollution and low birthweight: a European cohort study (ESCAPE). Lancet Respir. Med. 1, 695–704. https://doi.org/10.1016/S2213-2600(13)70192-9

Perrone, M.R., Bertoli, I., Romano, S., Russo, M., Rispoli, G., Pietrogrande, M.C., 2019. PM2.5

and PM10 oxidative potential at a Central Mediterranean Site: Contrasts between dithiothreitol- and ascorbic acid-measured values in relation with particle size and chemical composition. Atmos. Environ. 210, 143–155. https://doi.org/10.1016/j.atmosenv.2019.04.047

Pietrogrande, M.C., Dalpiaz, C., Dell'Anna, R., Lazzeri, P., Manarini, F., Visentin, M., Tonidandel, G., 2018. Chemical composition and oxidative potential of atmospheric coarse particles at an industrial and urban background site in the alpine region of northern Italy. Atmos. Environ. 191, 340–350. https://doi.org/10.1016/j.atmosenv.2018.08.022

Pirjola, L., Johansson, C., Kupiainen, K., Stojiljkovic, A., Karlsson, H., Hussein, T., 2010. Road dust emissions from paved roads measured using different mobile systems. J. Air Waste Manag. Assoc. 60, 1422–1433. https://doi.org/10.3155/1047-3289.60.12.1422

Piscitello, A., Bianco, C., Casasso, A., Sethi, R., 2021. Non-exhaust traffic emissions: Sources, characterization, and mitigation measures. Sci. Total Environ. 766, 144440. https://doi.org/10.1016/j.scitotenv.2020.144440

Pitiranggon, M., Johnson, S., Haney, J., Eisl, H., Ito, K., 2021. Long-term trends in local and transported PM2.5 pollution in New York City. Atmos. Environ. 248, 118238. https://doi.org/10.1016/j.atmosenv.2021.118238

Plachá, D., Peikertova, P., Kukutschova, J., Lee, P.W., Čabanová, K., Karas, J., Kuchařová, J., Filip, P., 2015. Identification of Organic Compounds Released from Low-Metallic Automotive Model Brake Pad and its Non-Airborne Wear Particles. SAE Int. J. Mater. Manuf. 9, 123–132. https://doi.org/10.4271/2015-01-2662

Poulakis, E., Theodosi, C., Bressi, M., Sciare, J., Ghersi, V., Mihalopoulos, N., 2015. Airborne

mineral components and trace metals in Paris region: spatial and temporal variability. Environ. Sci. Pollut. Res. 22, 14663–14672. https://doi.org/10.1007/s11356-015-4679-0

Puisney, C., Oikonomou, E.K., Nowak, S., Chevillot, A., Casale, S., Baeza-Squiban, A., Berret, J.F., 2018. Brake wear (nano)particle characterization and toxicity on airway epithelial cells: In vitro. Environ. Sci. Nano 5, 1036–1044. https://doi.org/10.1039/c7en00825b

Qu, J., Blau, P.J., Jolly, B.C., 2009. Oxygen-diffused titanium as a candidate brake rotor material. Wear 267, 818–822. https://doi.org/10.1016/j.wear.2008.12.044

Que, M., Tong, Y., Wei, G., Yuan, K., Wei, J., Jiang, Y., Zhu, H., Chen, Y., 2016. Safe and flexible ion gel based composite electrolyte for lithium batteries. J. Mater. Chem. A 4, 14132–14140. https://doi.org/10.1039/c6ta04914a

Querol, X., Alastuey, A., Moreno, T., Viana, M.M., Castillo, S., Pey, J., Rodríguez, S., Artiñano, B., Salvador, P., Sánchez, M., Garcia Dos Santos, S., Herce Garraleta, M.D., Fernandez-Patier, R., Moreno-Grau, S., Negral, L., Minguillón, M.C., Monfort, E., Sanz, M.J., Palomo-Marín, R., Pinilla-Gil, E., Cuevas, E., de la Rosa, J., Sánchez de la Campa, A., 2008. Spatial and temporal variations in airborne particulate matter (PM10 and PM2.5) across Spain 1999-2005. Atmos. Environ. 42, 3964–3979. https://doi.org/10.1016/j.atmosenv.2006.10.071

Querol, X., Viana, M., Alastuey, A., Amato, F., Moreno, T., Castillo, S., Pey, J., de la Rosa, J., Sánchez de la Campa, A., Artíñano, B., Salvador, P., García Dos Santos, S., Fernández-Patier, R., Moreno-Grau, S., Negral, L., Minguillón, M.C., Monfort, E., Gil, J.I., Inza, A., Ortega, L.A., Santamaría, J.M., Zabalza, J., 2007. Source origin of trace elements in PM from regional background, urban and industrial sites of Spain. Atmos. Environ. 41, 7219–

7231. https://doi.org/10.1016/j.atmosenv.2007.05.022

Raaschou-Nielsen, O., Beelen, R., Wang, M., Hoek, G., Andersen, Z.J., Hoffmann, B., Stafoggia, M., Samoli, E., Weinmayr, G., Dimakopoulou, K., Nieuwenhuijsen, M., Xun, W.W., Fischer, P., Eriksen, K.T., Sørensen, M., Tjønneland, A., Ricceri, F., de Hoogh, K., Key, T., Eeftens, M., Peeters, P.H., Bueno-de-Mesquita, H.B., Meliefste, K., Oftedal, B., Schwarze, P.E., Nafstad, P., Galassi, C., Migliore, E., Ranzi, A., Cesaroni, G., Badaloni, C., Forastiere, F., Penell, J., De Faire, U., Korek, M., Pedersen, N., Östenson, C.G., Pershagen, G., Fratiglioni, L., Concin, H., Nagel, G., Jaensch, A., Ineichen, A., Naccarati, A., Katsoulis, M., Trichpoulou, A., Keuken, M., Jedynska, A., Kooter, I.M., Kukkonen, J., Brunekreef, B., Sokhi, R.S., Katsouyanni, K., Vineis, P., 2016. Particulate matter air pollution components and risk for lung cancer. Environ. Int. 87, 66–73. https://doi.org/10.1016/j.envint.2015.11.007

Rao, L., Zhang, L., Wang, X., Xie, T., Zhou, S., Lu, S., Liu, X., Lu, H., Xiao, K., Wang, W., Wang, Q., 2020. Oxidative potential induced by ambient particulate matters with acellular assays: A review. Processes 8, 1–21. https://doi.org/10.3390/pr8111410

Ren, A., Qiu, X., Jin, L., Ma, J., Li, Z., Zhang, L., Zhu, H., Finnell, R.H., Zhu, T., 2011. Association of selected persistent organic pollutants in the placenta with the risk of neural tube defects. Proc. Natl. Acad. Sci. U. S. A. 108, 12770–12775. https://doi.org/10.1073/pnas.1105209108

Rexeis, M., Hausberger, S., 2009. Trend of vehicle emission levels until 2020 - Prognosis based on current vehicle measurements and future emission legislation. Atmos. Environ. 43, 4689–4698. https://doi.org/10.1016/j.atmosenv.2008.09.034

Rietmann, N., Hügler, B., Lieven, T., 2020. Forecasting the trajectory of electric vehicle sales and the consequences for worldwide CO2 emissions. J. Clean. Prod. 261, 121038. https://doi.org/10.1016/j.jclepro.2020.121038

Rietmann, N., Lieven, T., 2019. How policy measures succeeded to promote electric mobility – Worldwide review and outlook. J. Clean. Prod. 206, 66–75. https://doi.org/10.1016/j.jclepro.2018.09.121

Rivas, I., Mazaheri, M., Viana, M., Moreno, T., Clifford, S., He, C., Bischof, O.F., Martins, V., Reche, C., Alastuey, A., Alvarez-Pedrerol, M., Sunyer, J., Morawska, L., Querol, X., 2017. Identification of technical problems affecting performance of DustTrak DRX aerosol monitors. Sci. Total Environ. 584–585, 849–855. https://doi.org/10.1016/j.scitotenv.2017.01.129

Rogge, W.F., Hildemann, L.M., Mazurek, M.A., Cass, G.R., Simoneit, B.R.T., 1993. Sources of Fine Organic Aerosol. 3. Road Dust, Tire Debris, and Organometallic Brake Lining Dust: Roads as Sources and Sinks. Environ. Sci. Technol. 27, 1892–1904. https://doi.org/10.1021/es00046a019

Rönkkö, T.J., Jalava, P.I., Happo, M.S., Kasurinen, S., Sippula, O., Leskinen, A., Koponen, H., Kuuspalo, K., Ruusunen, J., Väisänen, O., Hao, L., Ruuskanen, A., Orasche, J., Fang, D., Zhang, L., Lehtinen, K.E.J., Zhao, Y., Gu, C., Wang, Q., Jokiniemi, J., Komppula, M., Hirvonen, M.R., 2018. Emissions and atmospheric processes influence the chemical composition and toxicological properties of urban air particulate matter in Nanjing, China. Sci. Total Environ. 639, 1290–1310. https://doi.org/10.1016/j.scitotenv.2018.05.260

Rossini, P., Guerzoni, S., Molinaroli, E., Rampazzo, G., De Lazzari, A., Zancanaro, A., 2005.

Atmospheric bulk deposition to the lagoon of Venice: Part I. Fluxes of metals, nutrients and organic contaminants. Environ. Int. 31, 959–974. https://doi.org/10.1016/j.envint.2005.05.006

Sadagopan, P., Natarajan, H.K., Praveen Kumar, J., 2018. Study of silicon carbide-reinforced aluminum matrix composite brake rotor for motorcycle application. Int. J. Adv. Manuf. Technol. 94, 1461–1475. https://doi.org/10.1007/s00170-017-0969-7

Sadiktsis, I., Bergvall, C., Johansson, C., Westerholm, R., 2012. Automobile tires-A potential source of highly carcinogenic dibenzopyrenes to the environment. Environ. Sci. Technol. 46, 3326–3334. https://doi.org/10.1021/es204257d

Salminen, H., 2014. Parametrizing tyre wear using a brush tyre mode. Royal Institute of Technology, Stockholm.

Salomons, W., Förstner, U., 1984. Metals in the Hydrocycle. Springer, Berlin. https://doi.org/10.1007/978-3-642-69325-0

Samoli, E., Atkinson, R.W., Analitis, A., Fuller, G.W., Green, D.C., Mudway, I., Anderson, H.R., Kelly, F.J., 2016. Associations of short-term exposure to traffic-related air pollution with cardiovascular and respiratory hospital admissions in London, UK. Occup. Environ. Med. 73, 300–307. https://doi.org/10.1136/oemed-2015-103136

Sanchez, K.A., Foster, M., Nieuwenhuijsen, M.J., May, A.D., Ramani, T., Zietsman, J., Khreis, H., 2020. Urban policy interventions to reduce traffic emissions and traffic-related air pollution: Protocol for a systematic evidence map. Environ. Int. 142. https://doi.org/10.1016/j.envint.2020.105826

Sanders, P.G., Xu, N., Dalka, T.M., Maricq, M.M., 2003. Airborne brake wear debris: Size distributions, composition, and a comparison of dynamometer and vehicle tests. Environ. Sci. Technol. 37, 4060–4069. https://doi.org/10.1021/es034145s

Sapkota, A., Chelikowsky, A.P., Nachman, K.E., Cohen, A.J., Ritz, B., 2012. Exposure to particulate matter and adverse birth outcomes: A comprehensive review and meta-analysis. Air Qual. Atmos. Heal. 5, 369–381. https://doi.org/10.1007/s11869-010-0106-3

Schauer, J.J., Lough, G.C., Shafer, M.M., Christensen, W.F., Arndt, M.F., DeMinter, J.T., Park, J.S., 2006. Characterization of metals emitted from motor vehicles. Res. Rep. Health. Eff. Inst.

Selvaraju, P.N., Parammasivam, K.M., 2019. Empirical and numerical analysis of aerodynamic drag on a typical SUV car model at different locations of vortex generator. J. Appl. Fluid Mech. 12, 1487–1496. https://doi.org/10.29252/JAFM.12.05.29674

Seo, H., Joo, B., Park, J., Kim, Y.C., Lee, J.J., Jang, H., 2021. Effect of disc material on particulate matter emissions during high-temperature braking. Tribol. Int. 154, 106713. https://doi.org/10.1016/j.triboint.2020.106713

Sethupathi, P.B., Chandradass, J., Saibalaji, M.A., 2021. Comparative study of disc brake pads sold in Indian market — Impact on safety and environmental aspects. Environ. Technol. Innov. 21, 101245. https://doi.org/10.1016/j.eti.2020.101245

Shiraiwa, M., Ueda, K., Pozzer, A., Lammel, G., Kampf, C.J., Fushimi, A., Enami, S., Arangio, A.M., Fröhlich-Nowoisky, J., Fujitani, Y., Furuyama, A., Lakey, P.S.J., Lelieveld, J., Lucas, K., Morino, Y., Pöschl, U., Takahama, S., Takami, A., Tong, H., Weber, B., Yoshino, A., Sato, K., 2017. Aerosol Health Effects from Molecular to Global Scales. Environ. Sci.

Technol. 51, 13545–13567. https://doi.org/10.1021/acs.est.7b04417

Shirmohammadi, F., Hasheminassab, S., Wang, D., Saffari, A., Schauer, J.J., Shafer, M.M., Delfino, R.J., Sioutas, C., 2015. Oxidative potential of coarse particulate matter (PM10-2.5) and its relation to water solubility and sources of trace elements and metals in the Los Angeles Basin. Environ. Sci. Process. Impacts 17, 2110–2121. https://doi.org/10.1039/c5em00364d

Shirmohammadi, F., Hasheminassab, S., Wang, D., Schauer, J.J., Shafer, M.M., Delfino, R.J., Sioutas, C., 2016. The relative importance of tailpipe and non-tailpipe emissions on the oxidative potential of ambient particles in Los Angeles, CA. Faraday Discuss. 189, 361–380. https://doi.org/10.1039/c5fd00166h

Shirmohammadi, F., Wang, D., Hasheminassab, S., Verma, V., Schauer, J.J., Shafer, M.M., Sioutas, C., 2017. Oxidative potential of on-road fine particulate matter (PM2.5) measured on major freeways of Los Angeles, CA, and a 10-year comparison with earlier roadside studies. Atmos. Environ. 148, 102–114. https://doi.org/10.1016/j.atmosenv.2016.10.042

Sicard, P., Khaniabadi, Y.O., Perez, S., Gualtieri, M., De Marco, A., 2019. Effect of O3, PM10 and PM2.5 on cardiovascular and respiratory diseases in cities of France, Iran and Italy. Environ. Sci. Pollut. Res. 26, 32645–32665. https://doi.org/10.1007/s11356-019-06445-8

Simons, A., 2016. Road transport: new life cycle inventories for fossil-fuelled passenger cars and non-exhaust emissions in ecoinvent v3. Int. J. Life Cycle Assess. 21, 1299–1313. https://doi.org/10.1007/s11367-013-0642-9

Sjödin, Å., Ferm, M., Björk, A., Rahmberg, M., Gudmundsson, E., Swietlicki, E., Johansson, C., Gustafsson, M., Blomqvist, G., 2010. Wear particles from road traffic - a field , laboratory

and modelling study. Gotenberg.

Smith, D.L., Najm, W.G., Lam, A.H., 2003. Analysis of braking and steering performance in car-following scenarios. SAE Tech. Pap. https://doi.org/10.4271/2003-01-0283

Sommer, F., Dietze, V., Baum, A., Sauer, J., Gilge, S., Maschowski, C., Gieré, R., 2018. Tire abrasion as a major source of microplastics in the environment. Aerosol Air Qual. Res. 18, 2014–2028. https://doi.org/10.4209/aaqr.2018.03.0099

Spada, N.J., Cheng, X., White, W.H., Hyslop, N.P., 2018. Decreasing Vanadium Footprint of Bunker Fuel Emissions. Environ. Sci. Technol. 52, 11528–11534. https://doi.org/10.1021/acs.est.8b02942

Srimuruganandam, B., Shiva Nagendra, S.M., 2012. Application of positive matrix factorization in characterization of PM 10 and PM 2.5 emission sources at urban roadside. Chemosphere 88, 120–130. https://doi.org/10.1016/j.chemosphere.2012.02.083

Sternbeck, J., Sjödin, Å., Andréasson, K., 2002. Metal emissions from road traffic and the influence of resuspension - Results from two tunnel studies. Atmos. Environ. 36, 4735–4744. https://doi.org/10.1016/S1352-2310(02)00561-7

Strak, M., Janssen, N., Beelen, R., Schmitz, O., Vaartjes, I., Karssenberg, D., van den Brink, C., Bots, M.L., Dijst, M., Brunekreef, B., Hoek, G., 2017. Long-term exposure to particulate matter, NO2 and the oxidative potential of particulates and diabetes prevalence in a large national health survey. Environ. Int. 108, 228–236. https://doi.org/10.1016/j.envint.2017.08.017

Strak, M., Janssen, N.A.H., Godri, K.J., Gosens, I., Mudway, I.S., Cassee, F.R., Lebret, E.,

Kelly, F.J., Harrison, R.M., Brunekreef, B., Steenhof, M., Hoek, G., 2012. Respiratory health effects of airborne particulate matter: The role of particle size, composition, and oxidative potential-the RAPTES project. Environ. Health Perspect. 120, 1183–1189. https://doi.org/10.1289/ehp.1104389

Sturk, D., Rosell, L., Blomqvist, P., Tidblad, A.A., 2019. Analysis of li-ion battery gases vented in an inert atmosphere thermal test chamber. Batteries 5, 1–17. https://doi.org/10.3390/batteries5030061

Su, J.G., Meng, Y.Y., Pickett, M., Seto, E., Ritz, B., Jerrett, M., 2016. Identification of Effects of Regulatory Actions on Air Quality in Goods Movement Corridors in California. Environ. Sci. Technol. 50, 8687–8696. https://doi.org/10.1021/acs.est.6b00926

Sundarkrishnaa, K., 2015. Friction Material Composites Copper-/Metal-Free Material Design Perspective, 2nd ed. Springer International Publishing.

Taghvaee, S., Sowlat, M.H., Diapouli, E., Manousakas, M.I., Vasilatou, V., Eleftheriadis, K., Sioutas, C., 2019. Source apportionment of the oxidative potential of fine ambient particulate matter (PM 2.5) in Athens, Greece. Sci. Total Environ. 653, 1407–1416. https://doi.org/10.1016/j.scitotenv.2018.11.016

Tapparo, A., Di Marco, V., Badocco, D., D'Aronco, S., Soldà, L., Pastore, P., Mahon, B.M., Kalberer, M., Giorio, C., 2020. Formation of metal-organic ligand complexes affects solubility of metals in airborne particles at an urban site in the Po valley. Chemosphere 241, 1–13. https://doi.org/10.1016/j.chemosphere.2019.125025

Taylor, S.R., McLennan, S., 1985. The continental crust: Its composition and evolution. Blackwell, Oxford.

Thorpe, A., Harrison, R.M., 2008. Sources and properties of non-exhaust particulate matter from road traffic: A review. Sci. Total Environ. 400, 270–282. https://doi.org/10.1016/j.scitotenv.2008.06.007

Timmers, V.R.J.H., Achten, P.A.J., 2018. Non-Exhaust PM Emissions From Battery Electric Vehicles, Non-Exhaust Emissions. Elsevier Inc. https://doi.org/10.1016/b978-0-12-811770-5.00012-1

Timmers, V.R.J.H., Achten, P.A.J., 2016. Non-exhaust PM emissions from electric vehicles. Atmos. Environ. 134, 10–17. https://doi.org/10.1016/j.atmosenv.2016.03.017

USEPA, 2020. Brake and Tire Wear Emissions from Onroad Vehicles in MOVES3 Brake and Tire Wear Emissions.

Valdés, A., Zanobetti, A., Halonen, J.I., Cifuentes, L., Morata, D., Schwartz, J., 2012. Elemental concentrations of ambient particles and cause specific mortality in Santiago, Chile: A time series study. Environ. Heal. A Glob. Access Sci. Source 11, 1–8. https://doi.org/10.1186/1476-069X-11-82

Vardoulakis, S., Giagloglou, E., Steinle, S., Davis, A., Sleeuwenhoek, A., Galea, K.S., Dixon, K., Crawford, J.O., 2020. Indoor exposure to selected air pollutants in the home environment: A systematic review. Int. J. Environ. Res. Public Health 17, 1–24. https://doi.org/10.3390/ijerph17238972

Veld, M. in ’t, Alastuey, A., Pandolfi, M., Amato, F., Pérez, N., Reche, C., Via, M., Minguillón, M.C., Escudero, M., Querol, X., 2021. Compositional changes of PM2.5 in NE Spain during 2009–2018: A trend analysis of the chemical composition and source apportionment. Sci. Total Environ. 795, 148728. https://doi.org/10.1016/j.scitotenv.2021.148728

Verma, P.C., Alemani, M., Gialanella, S., Lutterotti, L., Olofsson, U., Straffelini, G., 2016. Wear debris from brake system materials: A multi-analytical characterization approach. Tribol. Int. 94, 249–259. https://doi.org/10.1016/j.triboint.2015.08.011

von Schneidemesser, E., Zhou, J., Stone, E.A., Schauer, J.J., Qasrawi, R., Abdeen, Z., Shpund, J., Vanger, A., Sharf, G., Moise, T., Brenner, S., Nassar, K., Saleh, R., Al-Mahasneh, Q.M., Sarnat, J.A., 2010. Seasonal and spatial trends in the sources of fine particle organic carbon in Israel, Jordan, and Palestine. Atmos. Environ. 44, 3669–3678. https://doi.org/10.1016/j.atmosenv.2010.06.039

Von Uexküll, O., Skerfving, S., Doyle, R., Braungart, M., 2005. Antimony in brake pads-a carcinogenic component? J. Clean. Prod. 13, 19–31. https://doi.org/10.1016/j.jclepro.2003.10.008

Vontorová, J., Dobiáš, V., Mohyla, P., 2017. Utilization of GDOES for the study of friction layers formed on the surface of brake discs during the friction process. Chem. Pap. 71, 1507–1514. https://doi.org/10.1007/s11696-017-0145-4

Wagner, S., Hüffer, T., Klöckner, P., Wehrhahn, M., Hofmann, T., Reemtsma, T., 2018. Tire wear particles in the aquatic environment - A review on generation, analysis, occurrence, fate and effects. Water Res. 139, 83–100. https://doi.org/10.1016/j.watres.2018.03.051

Wahlström, J., 2015. A comparison of measured and simulated friction, wear, and particle emission of disc brakes. Tribol. Int. 92, 503–511. https://doi.org/10.1016/j.triboint.2015.07.036

Wahlström, J., Olander, L., Olofsson, U., 2010a. Size, shape, and elemental composition of airborne wear particles from disc brake materials. Tribol. Lett. 38, 15–24.

https://doi.org/10.1007/s11249-009-9564-x

Wahlström, J., Söderberg, A., Olander, L., Jansson, A., Olofsson, U., 2010b. A pin-on-disc simulation of airborne wear particles from disc brakes. Wear 268, 763–769. https://doi.org/https://doi.org/10.1016/j.wear.2009.11.014

Wahlström, J., Söderberg, A., Olofsson, U., 2009. Simulation of airborne wear particles from disc brakes. SAE Tech. Pap. https://doi.org/10.4271/2009-01-3040

Wallenborn, J.G., Schladweiler, M.J., Richards, J.H., Kodavanti, U.P., 2009. Differential pulmonary and cardiac effects of pulmonary exposure to a panel of particulate matter-associated metals. Toxicol. Appl. Pharmacol. 241, 71–80. https://doi.org/10.1016/j.taap.2009.08.003

Wang, A., Kadam, S., Li, H., Shi, S., Qi, Y., 2018. Review on modeling of the anode solid electrolyte interphase (SEI) for lithium-ion batteries. npj Comput. Mater. 4. https://doi.org/10.1038/s41524-018-0064-0

Wang, B., Eum, K. Do, Kazemiparkouhi, F., Li, C., Manjourides, J., Pavlu, V., Suh, H., 2020. The impact of long-term PM2.5 exposure on specific causes of death: Exposure-response curves and effect modification among 53 million U.S. Medicare beneficiaries. Environ. Heal. A Glob. Access Sci. Source 19, 1–12. https://doi.org/10.1186/s12940-020-00575-0

Wang, J.M., Jeong, C.H., Hilker, N., Healy, R.M., Sofowote, U., Debosz, J., Su, Y., Munoz, A., Evans, G.J., 2021. Quantifying metal emissions from vehicular traffic using real world emission factors. Environ. Pollut. 268, 115805. https://doi.org/10.1016/j.envpol.2020.115805

Wang, L., Yu, Y., Huang, K., Zhang, Z., Li, X., 2020. The inharmonious mechanism of CO2, NOx, SO2, and PM2.5 electric vehicle emission reductions in Northern China. J. Environ. Manage. 274. https://doi.org/10.1016/j.jenvman.2020.111236

Wang, Q., Sun, J., Yao, X., Chen, C., 2006. Thermal Behavior of Lithiated Graphite with Electrolyte in Lithium-Ion Batteries. J. Electrochem. Soc. 153, A329. https://doi.org/10.1149/1.2139955

Wang, X., Grose, M.A., Caldow, R., Osmondson, B.L., Swanson, J.J., Chow, J.C., Watson, J.G., Kittelson, D.B., Li, Y., Xue, J., Jung, H., Hu, S., 2016. Improvement of Engine Exhaust Particle Sizer (EEPS) size distribution measurement - II. Engine exhaust particles. J. Aerosol Sci. 92, 83–94. https://doi.org/10.1016/j.jaerosci.2015.11.003

Wang, Y., Shi, L., Lee, M., Liu, P., Di, Q., Zanobetti, A., Schwartz, J.D., 2017. Long-term Exposure to PM 2.5 and Mortality among Older Adults in the Southeastern US. Epidemiology 28, 207–214. https://doi.org/10.1097/EDE.0000000000000614

Wei, Y., Han, I., Shao, M., Hu, M., Zhang, J.J., Tang, X., 2009. Article PM Constituents and Oxidative DNA Damage in Humans PM 2 . 5 Constituents and Oxidative DNA Damage in Humans. Environ. Sci. Technol. 43, 4757–4762.

Weichenthal, S., Shekarrizfard, M., Traub, A., Kulka, R., Al-Rijleh, K., Anowar, S., Evans, G., Hatzopoulou, M., 2019. Within-City Spatial Variations in Multiple Measures of PM2.5 Oxidative Potential in Toronto, Canada. Environ. Sci. Technol. 53, 2799–2810. https://doi.org/10.1021/acs.est.8b05543

Wik, A., Dave, G., 2009. Occurrence and effects of tire wear particles in the environment - A critical review and an initial risk assessment. Environ. Pollut. 157, 1–11.

https://doi.org/10.1016/j.envpol.2008.09.028

Wilken, S., Treskow, M., Scheers, J., Johansson, P., Jacobsson, P., 2013. Initial stages of thermal decomposition of LiPF6-based lithium ion battery electrolytes by detailed Raman and NMR spectroscopy. RSC Adv. 3, 16359–16364. https://doi.org/10.1039/c3ra42611d

Wilson, J.G., Kingham, S., Pearce, J., Sturman, A.P., 2005. A review of intraurban variations in particulate air pollution: Implications for epidemiological research. Atmos. Environ. 39, 6444–6462. https://doi.org/10.1016/j.atmosenv.2005.07.030

Windsor, S., 2014. Real world drag coefficient – is it wind averaged drag?, The International Vehicle Aerodynamics Conference. Woodhead Publishing Limited. https://doi.org/10.1533/9780081002452.1.3

Wu, Z., Liu, Y., Pan, G., 2009. A smart car control model for brake comfort based on car following. IEEE Trans. Intell. Transp. Syst. 10, 42–46. https://doi.org/10.1109/TITS.2008.2006777

Xu, C., Dai, Q., Gaines, L., Hu, M., Tukker, A., Steubing, B., 2020. Future material demand for automotive lithium-based batteries. Commun. Mater. 1. https://doi.org/10.1038/s43246-020-00095-x

Xu, X., Cook, R.L., Ilacqua, V.A., Kan, H., Talbott, E.O., Kearney, G., 2010. Studying associations between urinary metabolites of polycyclic aromatic hydrocarbons (PAHs) and cardiovascular diseases in the United States. Sci. Total Environ. 408, 4943–4948. https://doi.org/10.1016/j.scitotenv.2010.07.034

Yadav, S., Phuleria, H.C., 2020. Oxidative Potential of Particulate Matter: A Prospective

Measure to Assess PM Toxicity. Energy, Environ. Sustain. 333–356. https://doi.org/10.1007/978-981-15-0540-9_16

Yang, A., Hellack, B., Leseman, D., Brunekreef, B., Kuhlbusch, T.A.J., Cassee, F.R., Hoek, G., Janssen, N.A.H., 2015. Temporal and spatial variation of the metal-related oxidative potential of PM2.5 and its relation to PM2.5 mass and elemental composition. Atmos. Environ. 102, 62–69. https://doi.org/10.1016/j.atmosenv.2014.11.053

Yang, A., Janssen, N.A.H., Brunekreef, B., Cassee, F.R., Hoek, G., Gehring, U., 2016. Children's respiratory health and oxidative potential of PM2.5: The PIAMA birth cohort study. Occup. Environ. Med. 73, 154–160. https://doi.org/10.1136/oemed-2015-103175

Yang, F., Xie, Y., Deng, Y., Yuan, C., 2018. Predictive modeling of battery degradation and greenhouse gas emissions from U.S. state-level electric vehicle operation. Nat. Commun. 9, 1–10. https://doi.org/10.1038/s41467-018-04826-0

Yang, X., Jia, X., Dong, W., Wu, S., Miller, M.R., Hu, D., Li, H., Pan, L., Deng, F., Guo, X., 2018. Cardiovascular benefits of reducing personal exposure to traffic-related noise and particulate air pollution: A randomized crossover study in the Beijing subway system. Indoor Air 28, 777–786. https://doi.org/10.1111/ina.12485

Ye, D., Klein, M., Mulholland, J.A., Russell, A.G., Weber, R., Edgerton, E.S., Chang, H.H., Sarnat, J.A., Tolbert, P.E., Sarnat, S.E., 2018. Estimating acute cardiovascular effects of ambient PM2.5 metals. Environ. Health Perspect. 126, 1–10. https://doi.org/10.1289/EHP2182

Yu, G.H., Park, S., 2021. Chemical characterization and source apportionment of PM2.5 at an urban site in Gwangju, Korea. Atmos. Pollut. Res. 12, 101092.

https://doi.org/10.1016/j.apr.2021.101092

Zhang, X., Staimer, N., Tjoa, T., Gillen, D.L., Schauer, J.J., Shafer, M.M., Hasheminassab, S., Pakbin, P., Longhurst, J., Sioutas, C., Delfino, R.J., 2016. Associations between microvascular function and short-term exposure to traffic-related air pollution and particulate matter oxidative potential. Environ. Heal. A Glob. Access Sci. Source 15, 1–16. https://doi.org/10.1186/s12940-016-0157-5

Zhang, Y., Peng, M., Yu, C., Zhang, L., 2017. Burden of mortality and years of life lost due to ambient PM10 pollution in Wuhan, China. Environ. Pollut. 230, 1073–1080. https://doi.org/10.1016/j.envpol.2017.07.053

Zhang, Y., Wang, H., Li, W., Li, C., 2019a. Quantitative identification of emissions from abused prismatic Ni-rich lithium-ion batteries. eTransportation 2, 100031. https://doi.org/10.1016/j.etran.2019.100031

Zhang, Y., Wang, H., Li, W., Li, C., Ouyang, M., 2019b. Size distribution and elemental composition of vent particles from abused prismatic Ni-rich automotive lithium-ion batteries. J. Energy Storage 26, 100991. https://doi.org/10.1016/j.est.2019.100991

Zhao, J., Lewinski, N., Riediker, M., 2015. Physico-chemical characterization and oxidative reactivity evaluation of aged brake wear particles. Aerosol Sci. Technol. 49, 65–74. https://doi.org/10.1080/02786826.2014.998363

Zhou, Y., Wang, M., Hao, H., Johnson, L., Wang, H., Hao, H., 2015. Plug-in electric vehicle market penetration and incentives: a global review. Mitig. Adapt. Strateg. Glob. Chang. 20, 777–795. https://doi.org/10.1007/s11027-014-9611-2

Zhu, Y., Kuhn, T., Mayo, P., Hinds, W.C., 2006. Comparison of daytime and nighttime concentration profiles and size distributions of ultrafine particles near a major highway. Environ. Sci. Technol. 40, 2531–2536. https://doi.org/10.1021/es0516514